DETONATION DIFFRACTION INTO A CONFINED VOLUME

A Thesis

by

NOLAN LEE POLLEY

Submitted to the Office of Graduate Studies of
Texas A&M University
in partial fulfillment of the requirements for the degree of

MASTER OF SCIENCE

December 2010

Major Subject: Mechanical Engineering

Detonation Diffraction into a Confined Volume

DETONATION DIFFRACTION INTO A CONFINED VOLUME

A Thesis

by

NOLAN LEE POLLEY

Submitted to the Office of Graduate Studies of
Texas A&M University
in partial fulfillment of the requirements for the degree of

MASTER OF SCIENCE

Approved by:

Chair of Committee,	Eric L. Petersen
Committee Members,	Gerald Morrison
	M. Sam Mannan
Head of Department,	Dennis O'Neal

December 2010

Major Subject: Mechanical Engineering

ABSTRACT

Detonation Diffraction into a Confined Volume. (December 2010)

Nolan Lee Polley, B.S., University of Wisconsin-Madison

Chair of Advisory Committee: Dr. Eric L. Petersen

Detonation diffraction has been, and remains, an active area of research. However, detonation diffraction into a confined volume and, specifically the transformation of a planar detonation into a cylindrical detonation, is an area which has received little attention. Experimental work needs to be conducted on detonation diffraction into a confined volume to understand how the interaction of the diffracted shock wave with a confining wall impacts the detonation diffraction process. Therefore, a facility was constructed to study this problem, and experiments were conducted to determine under what conditions a planar detonation could be transformed successfully into a cylindrical detonation. Four different fuel-oxidizer mixtures, $C_2H_2 + 2.5\ O_2$, $C_2H_2 + 4\ O_2$, $C_2H_4 + 3\ O_2$ and $H_2 + 0.5\ O_2$, were tested in this study using a combination of pressure transducers and soot foil records as diagnostics. Three different regimes of successful transmission- spontaneous re-ignition, continuous reflected re-initiation, and discontinuous reflected re-initiation- were identified. The detonation cell size and the distance from the tube exit to the confining wall, or gap size, were determined to be the most important parameters in the transmission process, and a linear correlation for determining whether or not transmission will be successful for a given set of initial

conditions was developed for gap sizes between 10 and 35 mm. For gap sizes smaller than 10 mm or gap sizes larger than 35 mm the linear correlation does not apply. Finally, the results of this study are compared to results on detonation diffraction into a confined volume available in the literature and explanations for any disagreements are given. This study showed that when compared to transmission of a detonation into an unconfined volume, the transmission of a detonation into a confined volume, for the majority of gap sizes, is possible for a wider range of conditions. However, for extremely small gap sizes, when compared to transmission into an unconfined volume, the range of conditions for which successful transmission is possible into a confined volume is actually narrower.

DEDICATION

I would like to dedicate this thesis to my parents, Lorin and Kathy, and my sister Kellen for their constant support and guidance throughout my college career and life.

ACKNOWLEDGMENTS

There are many people that I would like to acknowledge who have helped make the research presented in this thesis possible. I'd like to thank my advisor, Dr. Eric Petersen, who has given me with the opportunity to be a research assistant for the past two years. I have been exposed to a variety of research topics, including the research presented in this thesis. I'd also like to thank Miles Egbert, an undergraduate researcher who has worked with me on this project for the past year, who has been a tremendous help and asset. I'd also like to acknowledge and thank my fellow graduate students Will Lowry, Kevin Kreitz, Brandon Rotavera, Nicole Donato and Chris Aul. Finally, I'd like to thank Holley Toschlog for her help and advice during the past two years.

NOMENCLATURE

λ	Detonation cell size
λ_s	Critical detonation cell size for transmission of a planar detonation into an unconfined volume
w	Width of confined volume
d	Diameter of obstacle
D	Diameter of detonation tube

TABLE OF CONTENTS

Page

CHAPTER Page

Page

LIST OF FIGURES

Page

Page

Page

Page

Page

Page

Page

Page

Page

LIST OF TABLES

Page

CHAPTER I

INTRODUCTION

There are two different modes of combustion, deflagrations and detonations. Lee (2008) defines a deflagration as a combustion wave which propagates "at relatively low subsonic velocities with respect to the reactants ahead of it." A detonation, on the other hand, is a coupled shock wave and reaction zone which propagates at supersonic speed with respect to the reactants ahead of it.

The change in thermodynamic states of the gases also differs between a deflagration and detonation. While the temperature rises across both waves, the pressure actually falls across a deflagration, while there is a sharp increase in pressure across a detonation.

ZND Model

The simplest model for a detonation wave is known as the Zeldovich-von Neumann- Doring (ZND) model. This model treats a detonation wave as a 1-D shock wave followed by a reaction zone, as seen in Fig. 1. In this model, the leading shock wave, travelling at the Chapman-Jouguet (CJ) speed, raises the temperature of the reactants to a sufficiently high temperature for chemical reactions to take place, and the release of energy from these reactions continues to propel the leading shock wave at the CJ speed. The intermediate state between the reactants and products in Fig. 1 is known as the Von Neumann state. The conditions at this state can be calculated using the

---

This thesis follows the style of *Combustion Science and Technology*.

Rankine-Hugoniot normal shock equations, and as Fig. 1 shows the pressure at this state is much higher than the final pressure. However, because distance between the leading normal shock and reaction zone is extremely small, in practice this state is not observed experimentally.

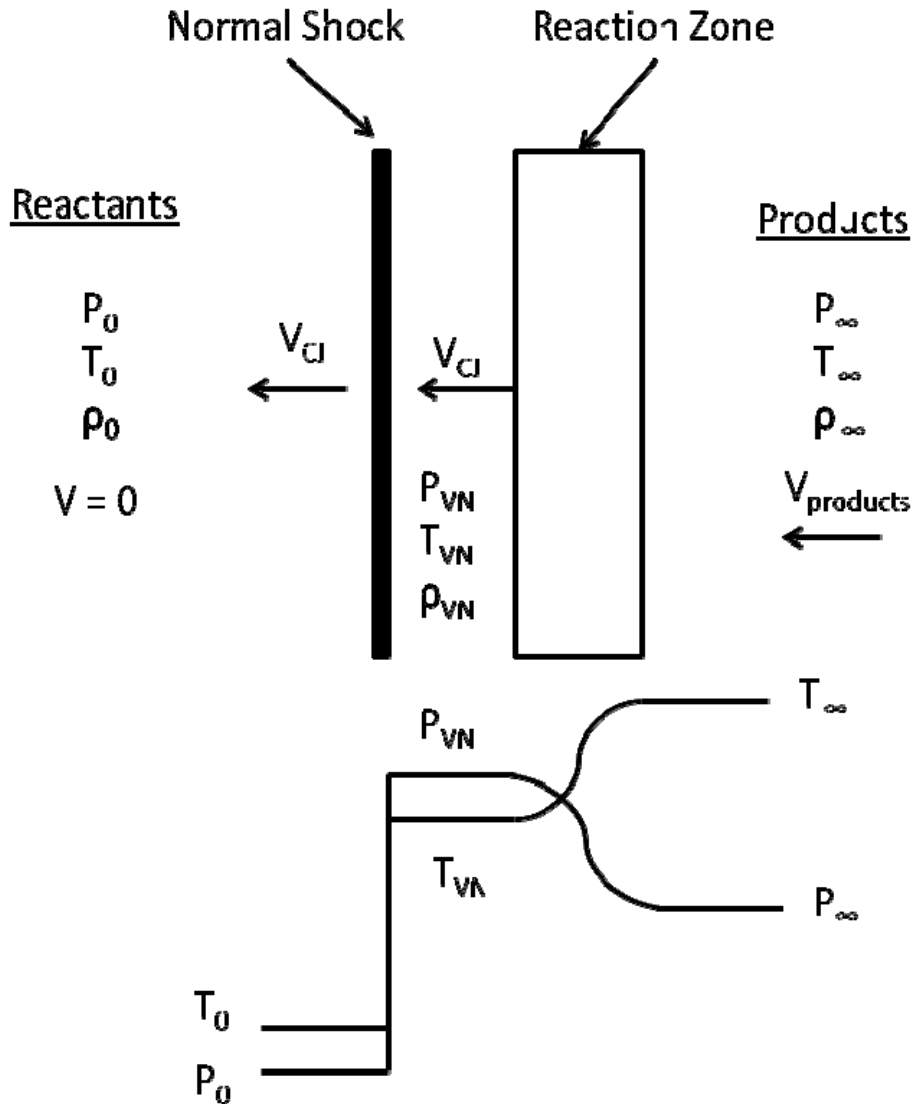

Figure 1 ZND model. Pressure and temperature variation across detonation wave in ZND model.

While a detonation wave actually possesses a complex, three-dimensional structure, the difference in thermodynamic states can be calculated quite accurately if it is treated as a one-dimensional wave. Browne et al. (2008b) published a report detailing the relevant jump conditions across both shock and detonation waves. A summary of the relevant equations is given in the following section.

First, energy, momentum and mass balances across the wave are conducted in a fixed-wave reference frame as shown in Fig. 2. The results of the balances are given in Eqs. (1-3).

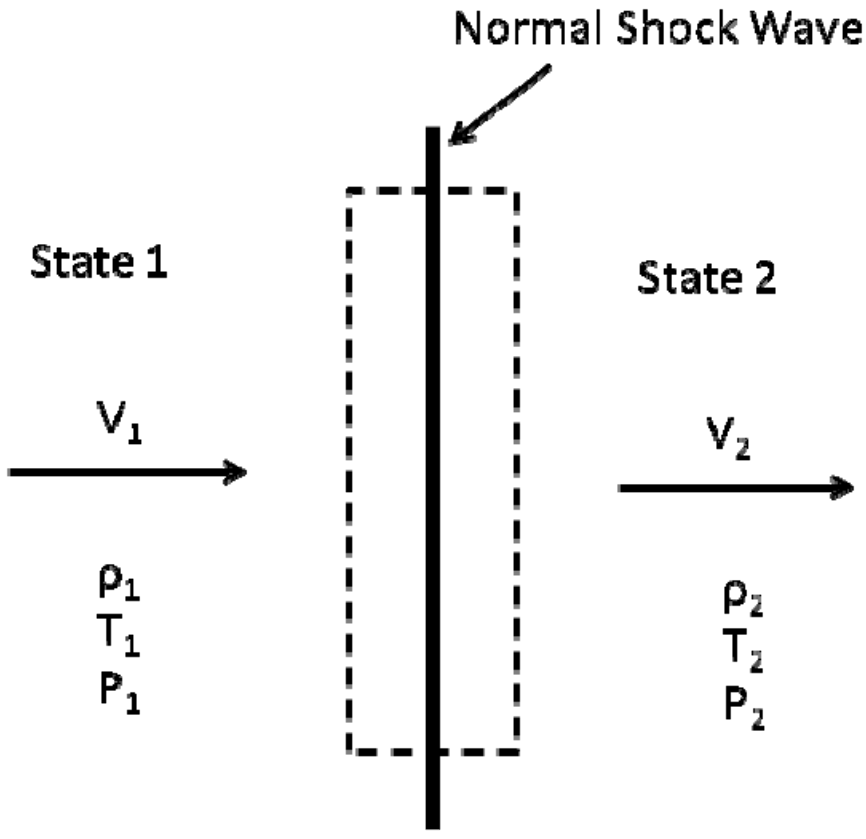

Figure 2 Jump conditions across detonation wave in the wave reference frame.

$$\rho_1 V_1 = \rho_2 V_2 \quad (1)$$

$$P_1 + \rho_1 V_1^2 = P_2 + \rho_2 V_2^2 \quad (2)$$

$$h_1 + \frac{V_1^2}{2} = h_2 + \frac{V_2^2}{2} \quad (3)$$

Browne et al. (2008b) also note that the entropy must increase across the wave, as expected, to satisfy the 2nd Law of thermodynamics.

$$\Delta h = (c_p T_2 - c_p T_1) - \mathrm{q} \quad (4)$$

$$P = \rho R T \quad (5)$$

$$a = \sqrt{\gamma R T} \quad (6)$$

$$M = \frac{v}{a} \quad (7)$$

$$\gamma = \frac{c_p}{c_v} \quad (8)$$

$$R = c_p - c_v \quad (9)$$

$$c_p = \gamma R/(\gamma - 1) \quad (10)$$

When the mass, momentum and energy balance equations are combined with Eqs. (4-10), the jump conditions for pressure and temperature across a planar detonation wave can be obtained. The final equations, as given by Browne et al. (2008b) are shown in Eqs. (11-12). The algebraic steps required to arrive at the final equations are shown in Appendix E**.** It is important to note that γ is not assumed to be a constant in the above equations because of the high temperatures present behind a detonation wave. The high temperatures reduce γ_2 sufficiently compared to γ_1 that gamma cannot be assumed constant across the wave.

$$P_2/P_1 = (1 + \gamma_1 M_1^2)/(1 + \gamma_2 M_2^2) \tag{11}$$

$$T_2/T_1 = (\gamma_1 R_1/\gamma_2 R_2)\left(\left({}^{1}/_{(\gamma_1 - 1)} + \tfrac{1}{2}M_1^2 + {}^{q}/_{a_1^2}\right)\Big/\left({}^{1}/_{(\gamma_2 - 1)} + \tfrac{1}{2}M_2^2\right)\right) \tag{12}$$

In order to solve the above equations, M_1 must be determined. To accomplish this, it is useful to plot the Hugoniot and Rayleigh lines on a Pv chart, as shown in Fig. 3.

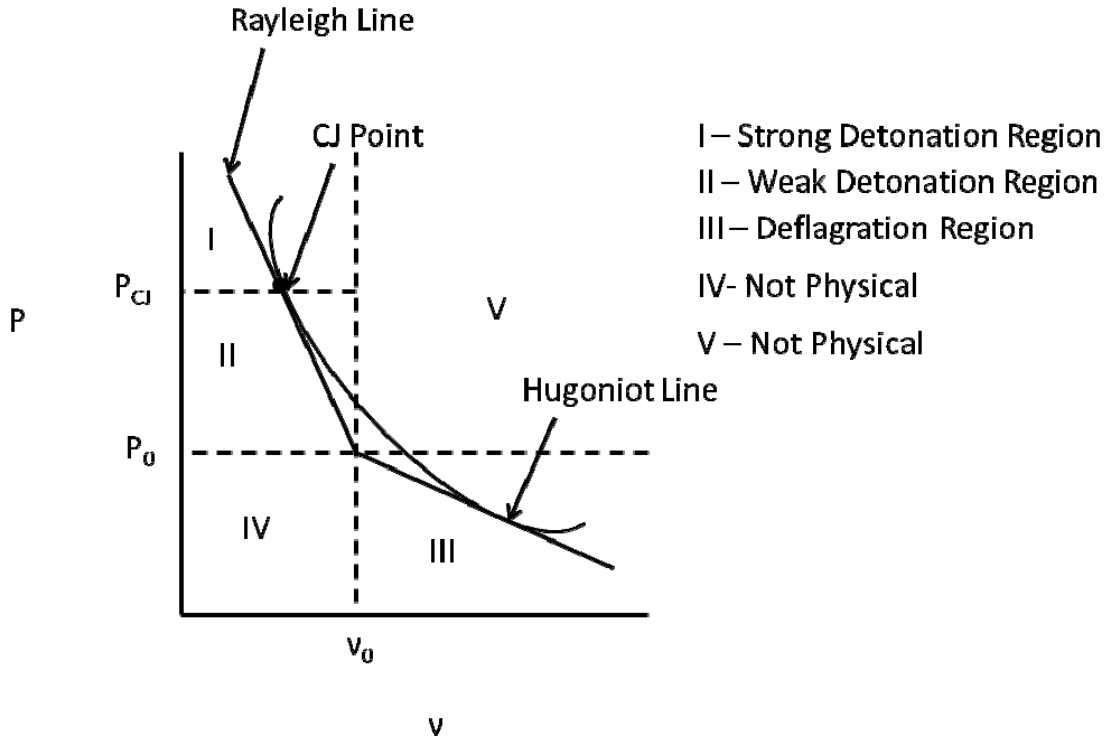

Figure 3 Rayleigh Line and Hugoniot line. Regions of strong detonations, weak detonations, and the Chapman-Jouguet (CJ) point are shown.

As shown in Fig. 3 there are three possible states for a detonation. A detonation can either be a strong detonation, where the flow behind the wave is subsonic, a weak detonation, where the flow behind the wave is supersonic, or a Chapman-Jouguet (CJ) detonation, where the flow behind the wave is sonic. The CJ condition exists when the Rayleigh and Hugoniot lines are tangent and have the same slope.

Typically, most detonation waves exist at the CJ condition because, since the flow behind the wave is sonic, no disturbances behind the detonation wave can propagate forward and affect the wave. However, both strong and weak detonations are also possible, although weak detonations are rarely observed experimentally.

Strong detonations are common and are typically observed experimentally following the deflagration-to detonation transition (DDT) or immediately following initiation, if the detonation wave were initiated using a high energy source such as a spark, laser or explosive. Because the flow behind the strong detonation wave is subsonic, disturbances from behind the wave affect the wave. As a result, strong detonations, also known as overdriven detonations, eventually decay to the CJ condition.

Using the condition that the Rayleigh and Hugoniot lines are tangent and have the same slope, it is possible to solve for the incident Mach number which satisfies these conditions. This result is known as the CJ Mach number. The solution, shown below, was given by Browne et al. (2008b)**.**

$$M_{CJ} = \sqrt{\left(\left((\gamma_2-1)(\gamma_2+1)q\right)\Big/\left(2\gamma_1(\gamma_1-1)\right)\right)+\left(\left((\gamma_1+\gamma_2)(\gamma_2-1)\right)\Big/\left(2\gamma_1(\gamma_1-1)\right)\right)} + \sqrt{\left(\left((\gamma_2-1)(\gamma_2+1)q\right)\Big/\left(2\gamma_1(\gamma_1-1)\right)\right)+\left(\left((\gamma_2-\gamma_1)(\gamma_2+1)\right)\Big/\left(2\gamma_1(\gamma_1-1)\right)\right)} \tag{13}$$

Finally, because at the CJ condition M_2 is equal to one, Eqs. (11-12) simplify to the following useful relations which can be used to calculate the change in thermodynamic states across a detonation wave.

$$P_{CJ}/P_1 = \left(1+\gamma_1 M_{CJ}^2\right)/(1+\gamma_2) \tag{14}$$

$$T_{CJ}/T_1 = (\gamma_1 R_1)/(\gamma_2 R_2)\left(\left(1/(\gamma_1 - 1) + \frac{1}{2}M_{CJ}^2 + q/a_1^2\right)/(1/(\gamma_2 - 1))\right) \quad (15)$$

Detonation Cellular Structure

While the ZND model treated a detonation wave as a 1-D shock wave followed by a reaction zone, in reality a detonation wave possesses a complex, 3-D structure. This 3-D structure can be visualized using soot foils, which record the path of the triple points present in a detonation. Lee (2008) and Lam et al. (2003) both offer excellent, more-detailed explanations of how the triple points actually write on the soot foil.

Figure 4 shows a representation of the typical cellular pattern recorded by a soot foil for a planar detonation wave. Ideally, the size of cells in a planar detonation wave is constant. However, in practice the cell size of a mixture can vary significantly depending on the degree of regularity of the mixture. Figure 5 shows an image of an experimental record from a cylindrical detonation where the cell size remained approximately constant. Further details on the experimental setup and the soot foils obtained are provided later in this thesis.

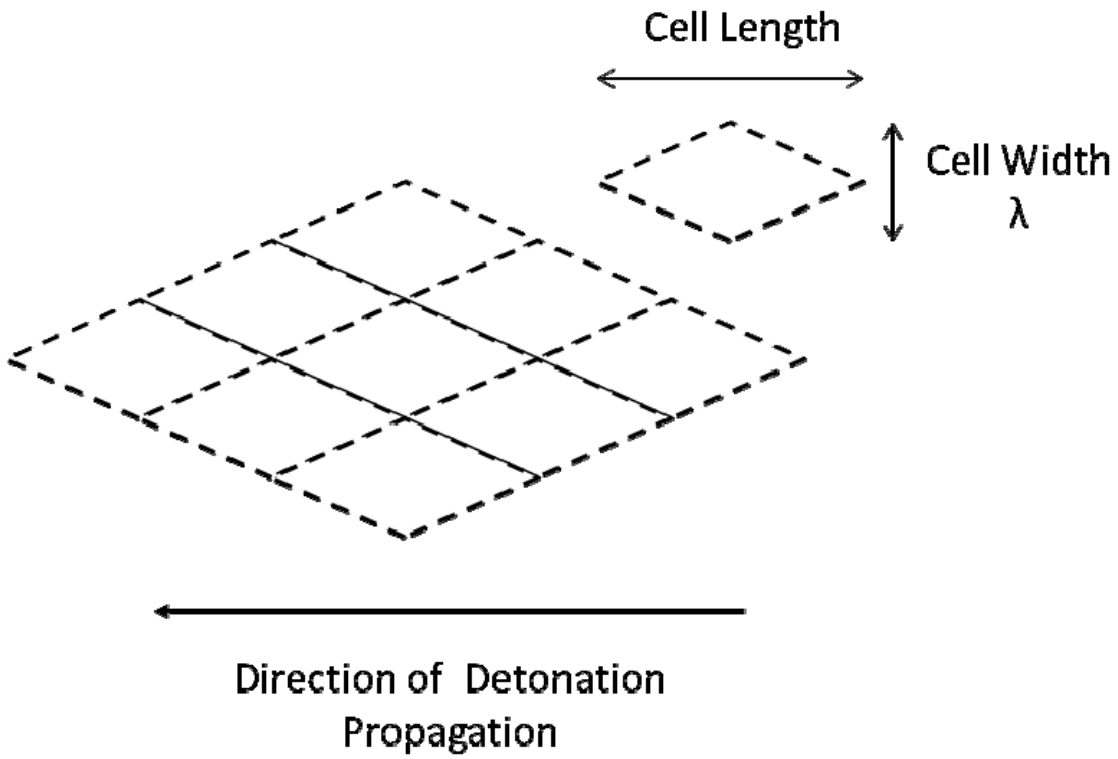

Figure 4 Detonation cell structure behind a planar detonation wave.

Figure 5 Experimental record of detonation wave cellular structure from the present study.

Figure 6 shows the cellular structure of a diverging detonation wave. The detonation cells grow larger in the direction of propagation. This is because the area of a diverging detonation front is increasing as it moves radially outwards, and additional transverse waves must be produced to maintain a constant cell size. If transverse waves are not produced at a fast enough rate, the detonation cells increase in size and the detonation wave will eventually fail. Figure 7 shows an image of an experimental record obtained of a diverging, cylindrical detonation which shows that the cell size grows in the direction of propagation. Both Lee (2008) and Vasil'ev (1998) provide a more detailed explanation of this phenomenon.

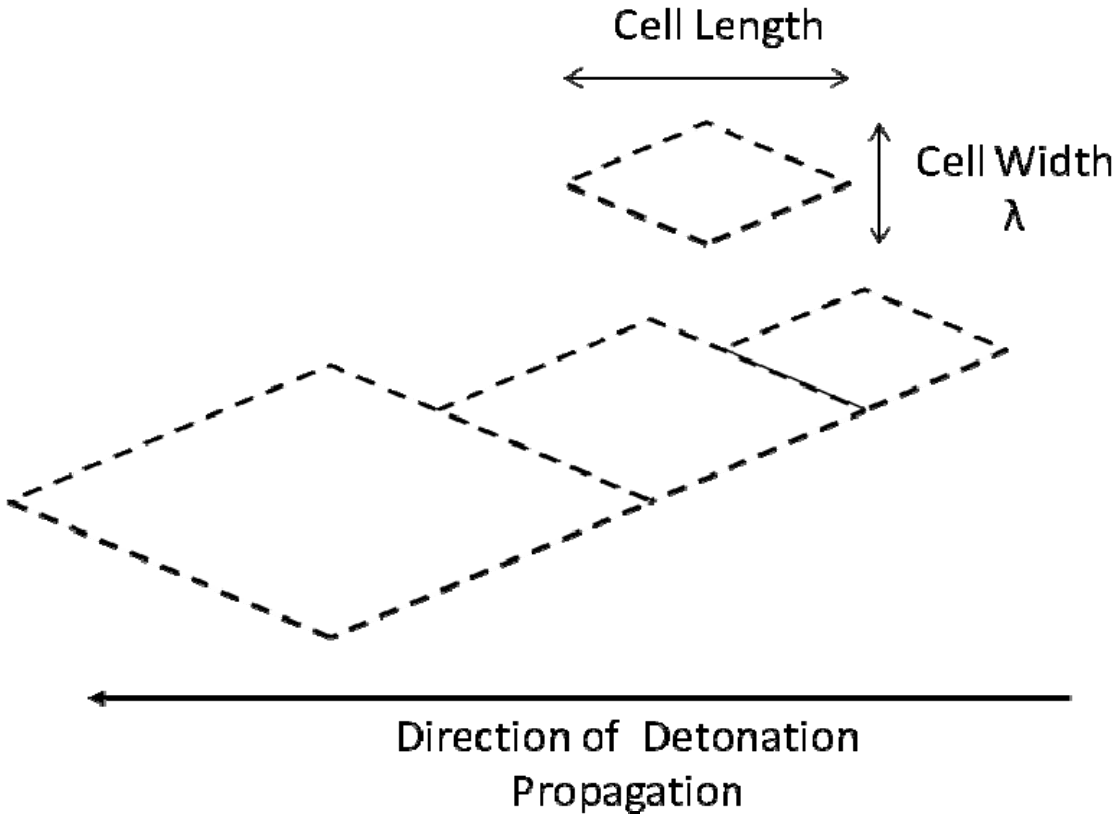

Figure 6 Detonation cellular structure for a diverging detonation wave. The cellular structure increases in the direction of propagation.

Figure 7 Experimental record of cellular structure for a diverging detonation wave from the present study. The cells grow larger as the detonation propagates radially outwards.

Introduction to Detonation Diffraction

Finally, an introduction to the detonation diffraction process is presented below. A more in-depth overview of the process is given in Chapter II. Detonation diffraction is another important aspect of detonation research as well as the focus of the current study. Detonation diffraction is simply defined as a detonation expanding from a smaller tube or channel into a larger confined or unconfined volume. Here, a confined volume is

defined as a volume where interaction between the detonation wave and a rigid wall is important in the transmission process, whereas there is no interaction between the detonation wave and a rigid wall in an unconfined volume.

As noted by Schultz (2000) on pgs. 4-6, a detonation diffracting into either an unconfined or confined volume will result in supercritical, critical, or subcritical transmission. In both supercritical and critical transmission, the detonation wave continues to propagate, while for subcritical transmission the leading shock wave and reaction zone decouple and the detonation wave fails to propagate.

Figures 8-11 graphically show the difference between supercritical and sub-critical transmission for diffraction into both unconfined and confined volumes. In supercritical transmission, the shock wave and reaction zone never decouple, while in critical transmission the shock wave and reaction zone begin to decouple; but re-initiation of the detonation wave occurs prior to complete failure of the detonation wave.

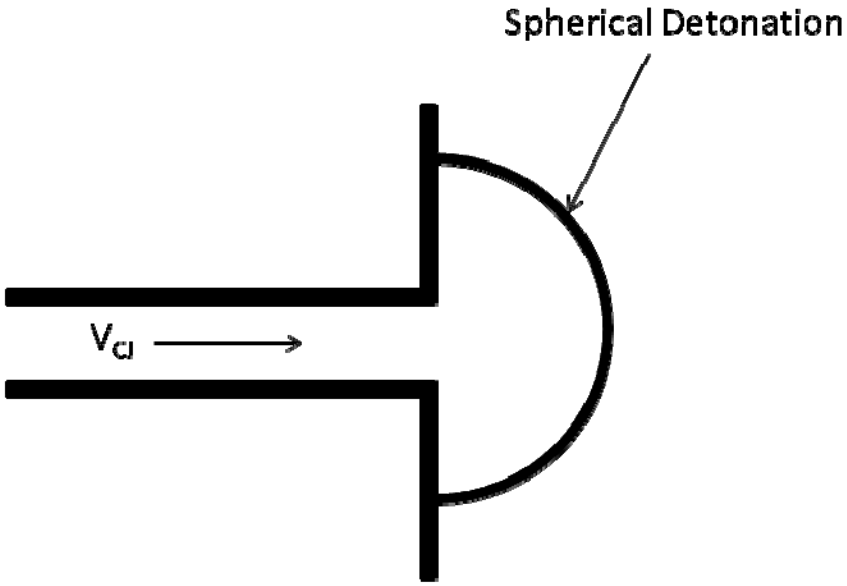

Figure 8 Supercritical transmission for a detonation diffracting into an unconfined volume. The shock wave and reaction zone remain coupled, and transmission of the detonation wave is successful.

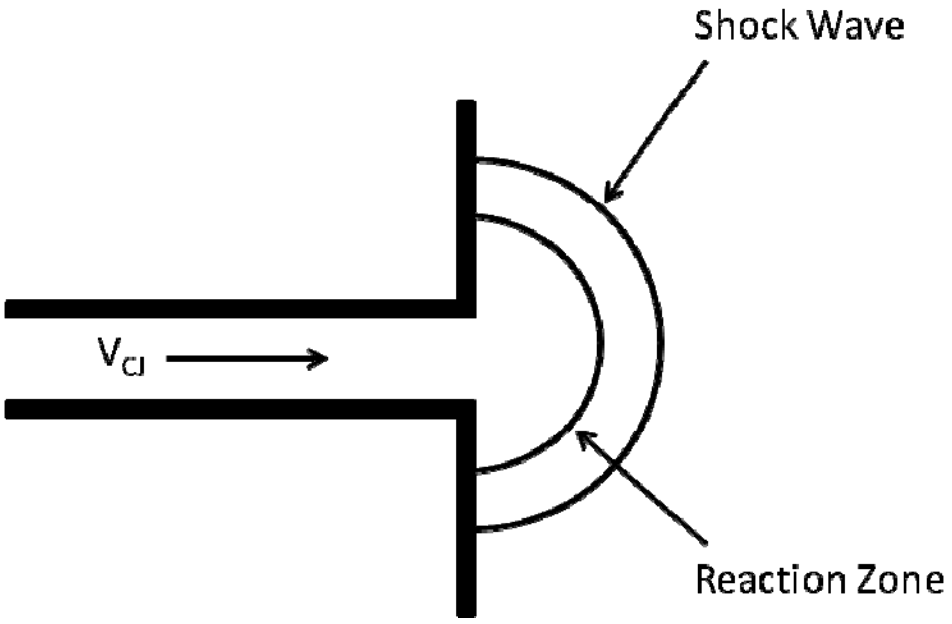

Figure 9 Subcritical transmission for a detonation diffracting into an unconfined volume. The shock wave and reaction zone decouple, and the transmission of the detonation fails and becomes a deflagration.

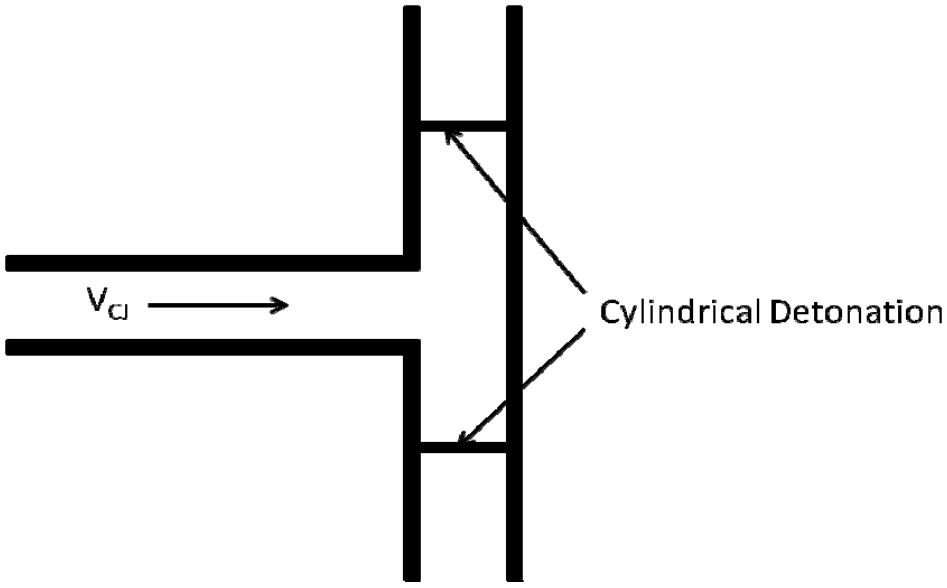

Figure 10 Supercritical transmission for a detonation diffracting into a confined volume. The shock wave and reaction zone remain coupled, and transmission of the detonation wave is successful.

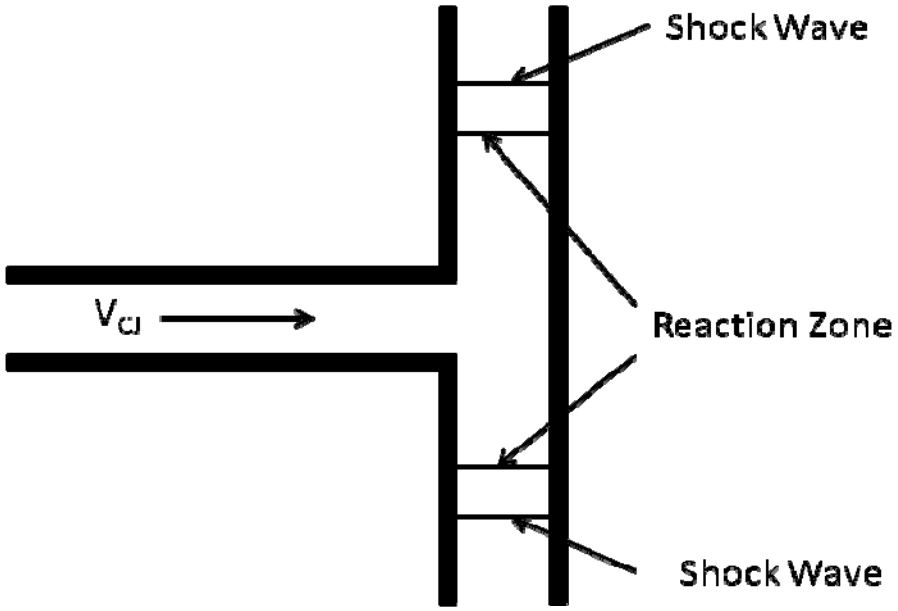

Figure 11 Subcritical transmission for a detonation diffracting into a confined volume. The shock wave and reaction zone decouple, and the transmission of the detonation fails and becomes a deflagration.

Detonation Diffraction Process

A simple diagram which illustrates the diffraction process and the reason why detonation diffraction results in failure of the detonation under certain conditions is shown in Fig. 12**.** To turn the flow, expansion waves are set up at the corners of the tube exit. These expansion waves propagate toward the tube axis at an angle of α. However, in addition to turning the flow, the expansion waves also lower the temperature of the gas behind the leading shock wave. The chemical reaction rate is extremely sensitive to temperature, and even a small drop in temperature behind the leading shock may slow the reaction rate sufficiently to allow the leading shock and reaction zone to decouple. For the shock wave and reaction zone to remain coupled, the energy release must occur very close to the leading shock wave.

During supercritical transmission, although the shock wave and reaction zone do decouple initially along the back wall, the detonation is re-initiated prior to the expansion waves reaching the tube axis and quenching the detonation. During sub-critical transmission, however, the detonation is not re-initiated prior to the expansion waves reaching the tube axis, and a fully decoupled shock wave and reaction zone result as the detonation fails.

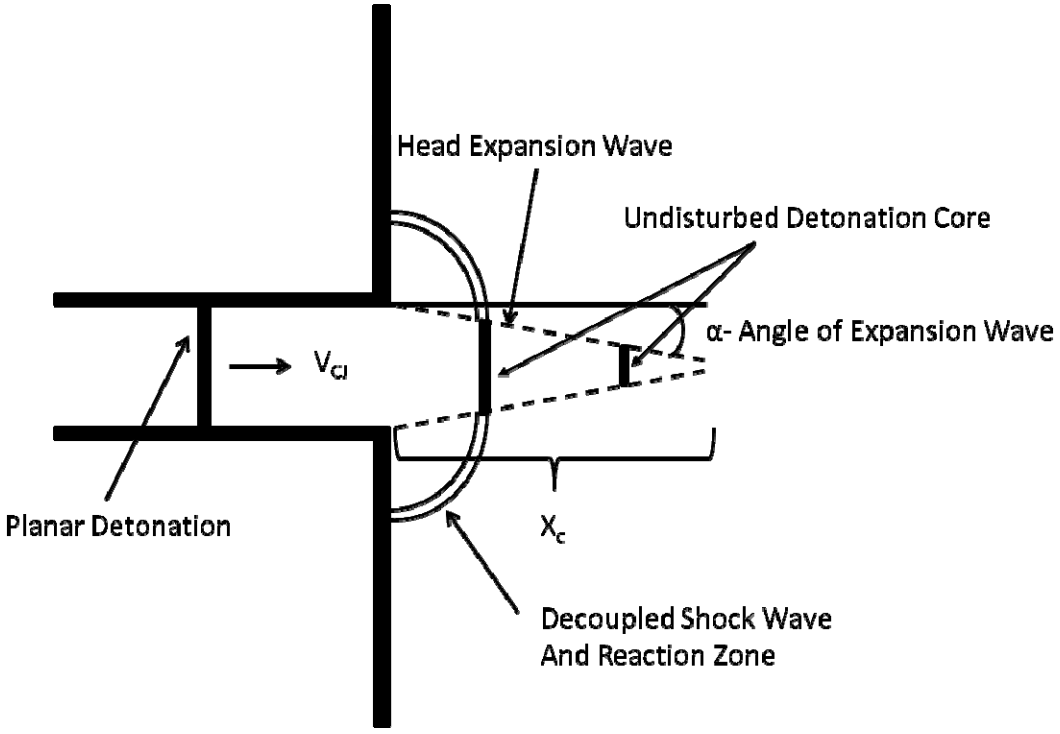

Figure 12 Representation of the detonation diffraction process. The expansion waves responsible for turning the flow propagate towards the center axis and are the reason for the failure of a diffracting detonation.

Summary

This thesis is divided into six chapters. Chapter II is a literature review of the previous work in detonation diffraction into an unconfined volume, detonation diffraction into a confined volume, cylindrical detonations, the deflagration-to-detonation transition process without obstacles and the deflagration-to-detonation transition process with obstacles. Chapter III presents calculations preformed to predict the velocity of a CJ detonation wave, the pressure rise across a CJ detonation wave and the equilibrium detonation cell size of a detonation wave for all four mixtures used in this study. Chapter IV presents an overview of the components of the experimental

facility and the experimental procedure used in the present study. Chapter V presents the results of the study in which critical conditions for successful transmission of a detonation into a confined volume are presented and the results are compared to the results of previous studies. Finally, a summary of the experimental results and conclusions obtained from the experiment is presented in Chapter VI while future recommendations are presented in Chapter VII.

CHAPTER II

LITERATURE REVIEW

Reviews of previous experimental and computational work on detonation diffraction relevant to the present study are reviewed in this chapter. The topics reviewed include detonation diffraction into both confined and unconfined volumes, cylindrical detonations, and the deflagration-to-detonation transition (DDT) process in both smooth and obstacle-filled tubes.

Unconfined Diffraction

When a planar detonation in a cylindrical tube is allowed to diffract into an unconfined volume, the detonation will either fail or successfully transform into a spherical detonation. For many fuel-oxygen-nitrogen mixtures, a relatively simple correlation of $d_c = 13\lambda$ is applicable for determining under what conditions transmission will be successful.

Schultz (2000) presents the timeline for the development of the $d_c \approx 13\lambda$ correlation. Mitrofanov and Soloukhin (1965) were the first to state that $d_c \approx 13\lambda$. However, initially this correlation was developed only for stoichiometric oxy-acetylene. Two important publications that extended the validity of the $d_c \approx 13\lambda$ to all fuel-oxygen-nitrogen mixtures were published by Edwards et al. (1981) and Knystautas et al. (1982). Knystautas et al. (1982) demonstrated the validity of the $d_c \approx 13\lambda$ correlation for mixtures of acetylene, hydrogen, ethylene, and propane with varying degrees of nitrogen dilution while, as Schultz (2000) notes, Edwards et al. (1981) found that for ethane and

propane mixtures, the critical diameter was 14λ, and for methane and acetone mixtures the critical diameter was 18λ. However, the results of Edwards et al. (1981) do not invalidate the global correlation but simply underscore the fact that it is just an approximation. This slight discrepancy is due in large part to the difficulty in obtaining accurate cell size data and the fact that analyzing soot foil records to determine cell size is often subject to interpretation.

An important publication to the present study was published by Matsui and Lee (1978). In this work, correlations for calculating the critical diameter were developed for a variety of fuel-oxygen mixtures over a wide range of initial pressures. While the goal of the study by Matsui and Lee (1978) was simply to develop correlations for the critical diameter for a variety of mixtures and not to validate the $d_c \approx 13\lambda$ correlation, the correlations presented allow for the cell size to be calculated by assuming the $d_c \approx 13\lambda$ is valid. All cell size data used in the present study were calculated from the correlations presented in the Matsui and Lee (1978) publication.

It is important to note that the $d_c \approx 13\lambda$ is only valid for fuel-oxygen or fuel-oxygen-nitrogen mixtures. If the diluent were changed to a monatomic gas, such as helium or argon, the critical diameter will change as well since the diluent affects the cellular regularity.

It is also important to note that the $d_c \approx 13\lambda$ correlation is purely empirical in nature. Achieving a better understanding of the detonation diffraction process into an unconfined volume has been and remains an active area of research. The work of Schultz (2000) was dedicated to developing a critical diffraction model to allow the sub-critical,

critical and super-critical conditions to be determined analytically. Arienti (2002) and Arienti and Shepherd (2005) performed numerical simulations of the detonation diffraction process. Pintgen and Shepherd (2009) have also recently performed experiments investigating the reason for the breakdown of the $d_c \approx 13\lambda$ correlation for mixtures containing a diluent other than nitrogen. The works cited above are only a very small portion of the recent publications in the area of detonation diffraction into an unconfined volume, but a more detailed review is beyond the scope of this work. The reader is encouraged to see the work of Schultz (2000) and Arenti (2002) for a more thorough review of the literature.

Confined Diffraction

While the diffraction of a detonation into an unconfined volume has been widely studied for decades, the diffraction of a detonation into a confined volume has received much less attention. As Schultz (2000) notes in his recommendations "confinement-induced re-initiations are also of scientific and practical interest to study and are directly related to detonation initiation by shock reflection and focusing."

One of the earliest studies which examined detonation diffraction into a confined volume was published by Murray and Lee (1983). This study examined the conditions necessary for the successful transformation of a planar detonation into a cylindrical detonation. Fig. 13 gives the dimensions of the facility used in their study.

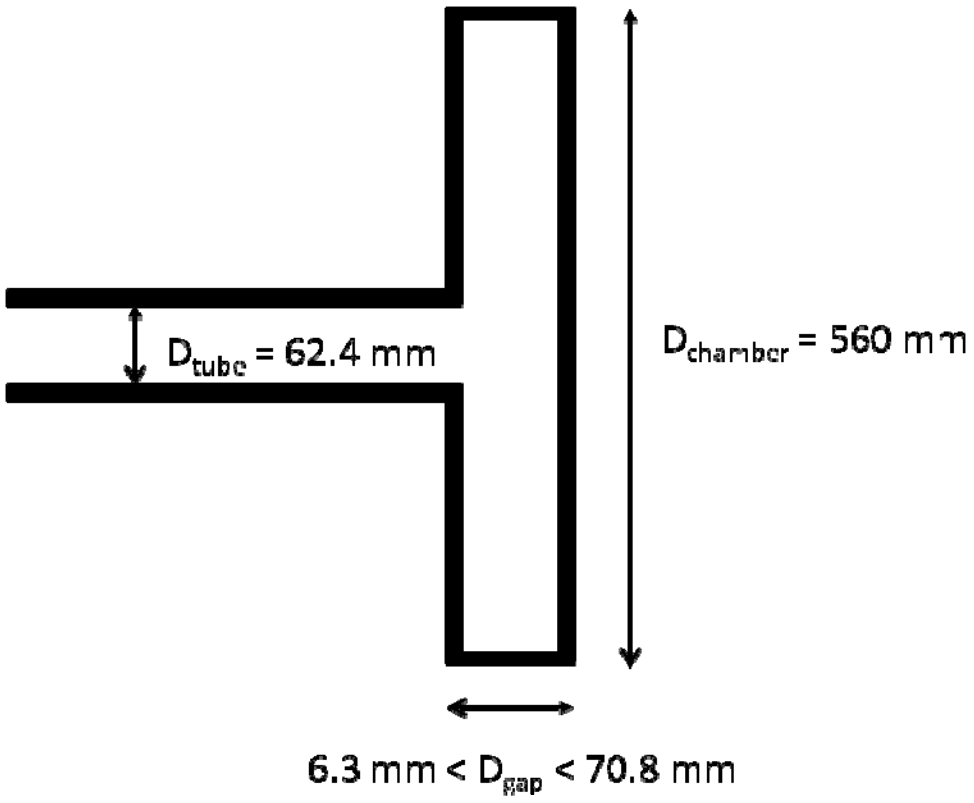

Figure 13 Dimensions of the facility used in the study by Murray and Lee (1983).

Murray and Lee (1983) found that two different modes of re-initiation were responsible for successful transmission of the planar detonation wave and that the gap size, the distance from the exit of the tube to the endwall, was an important parameter. The first mode of re-initiation, called "spontaneous re-initiation", occurred before the diffracted shock wave interacted with the endwall. The second mode of re-initiation, called "reflected re-initiation", occurred after the diffracted shock wave interacted with the endwall. They found that spontaneous re-initiation occurred when the gap size was greater than 11λ, while reflected re-initiation occurred when the gap size was between

5.7 and 11 λ. For gap sizes less than 5.7λ, they found that transmission of the detonation was not possible.

Sorin et al. (2009) performed experiments on detonation diffraction through different geometries. One of the geometries used in their study, called an “inverse tube”, resembled the facility used by Murray and Lee (1983). A schematic of the facility is shown in Fig. 14.

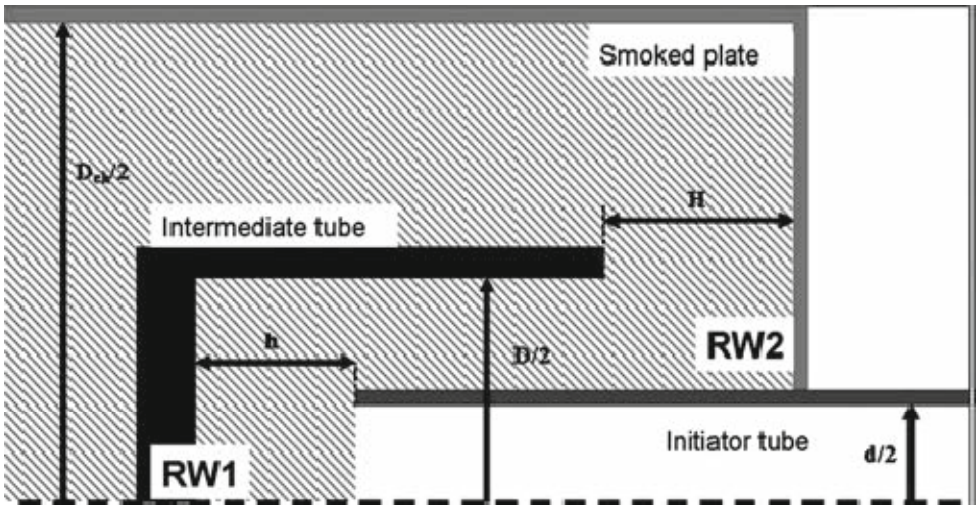

Figure 14 Facility used by Sorin et al. (2009). Figure taken from Sorin et. al. (2009). This geometry, called an "inverse tube", resembles the geometry used by Murray and Lee (1983).

While this geometry is similar to that of Murray and Lee (1983), the Sorin et al. experiment differs from their study because no back wall was present (but an intermediate tube was present). Nevertheless, Sorin et al. (2009) found that interaction with the walls did facilitate successful transmission. It was found that a value of h/d = 1.0 was the optimum condition for re-initiation at the front wall and that, as expected,

transmission was favored for smaller expansion ratios when the lateral wall was close to the tube due to interaction of the diffracted shock with the lateral wall.

Pantow et al. (1996) examined the influence of confinement on the transformation of a smaller planar detonation wave into a larger planar detonation wave. Figure 15 shows a schematic of their facility.

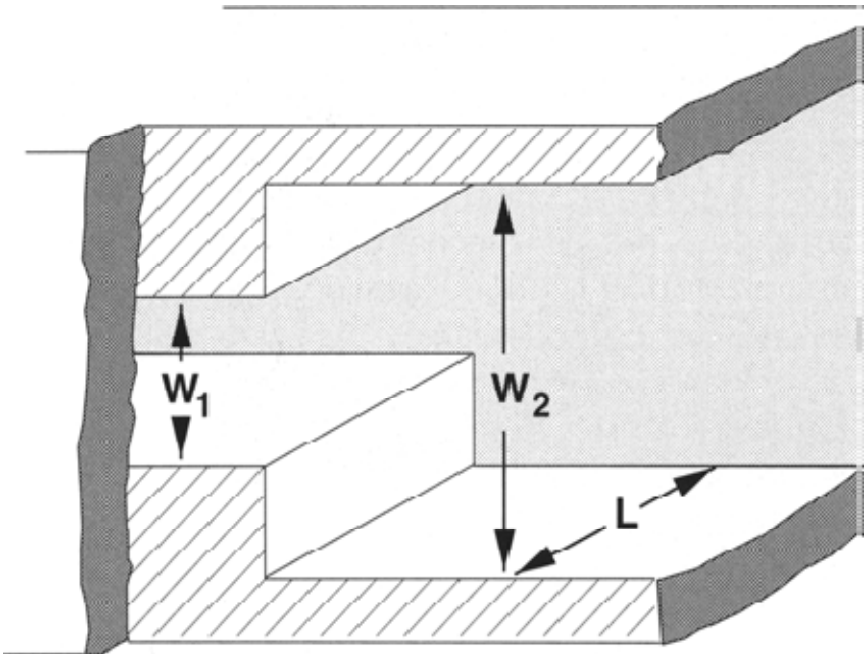

Figure 15 Facility used by Pantow et al. (1996). Figure taken from Pantow et al. (1996). This facility examined the diffraction of a detonation wave from a channel rather than a circular tube.

Pantow et al. (1996) found that the confinement allowed re-initiation to occur under conditions where the detonation would have failed if diffracting into an unconfined space. However, they noted that the "influence of the confining walls after the expansion diminishes with expansion factors (W_2/W_1) larger than five." This

observation makes sense because larger expansion ratios more closely resemble expansion into an unconfined volume. Figure 16 shows results obtained by Pantow et al. (1996) which compares numerical and experimental results.

Teodorczyk et al. (1989) studied the propagation of quasi-detonations, detonations propagating significantly below the CJ speed, in obstacle-filled tubes. They found that as the detonation wave diffracted over an obstacle, initially it began to fail as the shock wave and reaction zone decoupled. However, the detonation wave was re-initiated when the diffracted shock reflected from the tube walls.

Jones et al. (1995) conducted numerical simulations on detonation diffraction which showed that re-initiation of a detonation occurred after the diffracted shock had reflected from the tube walls.

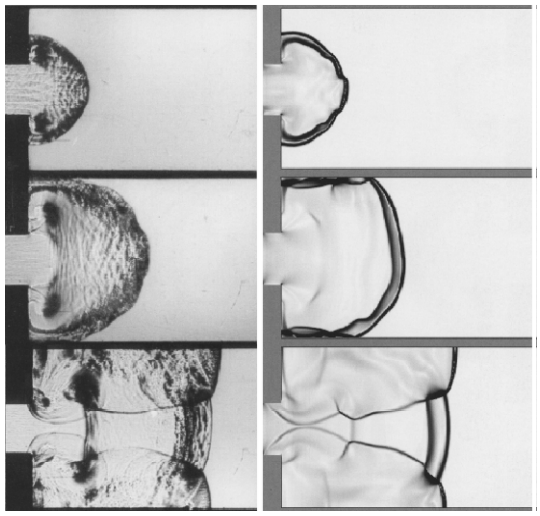

Figure 16 Experimental and numerical schlieren images obtained by Pantow et al. (1996). These images show the detonation is re-initiated by the reflection of the shock wave with the wall.

Ohyagi et al. (2002) showed experimentally that shock reflections from the tube wall allowed successful transmission of detonation waves for conditions which would have resulted in detonation failure if diffracting into an unconfined volume. However, this study also showed that for conditions when d/λ was much less than 13, even the reflected shock was not of sufficient strength to re-initiate the detonation.

Papalexandris et al. (2007) conducted numerical simulations on the diffraction of two-dimensional detonation waves from a smaller channel to a larger channel with varying expansion ratios. They showed that at the critical condition for transmission the reflection of the diffracted shock from the wall provided the mechanism for re-initiation, while for sub-critical conditions the temperatures behind the reflected shock were not high enough to allow the reaction zone and diffracted shock to re-couple. They also showed that the expansion ratio plays an important role in determining the successful or unsuccessful transmission. For example, for the same initial conditions transmission of the detonation may be successful with an expansion ratio of 2 but unsuccessful if the expansion ratio is increased to 3.

Brown and Thomas (2000) conducted experiments in which transition to detonation was initiated by the partial reflection of an incident shock from an obstacle in the tube. The reflection of the shock wave from this obstacle and the subsequent reflections from the walls of the tube produced conditions which resulted in transition to detonation.

Guo et al. (2007) conducted experiments on detonation diffraction into a 90-degree branched channel. Again, the reflection of the diffracted shock wave was important to the re-initiation mechanism in the branched channel.

Wang and Xu (2007) conducted experiments and numerical simulations on the detonation diffraction into a 90-degree branched channel. Their findings were similar to Guo et al. (2007), showing that the interaction of the leading shock wave with the wall was important in the re-initiation process.

The common thread between all studies involving detonation diffraction into a confined volume is that, typically, under conditions where a diffracting detonation would fail in an unconfined volume, the interaction between the diffracted shock wave and confining walls produces conditions where re-initiation of the detonation is possible.

Cylindrical Detonations

Diverging cylindrical detonations are an interesting topic of research, but again there have been relatively few studies which address this topic. The relevant studies which were found are reviewed below.

Lee (2008) on pgs. 189-190 notes that for a diverging cylindrical detonation to move at the CJ speed, transverse waves need to be created as the wave moves radially outward for the "average number of transverse waves per unit length along the circumference of the detonation front" to be constant. Without a sufficiently high production of these new transverse waves, the detonation cells grow bigger until the wave eventually fails.

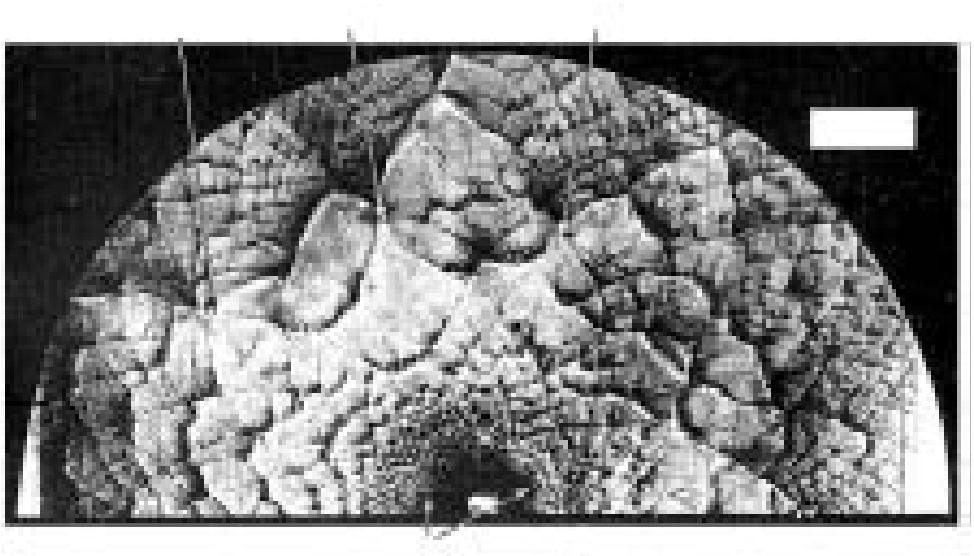

Figure 17 Soot foil record from Vasil'ev and Trotsyuk (2003). This record shows how the detonation cells initially grow in a diverging cylindrical detonation but eventually attain the expected, constant size.

Figure 17 shows a soot foil record of a diverging cylindrical detonation obtained by Vasil'ev and Trotsyuk (2003). This figure shows that the detonation cells do initially grow in size because the production of transverse waves is initially insufficient to sustain a constant cell size. However, near the edges the average cell size is much smaller, indicating that a sufficient number of transverse waves were produced to sustain this detonation. If the production of transverse waves had been insufficient, the cellular structure would have disappeared on the soot foil record.

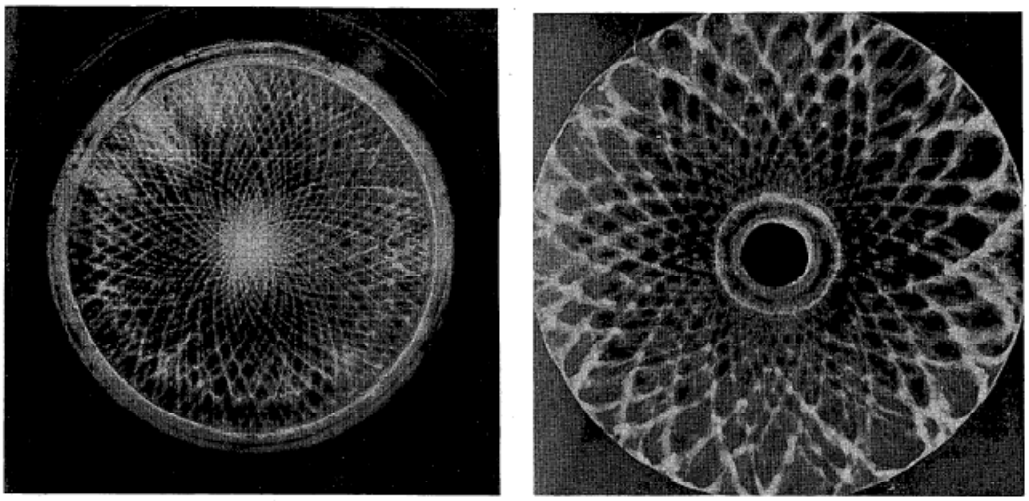

Figure 18 Open-shutter photographs from Guirao et al. (1989) of a successful diverging cylindrical detonation, left, and unsuccessful diverging cylindrical detonation, right.

Guirao et al. (1989) present open-shutter photographs of a self-sustaining cylindrical detonation and a failing cylindrical detonation. Figure 18 shows that detonation cell size remains constant as the wave expands radially outwards for the self-sustaining wave, while the cell size continually grows for the failing wave.

Lee (2008) on pg. 322 also notes that the pressure behind a diverging cylindrical detonation wave is slightly lower than the CJ pressure for a planar detonation wave with the same initial conditions. Lee (2008) on pg. 322 believes that curvature of the wave is most likely explanation for this phenomenon. This phenomenon was observed experimentally during the present study, as shown later.

DDT Without Obstacles

Finally, a brief overview of previous work on the DDT process is given below. Because a detonation was formed through this process in the current study, understanding the mechanics behind the DDT process was extremely important.

There are two mechanisms through which a detonation can be formed: direct initiation or a deflagration-to-detonation transition (DDT). Direct initiation of a detonation requires an initiator source with a high energy such as a high-powered spark, laser, or explosive. DDT, on the other hand, typically occurs after a combustible mixture is ignited using a weak ignition source, such as a glow plug or weak spark, and the as the resulting deflagration moves down a tube it accelerates and eventually suddenly transitions to a detonation.

The ignition source for the current study was a glow plug, and therefore understanding and minimizing the DDT length for test mixtures with initial pressures as low as 20 torr was crucial for the experiment.

First, the time and distance a deflagration must travel prior to transitioning into a detonation is affected by a number of factors. The most important factor is whether or not the space in which the detonation is propagating is filled with obstacles, such as orifice plates, or not.

There have been numerous studies on the DDT induction length in tubes without obstacles. Kuznetsov et al. (2005) notes that the tube diameter, initial pressure and temperature also all affect the DDT transition length in tubes without obstacles. Generally, the induction distance increases with increasing tube diameter and decreasing

initial pressure. Ciccarelli and Dorofeev (2008) also note that the wall roughness and mixture composition affect the DDT transition length in tubes without obstacles. Generally, induction distance increases with decreasing wall roughness. This is because the roughness of the wall aids in the acceleration of the flame due to its effect on the growth of the boundary layer. Ciccarelli and Dorofeev (2008) also provide equations to calculate run up distances for a variety of mixtures. Their calculations showed that run-up distances were strongly dependent on mixture composition due to the differences in mixture properties such as laminar flame velocity, laminar flame thickness, and kinematic viscosity.

The effect of tube diameter on the induction distance has been studied by Li et al. (2006), Bollinger and Edse (1959) and Baumann et al. (1961). All found that generally the induction distance increases with increasing tube diameter; although Bollinger and Edse (1959) note that the induction distance may increase with decreasing tube diameter for extremely small tubes due to wall quenching effects.

Finally, the effect of initial pressure on induction distance has been widely studied. A few of the studies, all of which show that detonation induction distance increases with decreasing initial pressure, were conducted by Bollinger (1964), Kuznetsov et al. (2005), Liberman et al. (2009) and Wang et al. (2000).

DDT With Obstacles

Because the physical size of a device, such as a pulse detonation engine or a laboratory experiment, is typically limited it can be beneficial to minimize the DDT

induction length. To minimize the detonation induction distance, obstacles such as an orifice plate or a Shchelkin spiral can be placed in the path of the flame to promote acceleration and subsequent transition to detonation. When obstacles are present, the blockage ratio (BR), shown in Eq. (16), and distance between obstacles have been found to be the most important parameters. Results from a few relevant studies are given below.

$$1 - (d/D)^2 \tag{16}$$

Generally, the results from studies utilizing obstacles to maximize flame acceleration and minimize the DDT length show that there is an optimum blockage ratio and obstacle spacing, shown by the results of the following studies. Peraldi et al. (1986) used blockage ratios of 0.43, 0.39 and 0.43 for 5-cm, 15-cm and 30-cm tubes, respectively, with an obstacle spacing of one tube diameter. These blockage ratios and this obstacle spacing were chosen based on the results of previous studies which suggested that these conditions provided maximum flame acceleration and highest terminal flame speeds. Lee et al. (2004) noted that "blockage ratios between 0.3 and 0.6 and sufficient obstacle spacing" were optimum for reducing the DDT induction length. Ciccarelli et al. (2005) found that for a BR of 0.43 the obstacle spacing had little effect on the flame acceleration, while for higher BRs the obstacle spacing had a significant effect on the flame acceleration. He also notes that the optimum obstacle spacing is one tube diameter.

CHAPTER III

CALCULATIONS

CJ Velocity and Pressure

The velocity of and pressure rise across a Chapman-Jouguet wave are unique to each mixture. These parameters can be calculated by hand using the method outlined in the Introduction or using the Shock and Detonation Toolbox, a computer program which can be downloaded from the website of Dr. Shepherd's research group at the California Institute of Technology. This software allows the detonation wave speed and pressure rise across the wave, as well as many other variables, to be calculated if the mixture composition, initial fill pressure and initial temperature are specified.

The results for the wave speed and pressure rise across a CJ detonation wave are plotted in Figs. 19-20 for the four different mixtures studied in the current study over a range of initial fill pressures with an initial temperature of 293 K. It is interesting to note that out of the four test mixtures shown, the wave speed for stoichiometric hydrogen-oxygen is the highest but has the smallest pressure rise.

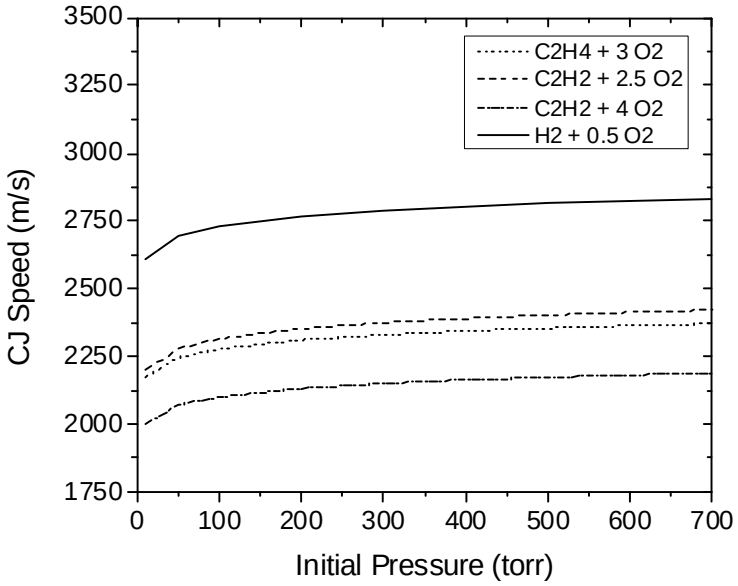

Figure 19 CJ velocity for four different mixtures used in the current study. The CJ velocity is a weak function of initial fill pressure.

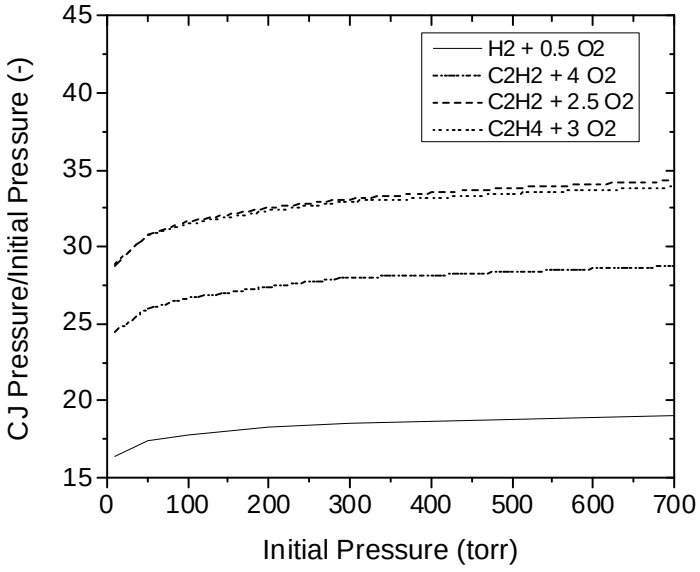

Figure 20 Pressure rise across a CJ wave for four different mixtures used in the current study. The pressure rise is a weak function of initial fill pressure.

Detonation Cell Size

Another important property of a mixture to this study was the detonation cell size. The detonation cell size is a function of both mixture and initial fill pressure. As noted by Schultz (2000) on pg. 3 of his thesis, when the cell size is manually sampled the minimum and maximum sizes "observed typically deviate from the average by +/- 50%." Shepherd (2009) also notes that the "value of cell size measurements is ultimately limited due to the lack of precision (a range of 50-100% is not uncommon)."

For the current study, direct measurement of the cell size over the entire range of experimental conditions for all mixtures was not feasible. However, because Murray and Lee (1983) had shown that the cell size was an extremely important parameter for detonation propagation into confined volumes, a way for calculating the cell size for all experimental conditions was needed. Thankfully, data from a previous study by Matsui and Lee (1978) were available and could be used to calculate the theoretical cell size for every experimental condition of interest herein.

In the study, Matsui and Lee (1978) performed experiments for a variety of mixtures and tube diameters, over a wide range of initial fill pressures to determine the critical diameter for transmission of a detonation into an unconfined volume. From these experiments, empirical correlations were developed to predict the critical initial pressure for transmission into an unconfined volume and were given in the form of Eq. (17), where P_c is given in torr and d_c is given in cm.

$$P_C = K*d_c^{-\alpha} \qquad (17)$$

Equation 17 can be rearranged into a more useful form for calculating the cell size, shown in Eq. (18).

$$\lambda = ((K/P_C)^{1/\alpha})/13 \quad (18)$$

To be able to directly solve for the cell size for a given mixture and initial pressure, the values of K and α are needed. The values of these constants were calculated by Mastui and Lee (1979), and their values for the four mixtures used in this study are given in Table 1.

Table 1 Coefficients for empirical relation developed by Mastui and Lee (1979) shown in Eq. (18). These correlations allow the cell size for a mixture to be calculated at a specified initial pressure

Mixture	**K**	**α**
$H_2 + 0.5\ O_2$	1452	0.928
$C_2H_2 + 4\ O_2$	287	0.884
$C_2H_2 + 2.5\ O_2$	127	0.882
$C_2H_4 + 3\ O_2$	508	0.918

The calculated cell sizes using the correlations of Matsui and Lee (1978) are shown in Fig. 21.

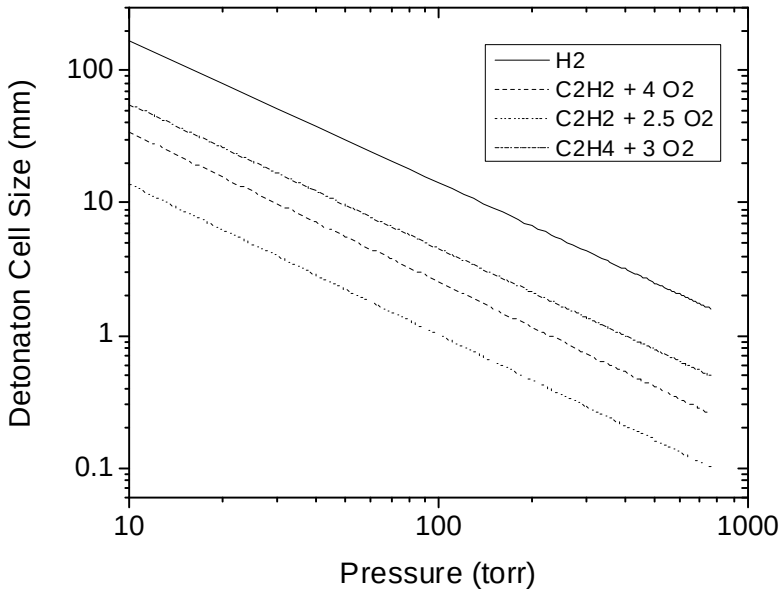

Figure 21 Calculated cell size based on the empirical correlations developed by Matsui and Lee (1978).

CHAPTER IV

EXPERIMENTAL

The facility used for this experiment was built from the ground up. The only exceptions to this statement are the mixing tank and manifold, which were already parts of the existing infrastructure in the laboratory. The important components of the facility are the detonation tube, ignition flange, expansion volume endwall, expansion volume back wall, expansion wall spacers, mixing tank, manifold, DAQ system, pressure diagnostics, and experimental stand. A more-detailed description of each of these components as well as an overview of the soot foil technique and experimental procedure are given in this chapter. A photograph of the overall facility is shown in Fig. 22**.** Drawings of the facility components are also given in Appendix F.

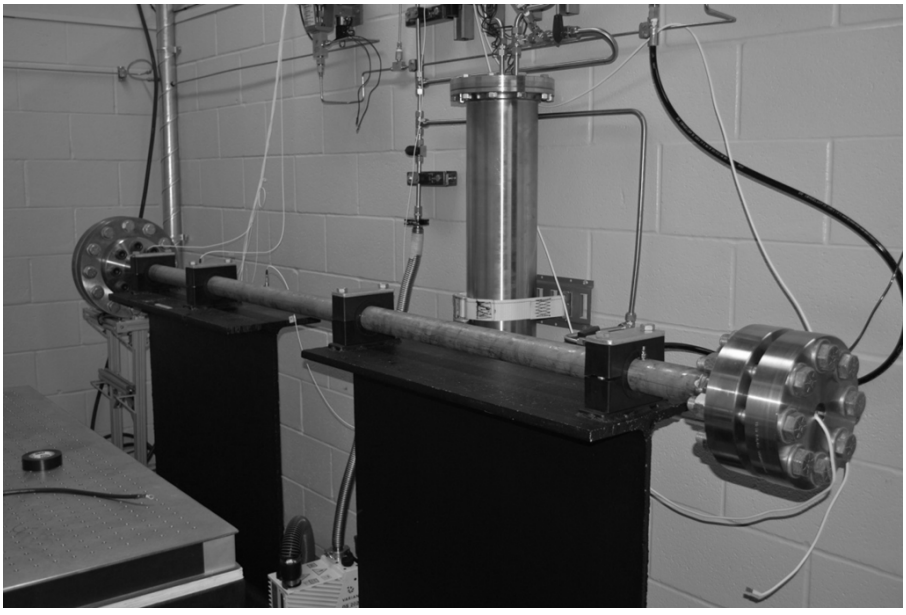

Figure 22 Photograph of detonation tube at TAMU with expansion volume attached (in background).

Detonation Tube

The detonation tube used in the current study was 2.75 m long with an ID of 3.8 cm and a wall thickness of 1.1 cm; it was constructed out of 304 stainless steel.

Expansion Volume

The goal of this thesis was to study detonation diffraction into a confined volume. To accomplish this goal, a confined volume, of adjustable width, was constructed and mounted to the end of the detonation tube.

The confined volume consists of multiple pieces: the endwall, back wall, and various spacers. Both the endwall and back wall of the expansion volume are made of 17-4 PH steel, 5 cm thick, and heat treated to condition H900. A cutaway view of the assembled expansion volume is shown in Fig. 23.

A 1-mm gap was machined into the endwall which provided the minimum gap spacing. In addition to this gap, four separate spacers could also be added to the experimental setup to change the gap spacing to the desired width. Two of the spacers, with widths of 12.7 mm and 25.4 mm, were made of 17-4 PH steel heat treated to condition H900. The other two spacers, with widths of 3.175 mm and 6.35 mm, were machined by Miles Egbert out of 6061-T6 aluminum in the Turbomachinery Laboratory machine shop.

To increase the number of gap sizes which could be achieved, o-ring grooves were machined into the spacers with widths of 25.4 mm and 6.35 mm. These o-ring

grooves allowed multiple spacers to be utilized during an experiment while still maintaining vacuum integrity of the vessel.

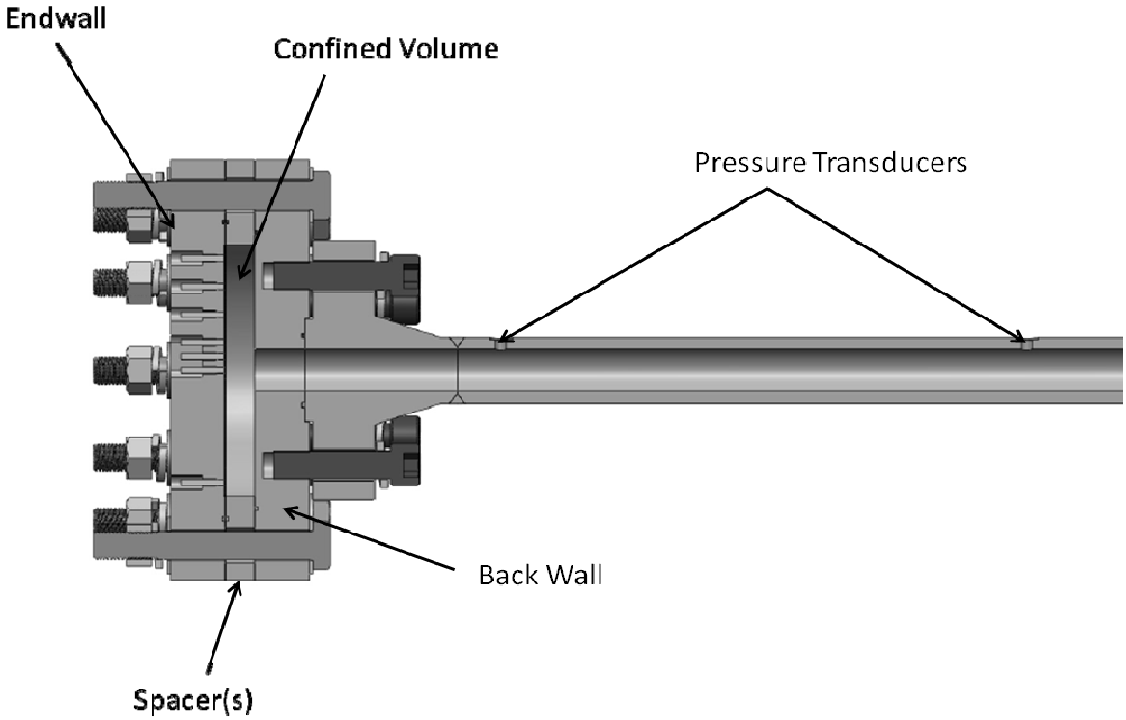

Figure 23 Cutaway of expansion volume and detonation tube. The size of the confined volume can be adjusted by adjusting the size of the spacers used.

Facility Capabilities

The capability of the facility is limited by the maximum test pressures which could be seen during a test. The maximum test pressure is a function of mixture composition, initial fill pressure and degree of overdrive. Also, Shepherd (1992) also notes that because of rapid application of the load a dynamic load factor, which converts the dynamic load into an equivalent static load, also needs to be taken into account.

However, for the quasi-static regime, where this facility should operate, the dynamic load factor is simply two.

For a CJ detonation wave the pressure behind an incident wave is typically between 15-35 times the initial pressure of the mixture, while the pressure behind a reflected CJ detonation is 2.4-2.5 times than the pressure behind an incident wave.

However, the potential for extremely high overpressures is possible when generating a detonation through a deflagration-to-detonation transition. These high overpressures are observed when the DDT event occurs very near to the endwall of the detonation tube. Because the detonation wave formed through the DDT event is initially overdriven, upon reflection extremely high pressures can be observed. Numerous studies, including those by Craven and Grieg (1968), Chan and Dewitt (1996), Dorofeev et al. (1996), Zhang et al. (1998) and Shepherd (1992), have investigated this phenomenon. This scenario represents a worst-case scenario and, while possible, is rarely accidentally observed. However, when this scenario does occur, the possibility for overpressures of 500 times the initial pressure is possible. Therefore, even though this scenario is unlikely, the experimental fill pressures should be limited so that the detonation tube will not fail even under this scenario.

For the detonation tube, Lame's equations for stress in a thick walled tube were used to calculate the maximum allowable pressure. Using these equations, the calculated yielding pressure of the detonation tube is approximately 850 bar and the calculated bursting pressure is 2000 bar. If the maximum allowable stress is taken to be one-half the yielding stress the static working pressure is 425 bar. Applying the dynamic load

factor means that the maximum test pressure should be limited to approximately 212.5 bar.

As previously noted, the expansion volume was made of 17-4 PH steel heat treated to condition H900 and 5.1 cm thick. At this condition the yield strength is 1227 MPa, the ultimate strength is 1386 MPa and the value of K_{IC} is 80 MPa-$m^{1/2}$.

Following the example of Shepherd (1992), the allowable pressure can be computed using the following equation, where S is the allowable stress, r_b is the bolt circle radius, t is the thickness of the endplate and C is 0.162.

$$\Delta P = (t/2r_b)^2(S/C) \tag{19}$$

It should be noted that the equation above assumes a constant pressure across the entire endplate, which is unlikely in the current experimental setup. However, assuming the pressure behind a reflected detonation exists across the entire cross section of the endplate represents a worst-case scenario for the current experimental setup.

Two different maximum allowable stresses can be defined. The first can be taken as one-half the yield strength, which is 613.5 MPa. The second can be calculated by using the leak-before-break criterion, which says that a crack can grow to a size larger than the thickness of a vessel before catastrophic failure occurs. A simple formula for the critical crack size is given in Eq. (20).

$$\sigma < K_{IC}/\sqrt{\pi a_c} \tag{20}$$

Solving Eq. (20) gives a maximum allowable stress of approximately 200 MPa. This value is less than the 613.5 MPa based on the yield strength, and therefore should be used as the maximum allowable stress.

If the maximum allowable working stress is assumed to be 100 MPa, one-half the maximum allowable stress, the resulting maximum allowable pressure is calculated to be 126 bar.

Finally, the limiting value for initial fill pressures can now be calculated based on the maximum allowable test pressure of 126 bar. As noted earlier, the highest test pressure occurs behind a reflected detonation and the value of this pressure depends on the mixture composition but is typically 37.5-87.5 times the initial fill pressure. Therefore, the maximum initial fill pressure for this facility should be between 1.4 and 3.4 bar depending upon the mixture composition.

However, for the current study the maximum initial fill pressure was around 0.5 bar and typical initial fill pressures were less than 0.2 bar. These fill pressures resulted in typical test pressures around 5 bar and a maximum test pressure of approximately 30 bar. The initial fill pressures were dictated by the cell size of the mixtures used and not the capability of the facility.

Mounting

The detonation tube was mounted to two steel I-beams using four Hydac pipe clamps, model HRES5S60, which were welded to the I-beams. These clamps contained rubber inserts which helped to securely hold the detonation tube in place during an

experiment. In addition to serving as a stand and elevating the detonation tube so that making experimental changes, such as changing spacers, was convenient, the I-beams also acted as an inertial mass for the experiment.

Ignition Source

The ignition source used for this set of experiments was an AC Delco 60G glow plug. Figure 24 shows that the glow plug protrudes only slightly through the ignition flange into the tube, where the combustible mixture is located. Using this ignition source, mixtures with initial pressures as low as 20 torr were able to be ignited. Typically, ignition was within 10-15 seconds once power was supplied to the glow plug, however, for mixtures near the 20-torr ignition limit power was supplied for up to 30 seconds to achieve ignition. For pressures under 20 torr it was not possible to achieve ignition.

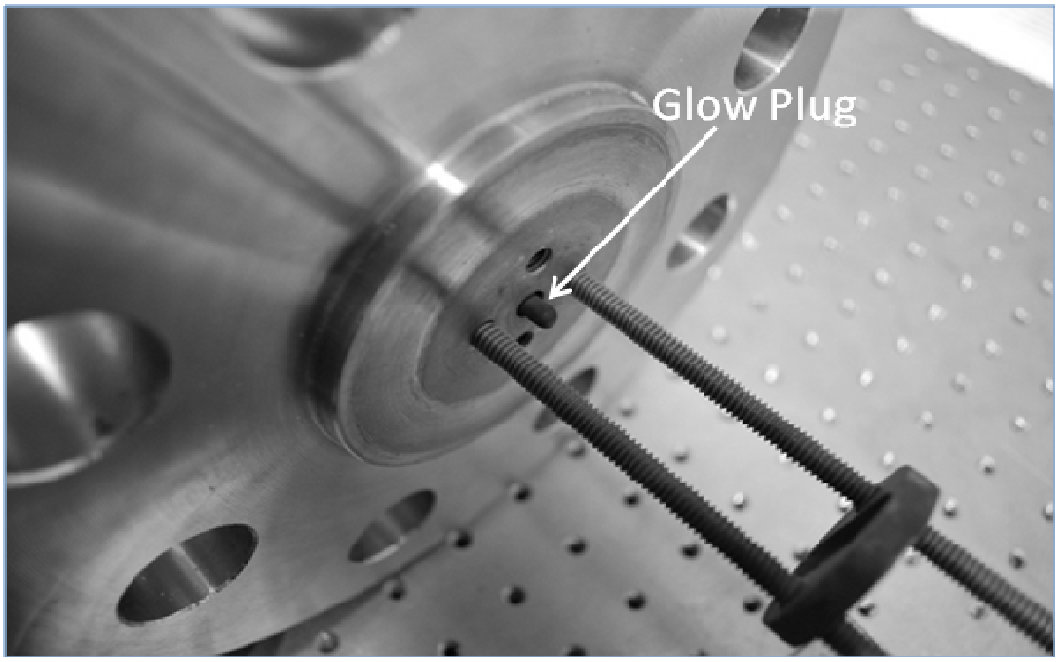

Figure 24 Photo of ignition flange, inside view. The end of the glow plug protrudes slightly into the tube and is responsible for initiating combustion.

Obstacles

As previously noted, the use of a glow plug as the ignition source meant that a detonation would need to be achieved though the DDT process. As mentioned in the Literature Review, the detonation induction length is a strong function of initial fill pressure. For the current study, typical initial fill pressures varied from 0.03 bar to approximately 0.5 bar. While data on the induction distance at sub-atmospheric conditions is limited, Bollinger (1964) and Kuznetsov et al. (2005) both reported induction distances for stoichiometric hydrogen-oxygen to be approximately 5 meters at an initial fill pressure of 0.2 bar. Ciccarelli and Dorofeev (2008) also showed that the detonation induction distances for stoichiometric hydrogen-air mixtures were significantly less than those for other hydrocarbons such as ethylene.

Therefore, because the length of the tube used in this study was limited to 2.75 m, it was clear that to achieve reliable CJ detonations at such low initial fill pressures, obstacles would be necessary.

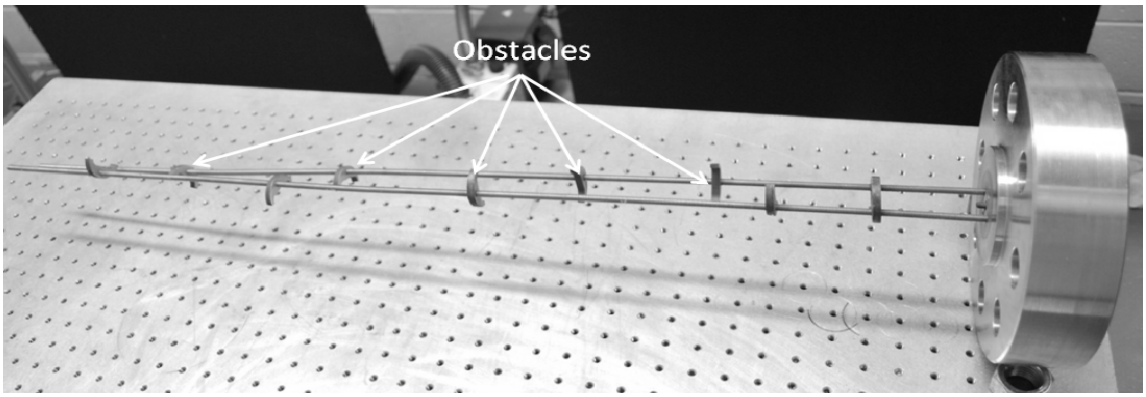

Figure 25 Obstacles used to promote DDT. The obstacles were held in place by two threaded, steel rods.

The obstacles used were steel washers of a slightly smaller diameter than the inside of the tube with a blockage ratio of approximately 0.41. This blockage ratio was chosen because it is close to the ideal blockage ratio cited by Peraldi et al. (1986). As seen in Fig. 25**,** there were a total of nine obstacles along the length of the tube spaced approximately one-to-three tube diameters apart from one another. Ciccarelli et al. (2005) found that for blockage ratios of 0.43 the obstacle spacing had little effect on flame acceleration. Because the goal of this research was not concerned with the DDT transition itself, but only required a CJ detonation wave be obtained prior to the end of the detonation tube, the placement or shape of the obstacles was not varied because this obstacle configuration was proven effective.

Manifold

As mentioned previously, the mixing manifold used for this study was already a part of the existing infrastructure in the laboratory. Figure 26 shows a photograph of the manifold used to make mixtures and vacuum or fill the detonation tube while Fig. 27 shows a schematic of the valve configuration which allowed the detonation tube to be filled, vacuumed or sealed.

Figure 26 Photo of the mixing manifold outside of the blast wall.

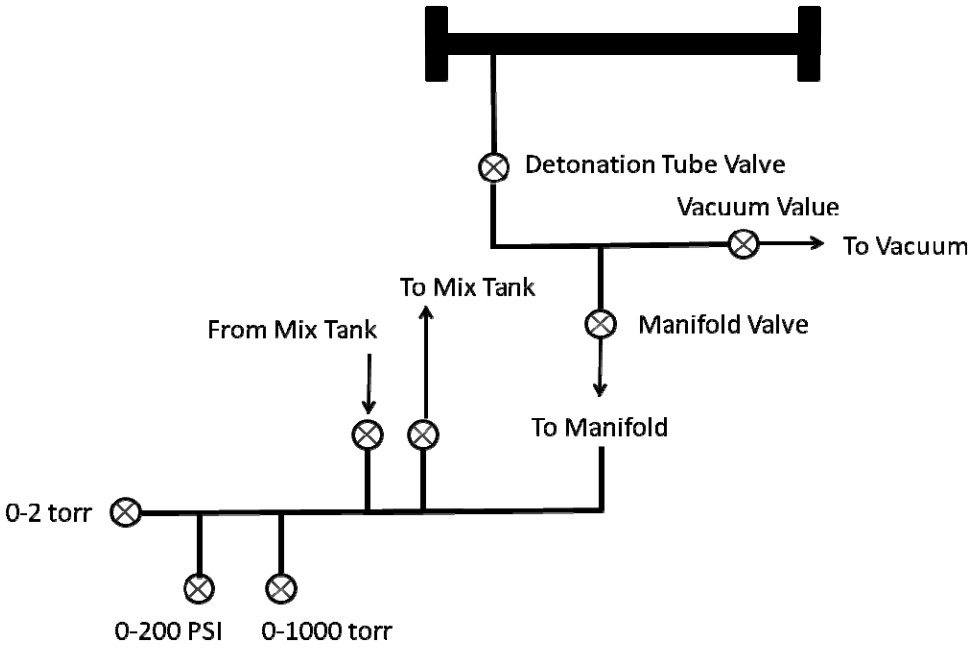

Figure 27 Simple schematic of the valve configuration for the detonation tube.

Diagnostics

Pressure transducers were the primary diagnostic in this experiment. Ports for up to thirteen pressure transducers were available for measurement. Eight transducers were mounted in the expansion volume and labeled E1-E8**,** as shown in Fig. 28. These transducers were used to monitor the propagation of the detonation wave in the expansion volume after diffraction and determine whether or not transmission of the detonation was successful. The other five ports were located along the length of the tube and labeled T1-T5, as shown in Fig. 29**.** These transducers were used to obtain the speed of the detonation wave in the main run-up tube prior to diffraction to verify that it was propagating at the CJ velocity.

The pressure transducers were PCB Model 113B22 piezoelectric units. They were flush mounted in both the detonation tube and expansion volume. The transducers had a measurement range of 34.475 MPa and a rise time of less than 1 μs. Because the temperatures behind a detonation wave propagating through a fuel-oxidizer mixture are extremely high, the pressure transducers were insulated from the thermal shock by a single layer of black electrical tape. This shield needed to be replaced often as older tape negatively impacted the quality of the pressure traces obtained during an experiment.

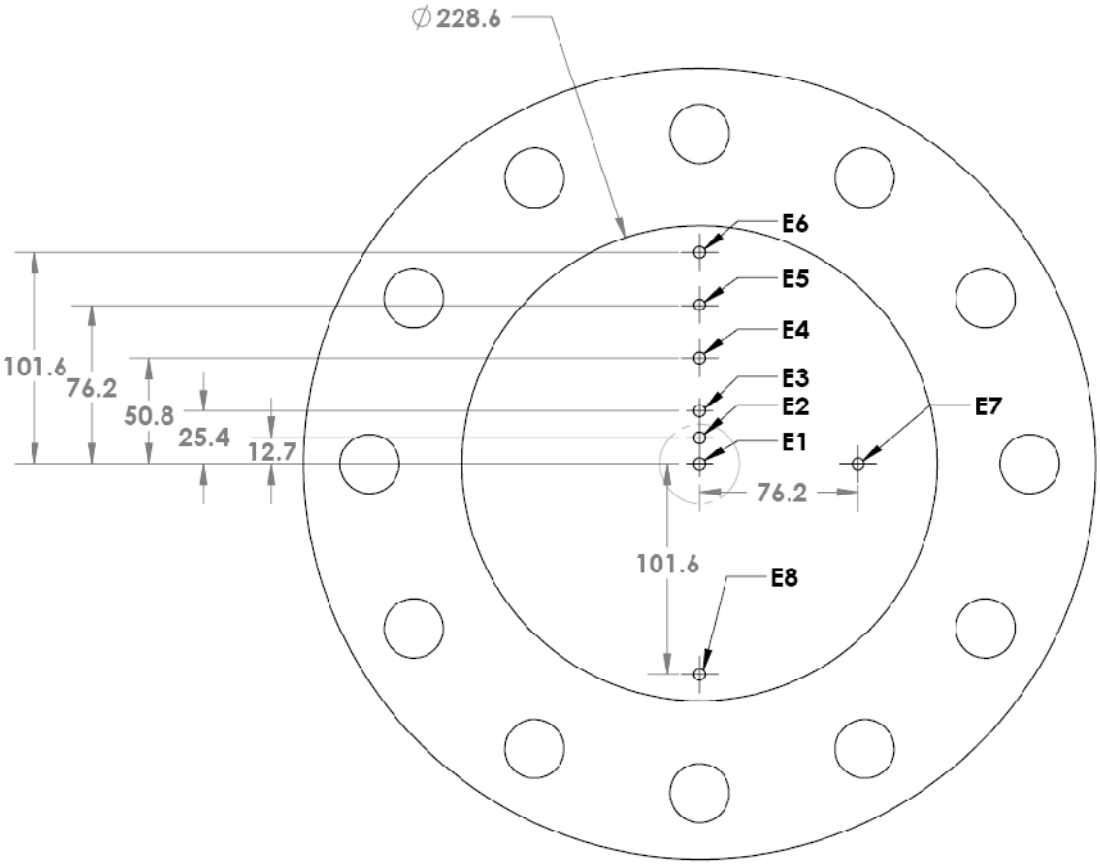

Figure 28 Positions of pressure sensors in expansion volume. Dimensions are in mm.

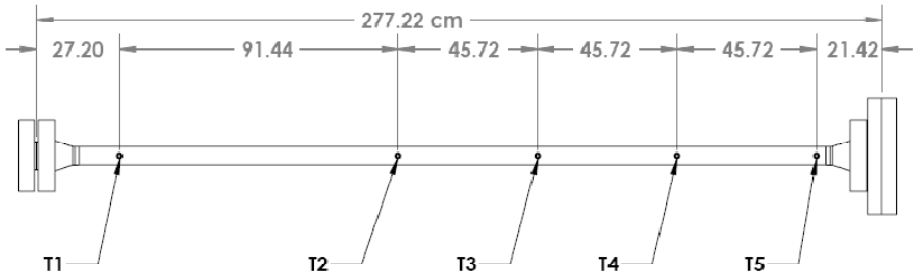

Figure 29 Positions of pressure sensors on detonation tube. Dimensions are in cm.

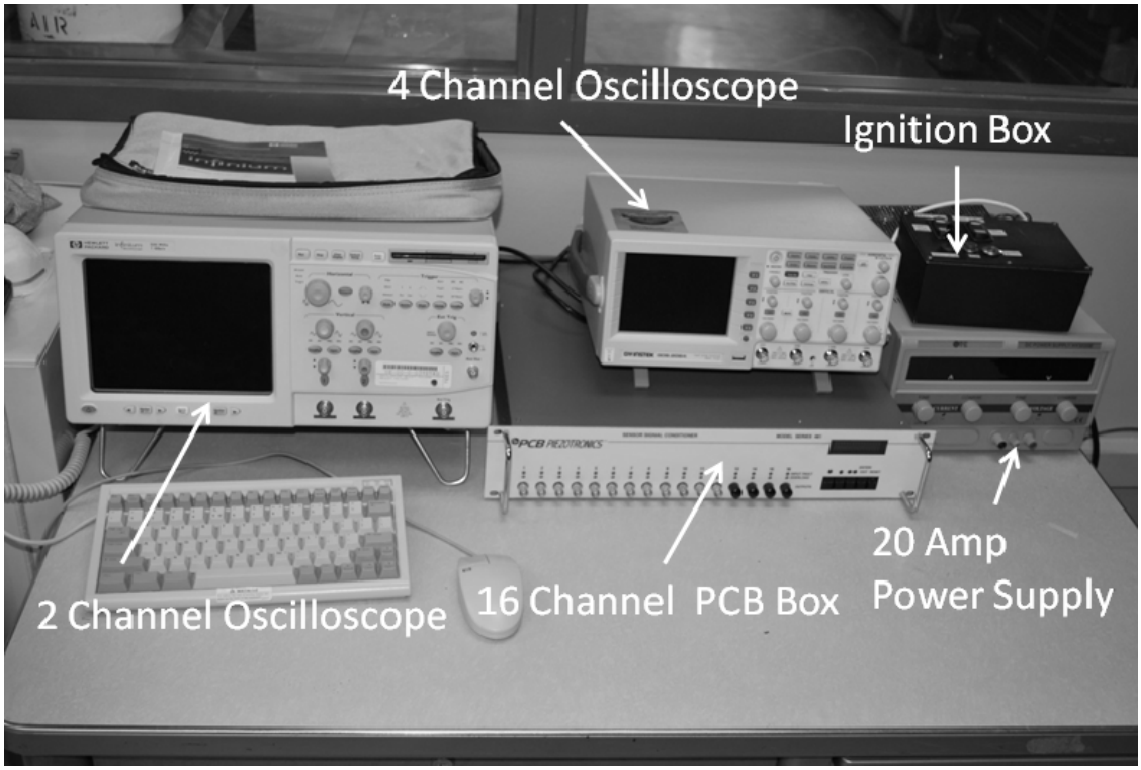

Figure 30 Components of DAQ system in the control room. Six pressure signals were collected each experiment, and all data were collected remotely.

To record the data during each experiment, two different oscilloscopes were used, which can be seen in Fig. 30. The first was a 4-channel oscilloscope, model GDS-2064. This oscilloscope had the capability to record up to 5000 pts/channel, 8 bits of vertical resolution and was used at a sampling rate of 1 MS/s. Typically, the transducers E1, E4, E5, and E6 were recorded using this oscilloscope. The second oscilloscope was a 2-channel HP Infinium Oscilloscope which had the ability to record up to 25000 pts/channel and was also used at a sampling rate of 1 MS/s. Typically, transducers T4 and T5 on the tube were recorded using this oscilloscope.

Soot Foil Technique

In addition to the pressure data obtained from each experiment, soot foils were used as a secondary diagnostic on select experiments. As mentioned in the Introduction, a soot foil is a metal or plastic sheet which is evenly coated with a fine layer of soot which allows the structure of the detonation wave to be visualized.

The method for producing high-quality soot foils was a trial-and-error process. The method of applying the soot to the foil and the type of material the foil was made out of were varied until the ideal combination was determined. Specifically, three different methods of coating the foil with soot and two different types of aluminum were used to identify the most effective method and material. A publication by Lam et al. (2003) and communications with Professor Joanna Austin of the University of Illinois Urbana-Champaign Aerospace Engineering Department (2010) were also extremely helpful in improving the technique.

First, two types of 0.02-in aluminum sheet, Alloy 1100 and Alloy 3003, were used to produce soot foils. However, only Alloy 3003 produced acceptable results. When Alloy 1100 was used, the results were extremely poor and nearly unreadable. All records in Appendix B are on 0.02-in, 3003 aluminum.

However, even when Alloy 3003 was used the method by which the soot was applied greatly affected the results. The first method attempted involved holding an aluminum sheet over an oxyacetylene torch which was run extremely rich. However, this method produced extremely thick, non-uniform coatings of soot which was not ideal, and this method was quickly abandoned.

In the second method, a kerosene-soaked rag was lit and a funnel, seen in Fig. 31, was then placed over the burning rag. The aluminum sheet was then held above the opening of the funnel and manually moved until a sufficient coating of soot was deposited onto the sheet. This method produced results which varied from experiment to experiment and were highly unpredictable. An important observation, and possible reason for the unpredictable results, was the fact that the soot deposited on the aluminum sheet could not be easily removed once applied.

Figure 31 Second method attempted to create high-quality soot foils. This method did not yield repeatable results.

The final, and most effective, method used the chimney shown in Fig. 32. A small kerosene rag, approximately 2-3 in^2, was lit, and the chimney was placed over the rag. The foil was then laid on top of the chimney, as shown in Fig. 33, and left until the fire was extinguished which typically took less than 30 seconds. This method produced a fine, uniform coating of soot which was easily wiped away with even slight contact. The foils produced using this method produced the highest-quality results and were extremely repeatable. This method was used for all runs after Run 266.

Figure 32 Chimney used in final method to produce soot foils. This method produced high-quality, repeatable results.

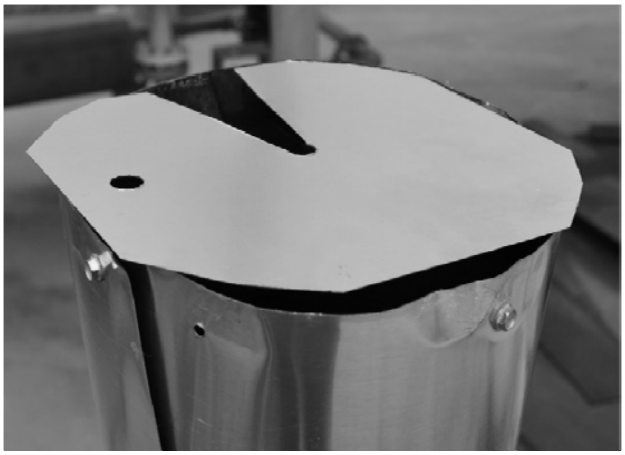

Figure 33 Close-up view of soot foil placed at top of chimney. The underside of the soot foil was evenly coated with soot after a small kerosene-soaked rag was burned.

Experimental Procedure

The same experimental procedure was followed for all experiments. The procedure was designed to allow repeatable data to be achieved as well as to ensure that the experiment was carried out safely. Fig. 27 can be referenced for valve locations.

First, the necessary spacer was installed to create an expansion volume with the desired gap size. After installing the necessary spacer, the detonation tube was then evacuated to at least 0.2 Torr, but typically the final pressure was less than 0.1 Torr. When evacuating the detonation tube the detonation tube, manifold and vacuum valves were all open.

After the tube had been evacuated, it was then filled to the desired initial fill pressure. When filling the tube the detonation tube and manifold valves as well as the valve from the mix tank were open while the valve to the vacuum was closed. If the initial fill pressure was higher than 70 torr, the tube was sealed and the fill lines between the tube and mix tank were evacuated. This was done to prevent the detonation from being able to propagate through the manifold should the valve sealing the detonation tube fail. The fill lines were evacuated by first closing the detonation tube valve and valve from the mix tank and then opening the vacuum valve.

However, if the test were conducted at very low initial fill pressures of less than 70 torr, the entire tube was evacuated to less than 0.2 Torr for a second time after the initial fill. The tube was then filled again to 70 torr before finally being evacuated to the desired initial fill pressure. This procedure was similar to the procedure followed by Murray and Lee (1983). It helped to ensure that prior to a test there was a high degree of

confidence in the composition of the test mixture. Ideally, by filling the detonation tube with the test mixture to 70 torr, evacuating it and then refilling the detonation tube again with the test mixture the majority of the 0.2-torr of residual gas should have the same composition as the test mixture.

After the detonation tube was filled to the desired initial pressure and sealed, the door to the blast room was sealed and everyone in the lab was notified that a test was being conducted. For any tests with potentially high pressures, the lab was emptied prior to an experiment.

Finally, the DAQ system was armed and the ignition switch, which delivered power to the glow plug, was pressed. However, to ensure that the glow plug could not be activated accidentally, a key, which activated a red LED light, needed to be turned to complete the circuit.

As previously mentioned, ignition typically occurred within 10-15 seconds after initiating the glow plug. However, at lower fill pressures ignition could take as long as 30 seconds. After the test was complete, the detonation tube was evacuated using a vacuum pump until at least 0.2 torr prior to the next test.

Mixture Uncertainty

Finally, having confidence in the mixture composition was extremely important for this study and the extreme care was taken when making the mixtures to ensure that the mixture composition was known. Because the mixtures used in this study were pure fuel-oxygen, mixtures were typically made only to 25 psi for safety.

Each mixture was made using the method of partial pressures and two different pressure transducers were used during the procedure. The first was an MKS Type 626 pressure transducer with a range of 0-1000 torr which was accurate to within 0.1 torr while the second transducer was a Sentra Model 255 0-200 psi gauge which was accurate to within 0.1 psi. For the highest degree of accuracy, the pressure of the constituent with the lowest mole fraction was measured using the MKS gauge while the pressure of the final constituent was measured using the Sentra gauge.

Table 2 below shows the relative uncertainty in mixture composition for all four mixtures assuming a final mixture pressure of 25 psi. The maximum Φ would occur if the maximum amount of fuel and minimum amount of oxygen were added while the minimum Φ would occur if the maximum amount of oxygen and minimum amount of fuel were added. For example, to calculate the maximum Φ for an H2 + 0.5 O2 mixture it was assumed that the mixture was composed of 430.7 torr of oxygen and 16.8 psi of hydrogen.

Table 2 Uncertainty in mixture composition made in mixing tank

Mixture	P_{fuel}	P_{O2}	Ideal φ	Max φ	Max φ % Error	Min φ	Min φ % Error
H_2 + 0.5 O_2	16.7 psi	430.8 torr	1	1.006	+/- 0.006 %	0.994	+/- 0.006 %
C_2H_2 + 2.5 O_2	369.3 torr	17.9 psi	1	1.006	+/- 0.006 %	0.994	+/- 0.006 %
C_2H_2 + 4 O_2	323.1 torr	18.8 psi	0.625	0.622	+/- 0.005 %	0.628	+/- 0.005 %
C_2H_4 + 3 O_2	258.5 torr	20 psi	1	1.006	+/- 0.006 %	0.994	+/- 0.006 %

The other source of uncertainty related to the mixture composition in this study is the mixture composition in the detonation tube prior to each experiment. The uncertainty of the mixture in the detonation tube is because the detonation tube could only be evacuated to a final pressure of 0.1- 0.2 torr prior to filling the tube with the test mixture and the composition of this residual gas was an unknown mixture of combustion products and air.

However, the largest change in equivalence ratio would occur if this residual gas were assumed to be pure oxygen. The calculations below detailing the maximum possible change in equivalence ratio were performed with this assumption.

As noted in the experimental procedure section, two different procedures for filling the detonation tube were followed depending upon the initial pressure. The first procedure involved only evacuating the tube to 0.1 – 0.2 torr and then filling the detonation tube to the desired initial pressure. This method was typically used for tests with initial fill pressures above approximately 70 torr. The second procedure involved evacuating the detonation tube to 0.1 – 0.2 torr, filling the detonation tube with the test mixture to 70 torr, re-evacuating the detonation tube to 0.2 torr and finally filling the detonation tube with the test mixture to the desired initial pressure. This method was typically used for experiments with initial fill pressures below 70 torr.

Tables 3-6 show why two different procedures were used. For low initial fill pressures the residual gas could have a potentially significant effect on the equivalence ratio of the mixture, while at higher initial fill pressures the residual gas has almost no effect on the equivalence ratio of the mixture. However, the potential negative effect of the residual gas on the equivalence ratio of the mixture at low initial pressure is eliminated by using the second experimental procedure.

Table 3 Uncertainty in H_2 + 0.5 O_2 mixture

Pressure (torr)	Worst Case Φ – No Refill	Worst Case Φ - Refill
20	0.971	1.000
40	0.985	1.000
60	0.990	1.000
80	0.993	1.000
100	0.994	1.000
200	0.997	1.000

Table 4 Uncertainty in C_2H_2 + 2.5 O_2 mixture

Pressure (torr)	Worst Case Φ – No Refill	Worst Case Φ - Refill
20	0.986	1.000
40	0.993	1.000
60	0.995	1.000
80	0.997	1.000
100	0.997	1.000
200	0.999	1.000

Table 5 Uncertainty in C_2H_2 + 4 O_2 mixture

Pressure (torr)	Worst Case Φ – No Refill	Worst Case Φ - Refill
20	0.617	0.625
40	0.621	0.625
60	0.622	0.625
80	0.623	0.625
100	0.623	0.625
200	0.624	0.625

Table 6 Uncertainty in C_2H_4 + 3 O_2 mixture

Pressure (torr)	Worst Case Φ – No Refill	Worst Case Φ - Refill
20	0.987	1.000
40	0.993	1.000
60	0.996	1.000
80	0.997	1.000
100	0.997	1.000
200	0.999	1.000

CHAPTER V

RESULTS

The results obtained during the present study are presented in this chapter. Records from pressure transducers T4, T5, E1, E4, E5, and E6 are referenced frequently. For clarification on the positions of these transducers Fig. 28 and Fig. 29 can be referenced.

Experimental vs. Theoretical CJ Speed

The overall goal of this experiment was to examine the behavior of a planar CJ detonation diffracting into a confined volume. For this reason, it first needed to be confirmed that a CJ detonation was in fact achieved during each experiment. This was accomplished by comparing the measured detonation velocity to the detonation velocity calculated using the SD Toolbox. A successful CJ wave was considered to have been obtained if the measured CJ speed was within +1% or -3% of the calculated CJ speed, which is the criteria that was used by Schultz (2000) in his thesis.

Figures 34-37 compare the experimental detonation velocities to the calculated CJ velocities for the four different mixtures used in this study. These figures show that a CJ detonation wave was obtained over the entire range of initial conditions for all mixtures.

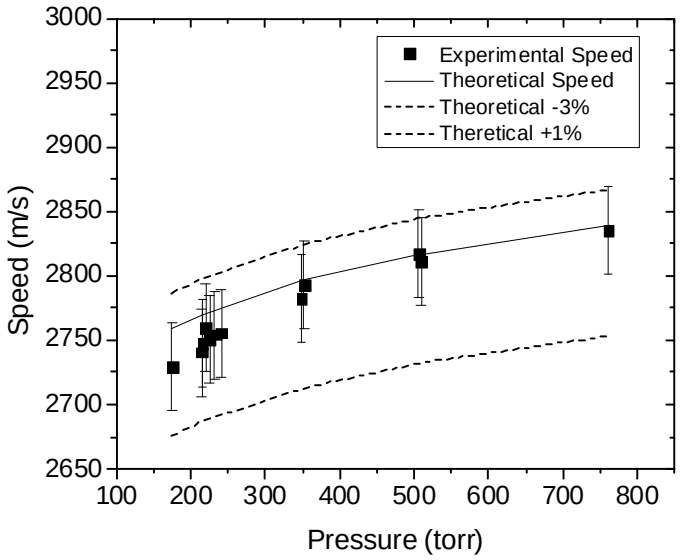

Figure 34 H_2 + 0.5 O_2 experimental vs. theoretical CJ velocity. The speeds obtained experimentally agree well with the theoretical CJ velocity.

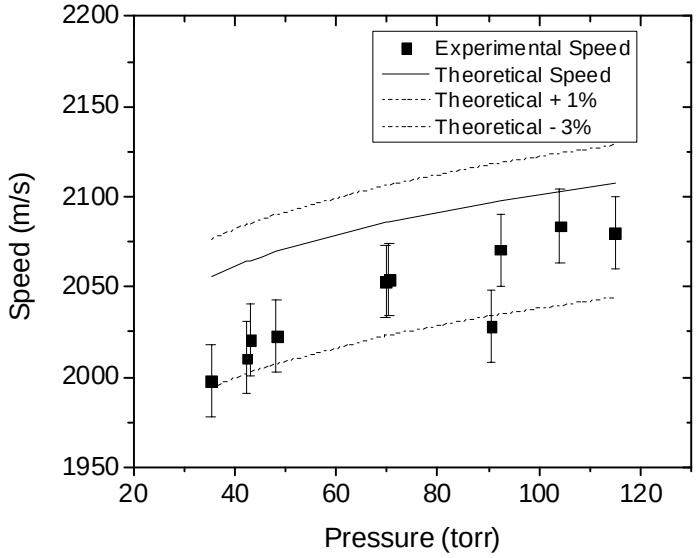

Figure 35 C_2H_2 + 4 O_2 experimental vs. theoretical CJ velocity. The speeds obtained experimentally agree well with the theoretical CJ velocity.

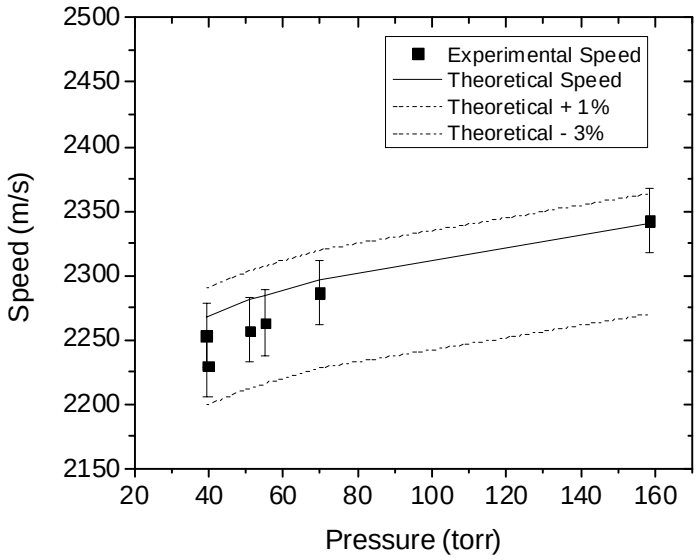

Figure 36 C_2H_2 + 2.5 O_2 experimental vs. theoretical CJ velocity. The speeds obtained experimentally agree well with the theoretical CJ velocity.

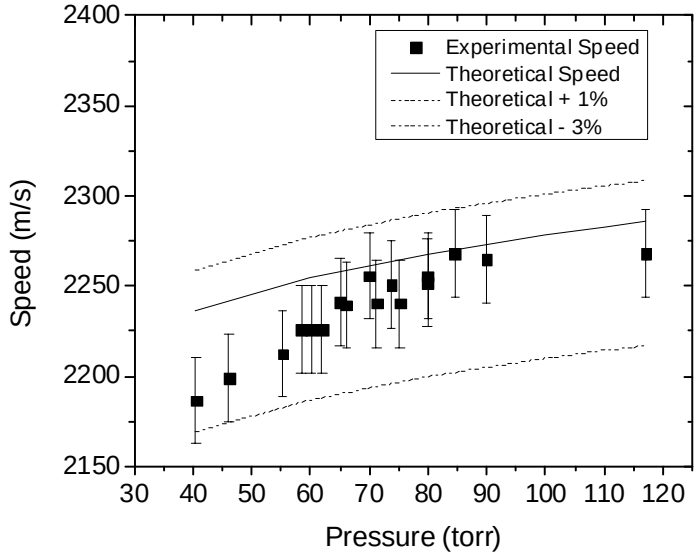

Figure 37 C_2H_4 + 4 O_2 experimental vs. theoretical CJ velocity. The speeds obtained experimentally agree well with the theoretical CJ velocity.

As noted by Schultz (2000), there are a number of factors that affect the uncertainty of the detonation velocity measurements such as the distance between transducers, the rise time of the transducer, the sampling rate of the DAQ and the detonation velocity.

The PCB 113B22 transducers had a rise time of less than 1 μs and the sampling rate used for all experiments was 1MS/s. These conditions are the same as those used by Schultz (2000) and result in an uncertainty of +/- 1 μs for the arrival of the detonation wave. Since two transducers are used to obtain the velocity, the measured time could differ from the actual time by +/- 2 μs. The distance between the transducers on the detonation tube was 45.72 cm while the distance between transducers E4-E5 and E5-E6 was 2.54 cm.

Since the theoretical timing, range of possible measured times, and distance between transducers is known the uncertainty in measured velocity can be calculated. The uncertainties in the measured velocities for all four mixtures are given in Table 7.

Table 7 Uncertainty associated with velocity measurements

Mixture	Theoretical CJ Speed	T4-T5 Measurement	T4-T5 % Error	E4-E5 or E5-E6 measurement	E4-E5 or E5-E6 % Error
H_2 + 0.5 O_2	2800 m/s	2766 – 2835 m/s	+1.24%, -1.21%	2294 – 3592 m/s	+28.3%, -18.1%
C_2H_2 + 2.5 O_2	2400 m/s	2375 – 2425 m/s	+1.06%, -1.03%	2019 – 2959 m/s	+23.3%, -15.9%
C_2H_2 + 4 O_2	2170 m/s	2150 – 2191 m/s	+0.96%, -0.94%	1853 – 2617 m/s	+20.6%, -14.6%
C_2H_4 + 3 O_2	2350 m/s	2326 – 2374 m/s	+1.03%, -1.01%	1983 – 2884 m/s	+22.7%, -15.6%

Experimental Incident and Reflected CJ Pressures

For further confirmation that a CJ detonation was successfully obtained during an experiment, the pressure traces from T4, T5, and E1 were compared to the calculated incident and reflected CJ pressures. Figure 38 and Fig. 39 are typical pressure traces obtained during an experiment. It can be seen in Fig. 38 that the magnitude of the incident pressure is approximately the CJ pressure, as expected.

Shepherd et al. (1991) show that the reflected pressure of a planar detonation is mixture insensitive and is approximately 2.5 times the magnitude of the CJ pressure. As

expected, Fig. 39 shows that the magnitude of the reflected pressure obtained experimentally is approximately 2.5.

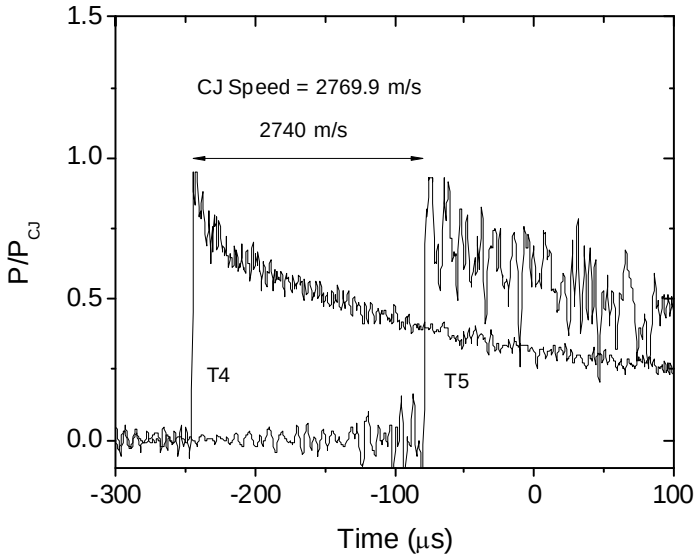

Figure 38 Typical trace showing that the incident pressure is approximately the CJ pressure as expected. The measured experimental speed is also very close to the theoretical CJ speed.

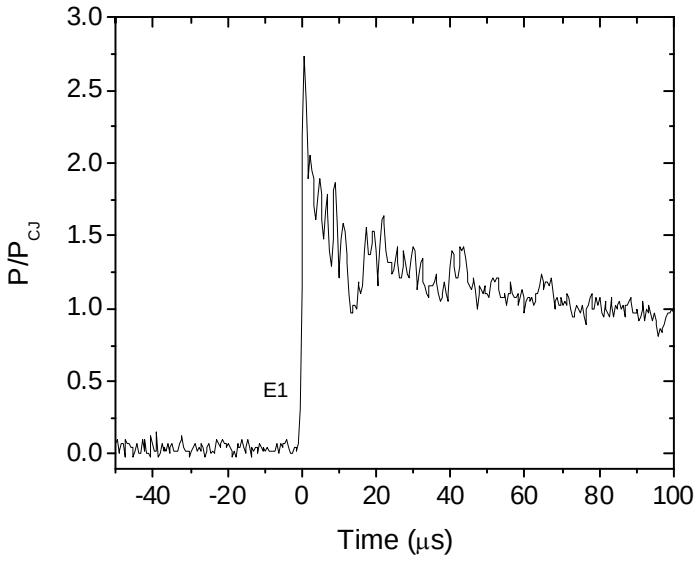

Figure 39 Typical trace showing the measured reflected pressure is approximately 2.5 times the CJ pressure as expected.

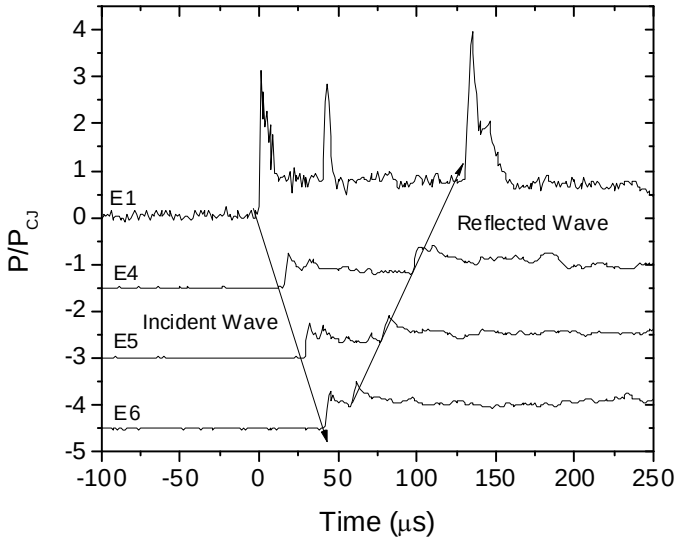

Figure 40 Typical experimental trace. The propagation of the incident wave and reflected shock wave in the expansion volume can be seen. The magnitude of the pressure at E1 is always higher than the magnitude of the pressure at E4, E5 or E6.

An example of a typical set of data obtained during an experiment is shown in Fig. 40. The value of the pressure in all runs has been normalized by the CJ pressure for the mixture calculated using the Shock and Detonation Toolbox programmed by Browne et al. (2008a). Also, for clarity, the traces of E4, E5 and E6 have been offset from zero, although the magnitude of each trace remains P/P_{CJ}.

There are a few main features of each experimental trace. First, the incident wave, either a decoupled shock or a detonation wave depending upon experimental conditions, moves radially outwards from E1 to E6. It can then be seen that the incident wave reflects from the boundary of the expansion volume and moves back radially towards the center. It should be noted that because this reflected wave is a converging cylindrical wave that its speed increases as it moves closer to the center. This increase in velocity also results in an increased pressure behind the wave. In fact, the pressure at the center of the expansion volume, where the converging waves meet can be very large, as shown by the magnitude of the third peak at E1 in Fig. 40.

By monitoring both the magnitude and speed of the incident wave as it travels radially outwards, it can be determined whether or not transmission of the planar detonation wave into the expansion volume was successful. In the section below the interpretation of the experimental data is explained in detail.

Regimes of Transmission

Pressure transducers were the primary diagnostic for determining whether or not successful transmission of a planar detonation into a cylindrical detonation occurred for

each run. Three distinct regimes of transmission were observed in the study, unsuccessful transmission, reflected re-initiation, or spontaneous re-initiation. Reflected re-initiation can be further subdivided into two categories, discontinuous or continuous. Each type of transmission is explained in more detail below.

Unsuccessful Transmission

A typical pressure trace for unsuccessful transmission is shown in Fig. 41. There are two major characteristics typically seen in an unsuccessful-transmission pressure trace. First, the radial velocity is well below V_{CJ}, typically about one-half V_{CJ}. Secondly, the magnitude of the pressure is below 0.5 P_{CJ} and usually decreases moving radially outwards.

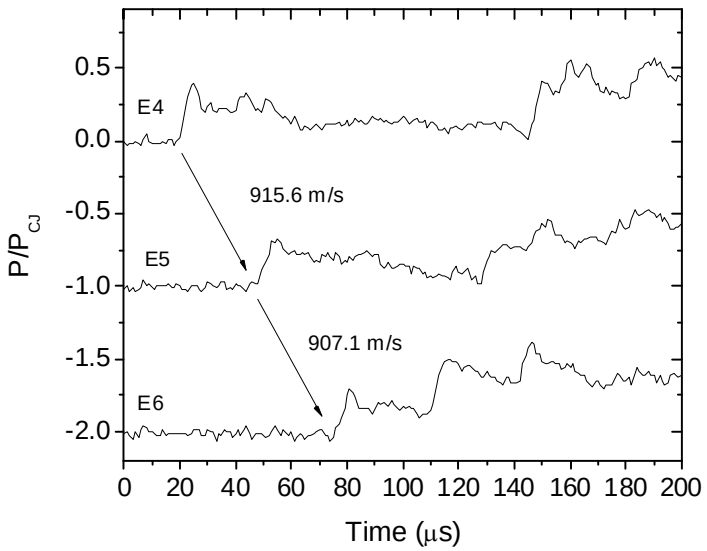

Figure 41 Unsuccessful transmission from Run 222. The low velocity and pressure rise are indications transmission was unsuccessful.

Figure 42 Soot foil record from Run 143 where transmission was unsuccessful. The cellular pattern disappears near the edges of the record indicating the detonation had failed.

Figure 42 shows a smoked foil record obtained during a run in which the detonation failed to propagate. It shows that the cell size increases with radial distance until the cellular structure finally disappears, indicating that the detonation failed. Because of the limited number of smoked foils available for testing, most smoked foils shown in the Appendix B are from successful transmissions since it was believed that those offered the most important and relevant information.

Discontinuous Reflected Re-initiation

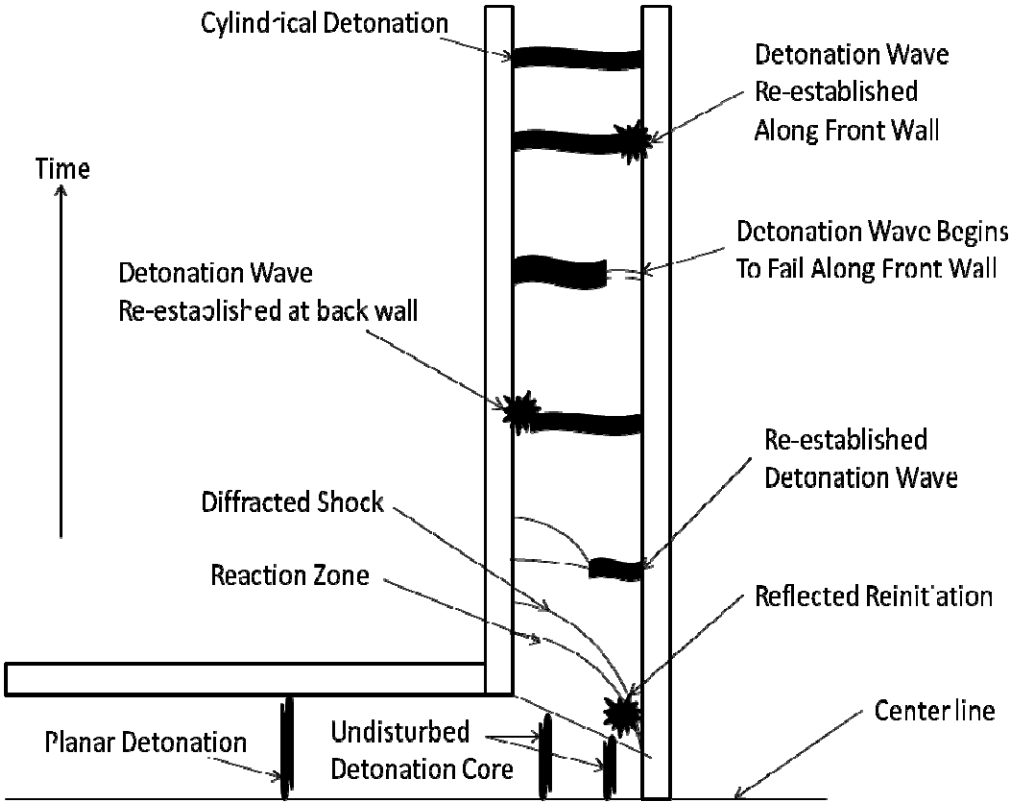

Figure 43 Discontinuous reflected re-initiation. The shock wave and reaction zone initially decouple along the back wall, the detonation is then re-initiated at the front wall and sweeps back to re-initiate the detonation at the back wall. However, the shock and reaction zone then decouple along the front wall before finally being re-initiated again to produce a stable, diverging cylindrical detonation.

As previously mentioned, reflected re-initiation can be divided into two sub-categories. The first, discontinuous reflected re-initiation is graphically represented in Fig. 43.

In discontinuous reflected re-initiation, initially the detonation is established along the front wall behind the reflected, diffracted shock wave. The re-established detonation then sweeps back toward the back wall until re-initiation occurs along the

back wall. It is this re-initiation that is the cause of the ring in Fig. 44. At this point, the detonation along the front wall begins to fail. However, in the same way that the re-established detonation along the front was able to re-establish the detonation along the back wall, the newly established detonation along the back wall now helps to re-establish the failing detonation on the front wall. Finally, a re-established cylindrical detonation propagates radially outwards.

This mode of re-initiation is responsible for the formation of the rings seen in Fig. 44 and Fig. 45. Murray and Lee (1983) stated that this ring shows the position of the decoupled shock wave and reaction zone at the time when re-initiation occurs. Typically, this ring is seen on the back wall because the shock wave and reaction zone along the back wall always decouple at the abrupt area expansion. The detonation wave is reformed along the back wall only after the detonation wave has re-formed at the front wall and has had time to sweep back to the back wall. However, in discontinuous reflected re-initiation, in addition to observing a ring on the back-wall soot foil record, a similar ring, at a larger radial diameter, was also observed on front-wall soot foil records. This ring on the front wall, seen in Fig. 45, must be formed by the same mechanism by which a ring is typically formed on the back wall. Therefore, because a ring is observed to form on the front wall under certain conditions it is clear that for a short period of time the shock wave and reaction zone do decouple along the front wall. However, it should be noted that after the detonation is re-established there is no indication that it may fail again as the cells do not grow appreciably in size near the edge of the soot foil.

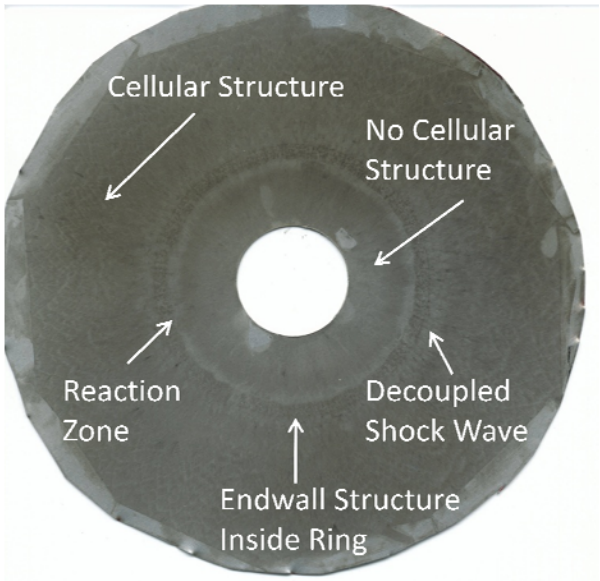

Figure 44 Back wall soot foil record from Run 244. The ring present in the soot foil record shows the position of the decoupled shockwave and reaction zone when the detonation was re-initiated at the back wall.

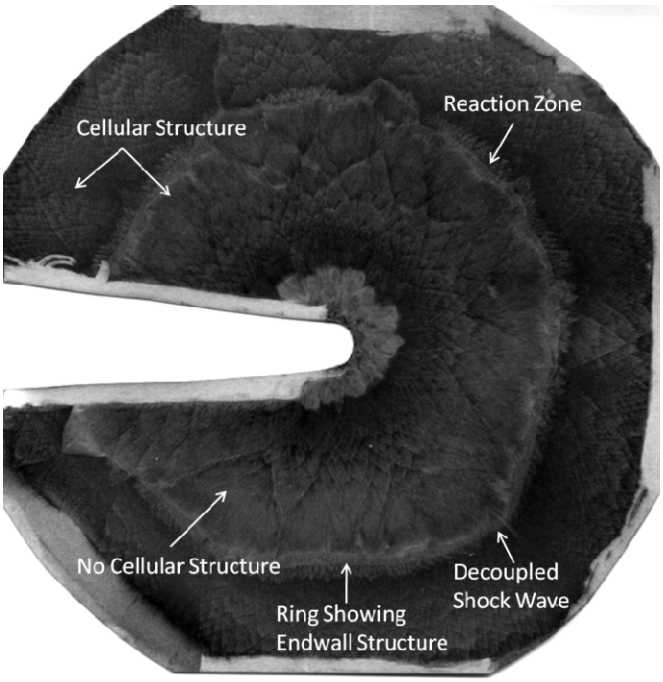

Figure 45 Front wall soot foil record from Run 368. Just as in Figure 41 a ring is present showing the position of the decoupled shock wave and reaction zone when the detonation was reinitiated at the front wall.

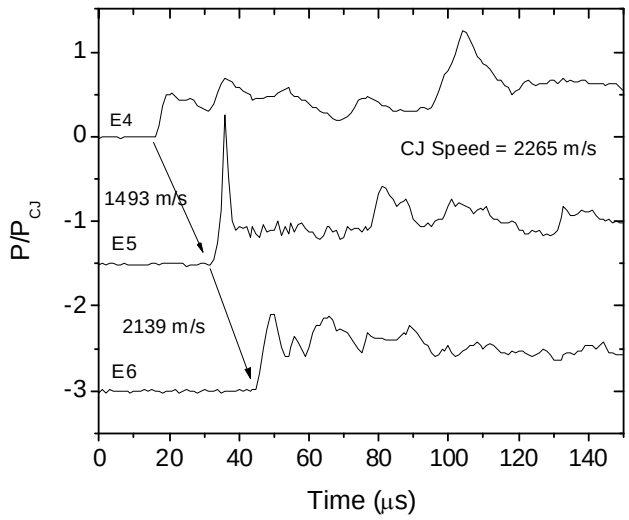

Figure 46 Pressure trace from Run 368 when discontinuous reflected re-initiation occurs. The wave speed from E4-E5 is much less than V_{CJ} but after re-initiation occurs, marked by the spike in pressure, the wave again moves at V_{CJ}. The location of the ring in Fig. 42 is consistent with the location of re-initiation seen in the pressure trace above.

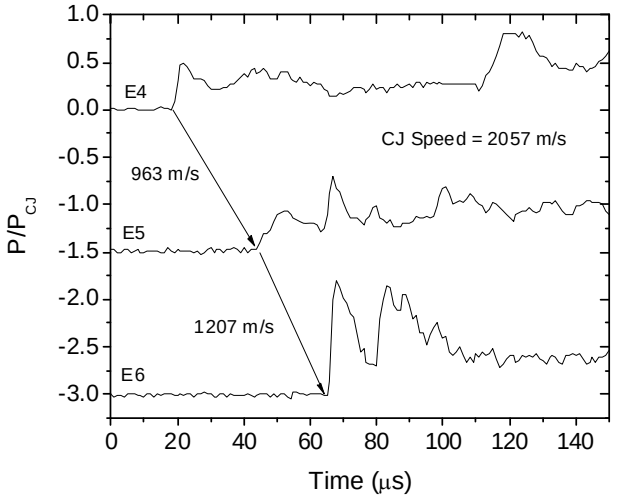

Figure 47 Pressure trace from Run 221 when discontinuous reflected re-initiation occurs. The location of re-initiation is at a larger radial distance compared to Run 368 in Fig. 43. However, the magnitude of pressure at E6 is much larger than it was at E4 or E5.

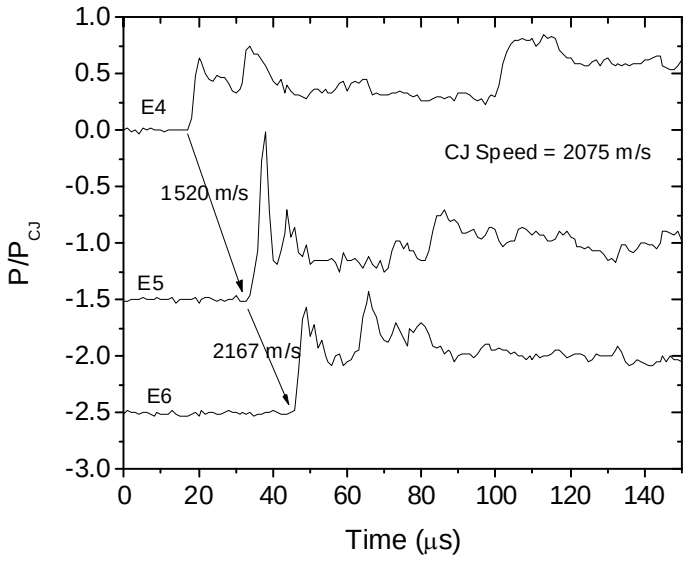

Figure 48 Pressure trace from Run 218 when discontinuous reflected re-initiation occurs. Similarly to Run 368 in Fig. 43, the wave speed from E4-E5 is much less than V_{CJ} but after re-initiation occurs, marked by the spike in pressure, the wave again moves at V_{CJ}.

Experimental results, pressure traces, and soot foil records for this method of re-initiation are shown in Figs. 44-48**.** The pressure traces in Figs. 46-48 indicate that at E4 the detonation wave has failed because the magnitude of the pressure is much lower than P_{CJ}. However, in Fig. 47**,** re-initiation appears to occur between E5 and E6 while in Fig. 46 and Fig. 48 the re-initiation occurs sooner, between E4 and E5. In Fig. 46-48, the speed between E5 and E6 is approximately equal to V_{CJ}, another indication that the detonation wave has been re-initiated.

It should be noted that usually, high quality pressure traces and front wall soot foil records could not be obtained during the same run. This situation was because of the way the soot foil was secured to the front wall. The soot foil was taped, with black

electrical tape, to the front wall and typically this tape also covered the pressure transducers, which resulted in multiple layers of tape on top of the transducers. These multiple layers of tape resulted in extremely poor pressure signals. However, fortunately, a few usable pressure traces were obtained from runs with front wall soot foils. These runs, such as Run 368, offer further insight into how this mode of re-initiation works.

First, the pressure signal shown in Fig. 46 indicates that the detonation wave has failed by the time it reached E4 and the lack of cellular structure at the radial location of E4 in the soot foil record of Fig. 45 also indicates that the detonation wave has failed. Secondly, the pressure trace from Fig. 46 indicates that re-initiation occurred somewhere between E4 and E5 and this is also the location of the ring in the soot foil record of Fig. 45. Finally, the pressure trace from Fig. 46 indicates that the detonation is sustained at E6 and the typical cellular structure evident outside of the ring in Fig. 45 confirms that a detonation is sustained. This pair of simultaneous records from Run 368 confirmed that the interpretation of the pressure traces shown in Figs. 47-48, for example, was correct, even though a corresponding soot foil record was not available for these particular experiments.

This method of reinitiation was observed in the pressure traces for gaps between 13.7 mm and 32.75 mm and when $w/\lambda < 5.5$. It was not observed in the pressure traces for gaps smaller than 13.7 mm because the re-initiation at the front wall occurred prior to the wave reaching E4. However, this method of reinitiation could be observed for gap sizes less than 13.7 mm using soot foil records. An example of a soot foil record for a gap size of 7.35 mm is shown in Fig. 49.

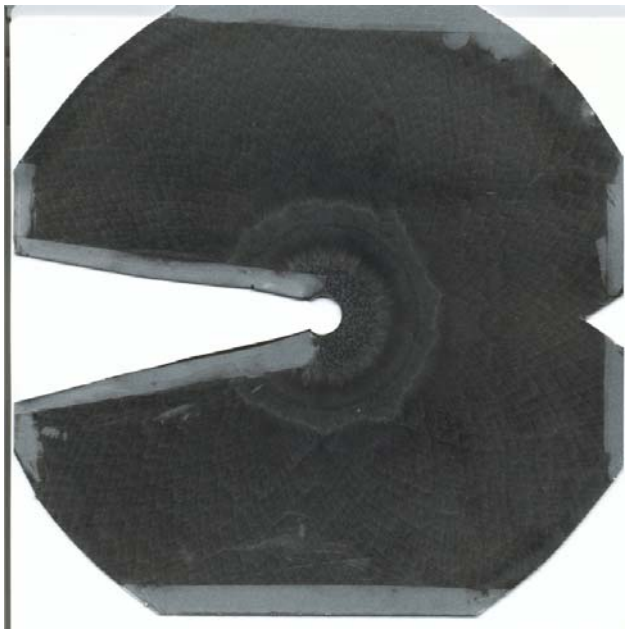

Figure 49 Front wall soot foil record from Run 275 showing discontinuous reflected re-initiation for a gap size of 7.35 mm. The ring shows that this method of re-initiation occured.

Continuous Reflected Re-initiation and Spontaneous Re-initiation

The final two methods of transmission, continuous reflected re-initiation and spontaneous re-initiation, are nearly impossible to distinguish by examining data from a single test. In both methods the detonation wave is re-established by the time it reaches E4 and moves at approximately the CJ speed as it moves radially outwards. The magnitude of the pressure at E4, E5 and E6 also remains nearly constant, at a value of approximately 0.7-0.8 P_{CJ}. It should be noted that this pressure deficiency is consistent with the findings of Lee (2008) on pg. 322. An example of a typical pressure trace obtained for either of these methods of transmission is shown in Fig. 50.

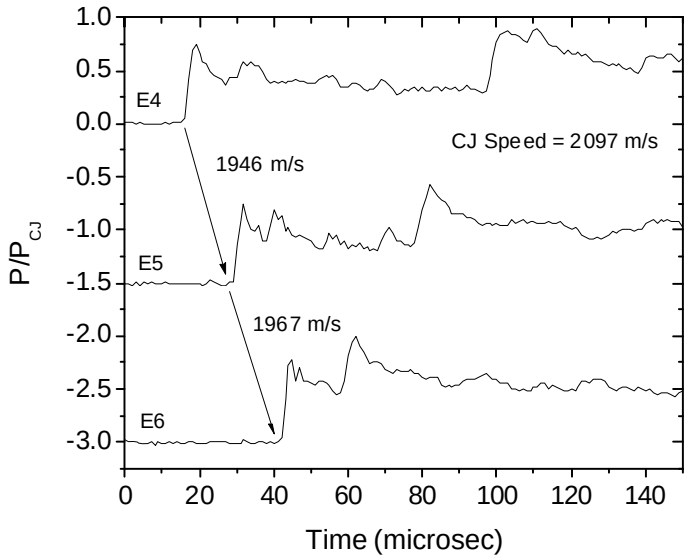

Figure 50 Pressure trace from Run 220 showing successful transmission. The magnitude of the pressure and speed of the wave are constant as the wave moves radially outwards and are both approximately at their CJ values.

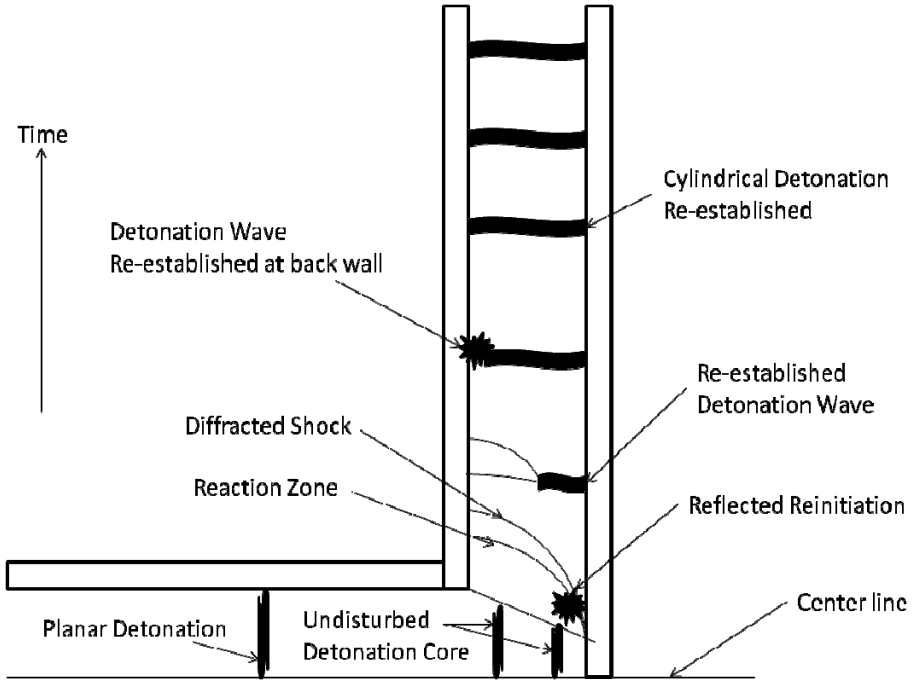

Figure 51 Graphical representation of the continuous reflected re-initiation process. Re-initiation occurs after the incident wave has reflected from the endwall.

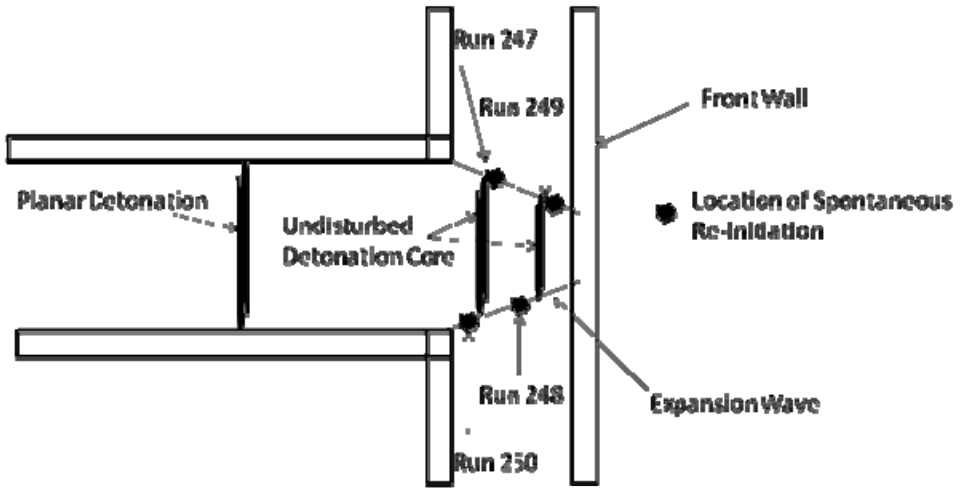

Figure 52 Graphical representation of the spontaneous re-initiation process. Re-initiation occurs prior to the incident wave interacting with the endwall.

Graphical representations of these re-initiation modes are shown in Fig. 51 and Fig. 52. The continuous reflected re-initiation process shown in Fig. 51 is nearly identical to the discontinuous reflected re-initiation process except that the detonation wave does not fail along the front wall. The method of re-initiation for the spontaneous re-initiation process is completely different because the detonation wave is re-initiated prior to the incident wave interacting with the endwall.

In both of these methods, because the detonation wave does not fail along the front wall, the ring seen in front wall soot foil records with discontinuous reflected re-initiation is not observed. The cellular structure in a soot foil record for these methods is continuous. An example of a soot foil record showing a soot foil record from either of these methods of re-initiation is shown in Fig. 53.

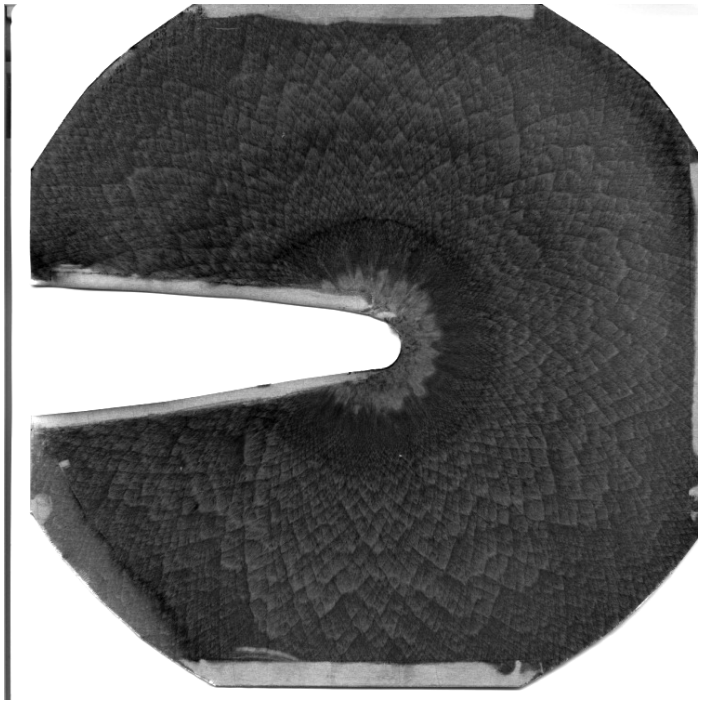

Figure 53 Soot foil record from Run 369. This is typical of the type of soot foil record seen for both continuous reflected re-initiation and spontanteous re-initiation. The ring evident with discontinuous reflected re-initiation is no longer present but the cellular strucutre is continuous.

Because these methods of re-initiation could not be distinguished by examining a single set of pressure traces, the results of Murray and Lee (1983) were used as a guide for determining whether continuous reflected re-initiation or spontaneous re-initiation occurred. The results of Murray and Lee (1983) indicated that spontaneous re-initiation occurred when w/λ was approximately 11. This finding means that the location of re-initiation will change as the sensitivity of the mixture is changed. For example, the re-initiation location for a more sensitive mixture, which has a smaller detonation cell size, will be closer to the tube exit than the re-initiation location for a less sensitive mixture. However, the location of reflected re-initiation, for a constant gap size, will be the same

regardless of mixture sensitivity. This result means that by comparing the pressure signals from multiple runs at different conditions it was possible to determine whether or not continuous reflected re-initiation or spontaneous re-initiation occurred. If runs when reflected re-initiation occurred are compared, the time at which the wave passes E4, E5 and E6 should be nearly identical, regardless of mixture sensitivity, because the location of re-initiation was the same. However, if runs when spontaneous re-initiation occurred are compared, the time at which the wave passes E4, E5 and E6 should be different depending on the sensitivity of the mixture. For example, the detonation wave from a more sensitive mixture should reach E4, E5 and E6 sooner than the detonation wave from a less sensitive mixture because re-initiation occurred sooner.

Table 8 gives the conditions for the runs plotted in Figs. 54-69. Figures 54-65 compares runs where reflected re-initiation is believed to have occurred and the timing of the pressure traces is nearly identical, as expected. Figures 66-69 compares runs where spontaneous re-initiation is believed to have occurred and, as expected, the arrival of the detonation wave at transducers E4, E5 and E6 depends on the sensitivity of the mixture.

Also, it should be noted, as shown in Table 8, that D/λ is less than 13 for the runs when reflected re-initiation occurs. While this would result in failure of the detonation wave diffracting into an unconfined volume, it does not result in failure of a detonation wave diffracting into a confined volume. However, because spontaneous re-initiation is the same method by which re-initiation occurs during detonation diffraction into an unconfined volume an additional constraint of $D/\lambda > 13$ must be satisfied for

spontaneous re-initiation to occur. Table 8 shows that for the runs plotted in Figs. 63-66 this criterion was satisfied.

Figures 54-65 also show that the shape of the normalized pressure signals are nearly identical. Every feature of the traces is evident in each run, showing that there is a physical reason for every feature in the trace and it is not just random noise. This high degree of reproducibility between pressure traces has been previously noted before by Liang et al. (2008) and Shepherd et al. (1989).

Table 8 List of conditions used to compare continuous reflected re-initiation and spontaneous re-initiation

Run	Mixture	Gap (mm)	w/λ	D/λ
127	H2 + 0.5 O2	26.4	5.17	7.47
135	H2 + 0.5 O2	26.4	5.71	8.26
130	H2 + 0.5 O2	26.4	6.31	9.13
131	H2 + 0.5 O2	26.4	8.56	12.38
108	H2 + 0.5 O2	39.1	8.51	8.31
109	H2 + 0.5 O2	39.1	6.06	5.91
114	H2 + 0.5 O2	39.1	6.89	6.73
115	H2 + 0.5 O2	39.1	7.64	7.46
170	C2H2 + 4 O2	13.7	9.2	25.63
171	C2H2 + 4 O2	13.7	8.61	23.98
172	C2H2 + 4 O2	13.7	7.88	21.96

Table 8 continued

Run	Mixture	Gap (mm)	w/λ	D/λ
175	C2H2 + 4 O2	13.7	6.10	17.00
176	C2H2 + 4 O2	13.7	5.40	15.06
250	C2H2 + 4 O2	26.4	24.21	35.01
247	C2H2 + 4 O2	26.4	21.51	31.11
248	C2H2 + 4 O2	26.4	16.45	23.79
249	C2H2 + 4 O2	26.4	12.79	18.49
251	C2H2 + 4 O2	26.4	8.23	11.90

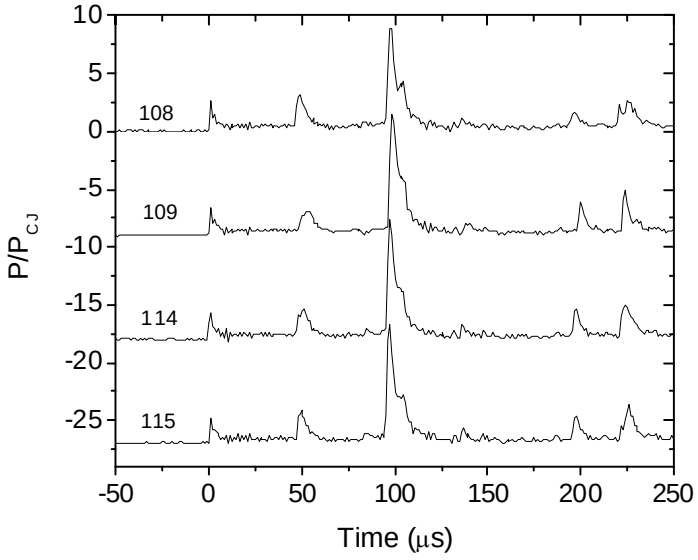

Figure 54 Reflected re-initiation with H_2 + 0.5 O_2 at E1 with 39.1-mm spacer.

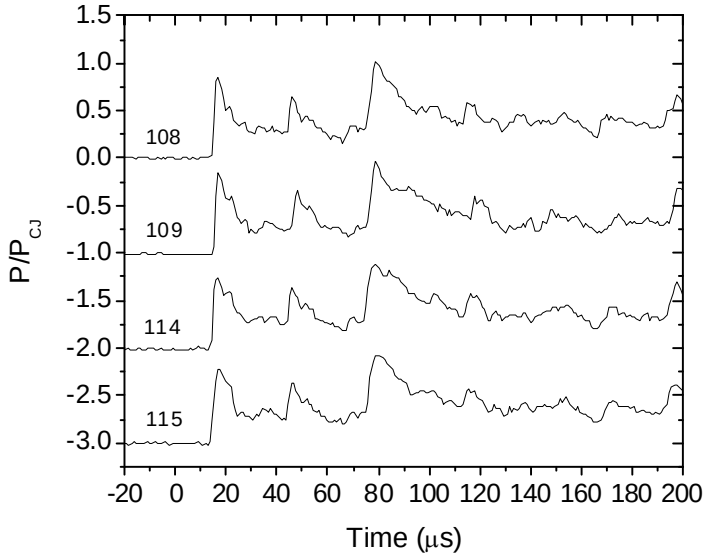

Figure 55 Reflected re-initiation with H_2 + 0.5 O_2 at E4 with 39.1-mm spacer.

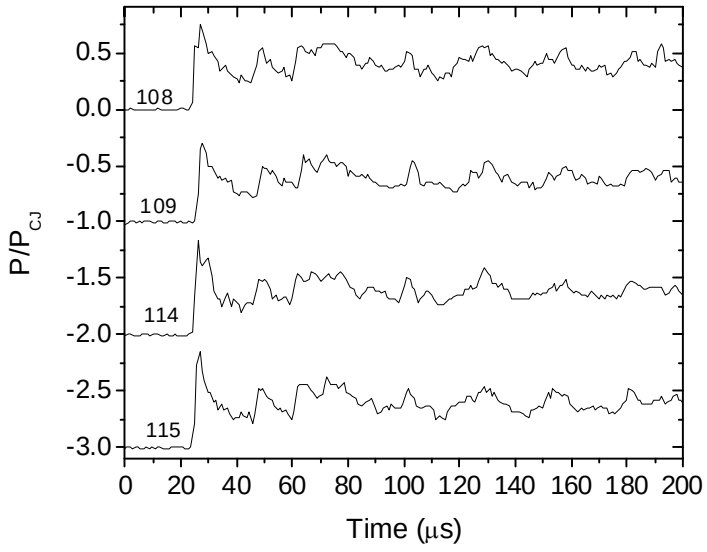

Figure 56 Reflected re-initiation with H_2 + 0.5 O_2 at E5 with 39.1-mm spacer.

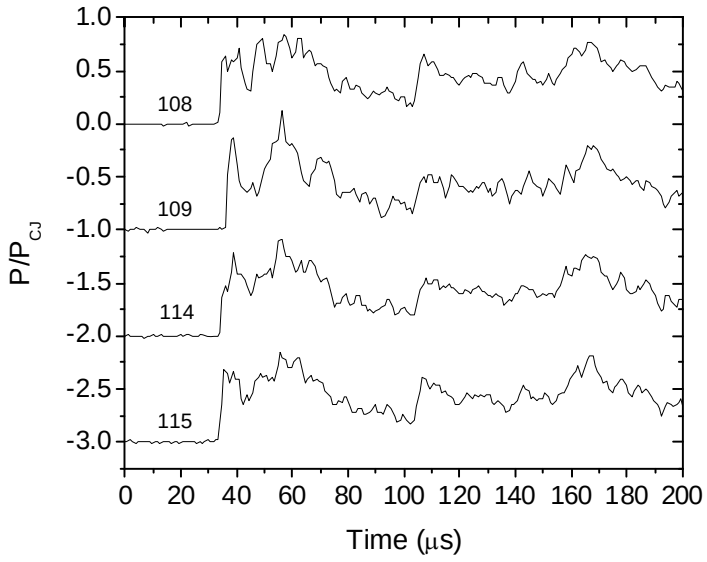

Figure 57 Reflected re-initiation with H_2 + 0.5 O_2 at E6 with 39.1-mm spacer.

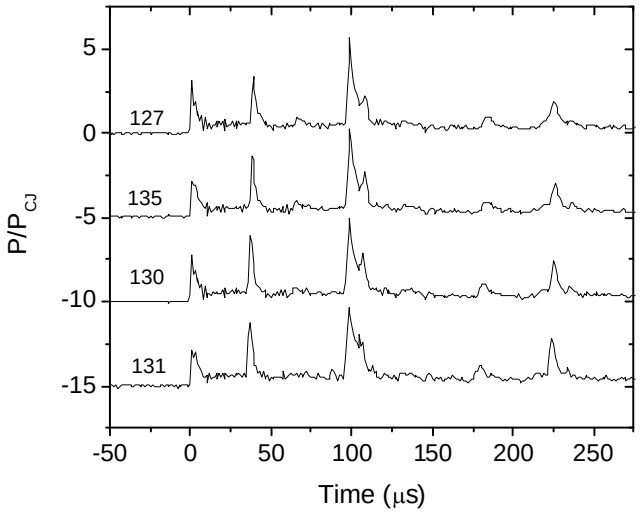

Figure 58 Reflected re-initiation with H_2 + 0.5 O_2 at E1 with 26.4-mm spacer.

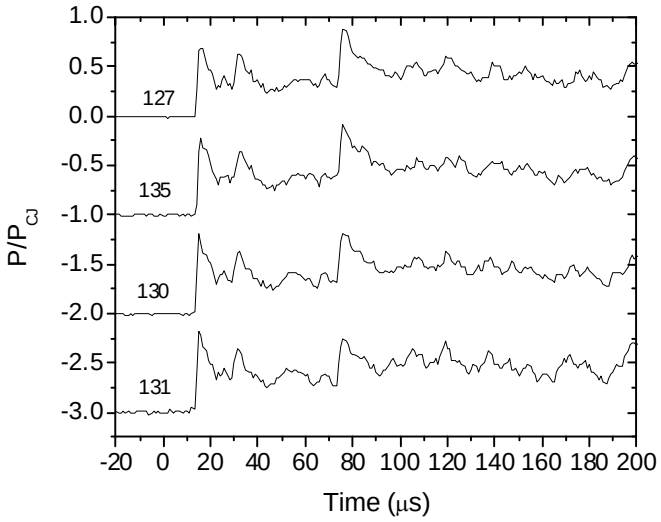

Figure 59 Reflected re-initiation with H_2 + 0.5 O_2 at E4 with 26.4-mm spacer.

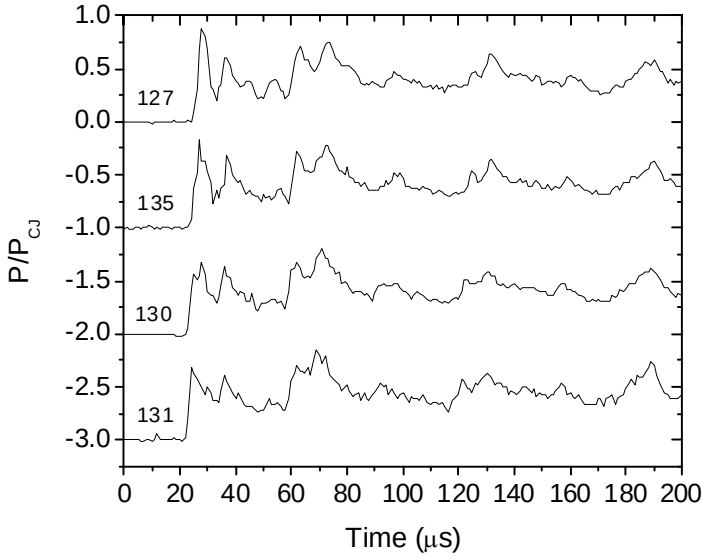

Figure 60 Reflected re-initiation with H_2 + 0.5 O_2 at E5 with 26.4-mm spacer.

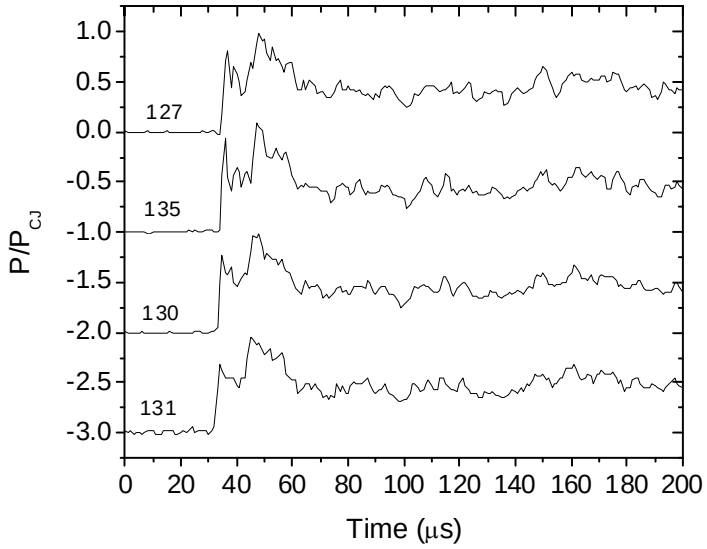

Figure 61 Reflected re-initiation with H_2 + 0.5 O_2 at E6 with 26.4 mm spacer.

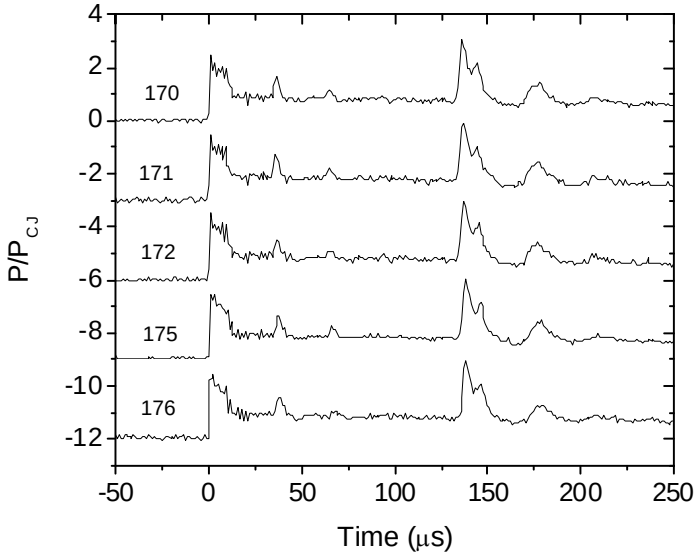

Figure 62 Reflected re-initiation with C_2H_2 + 4 O_2 at E1 with 13.7 mm spacer.

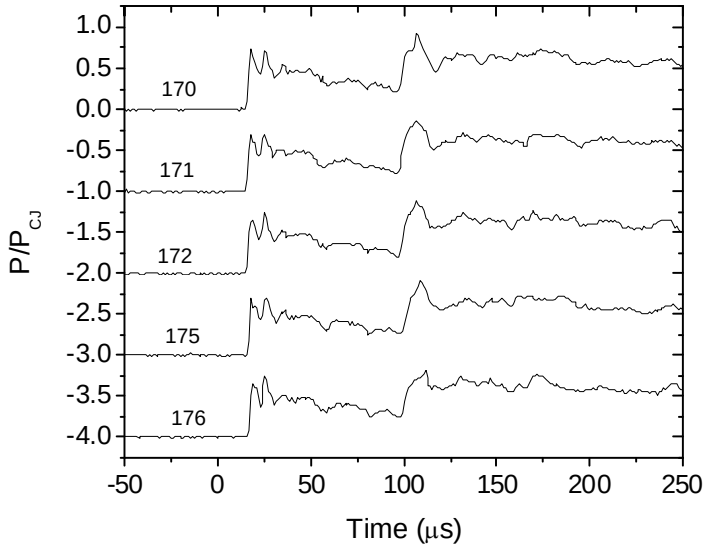

Figure 63 Reflected re-initiation with C_2H_2 + 4 O_2 at E4 with 13.7 mm spacer.

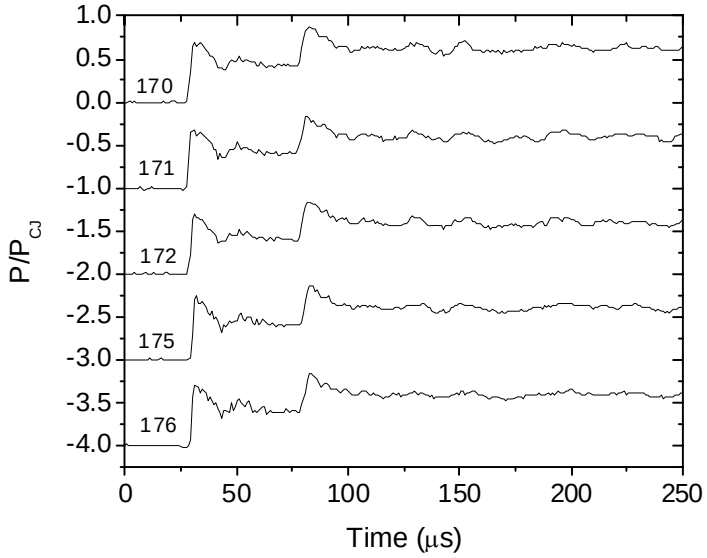

Figure 64 Reflected re-initiation with C_2H_2 + 4 O_2 at E5 with 13.7 mm spacer.

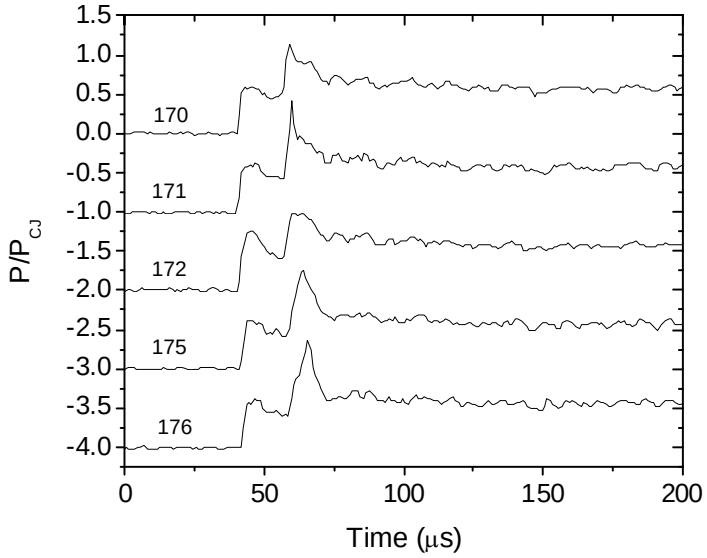

Figure 65 Reflected re-initiation with C_2H_2 + 4 O_2 at E6 with 13.7 mm spacer.

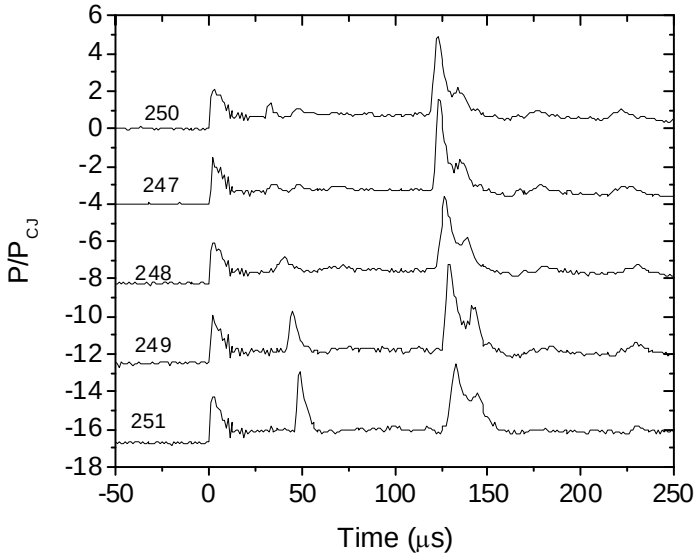

Figure 66 Spontaneous re-initiation with C_2H_2 + 4 O_2 at E1 with 26.4 mm spacer.

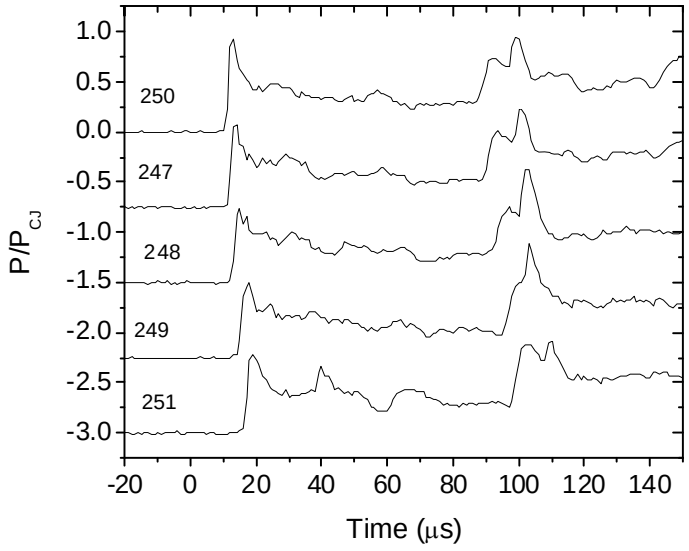

Figure 67 Spontaneous re-initiation with C_2H_2 + 4 O_2 at E4 with 26.4 mm spacer.

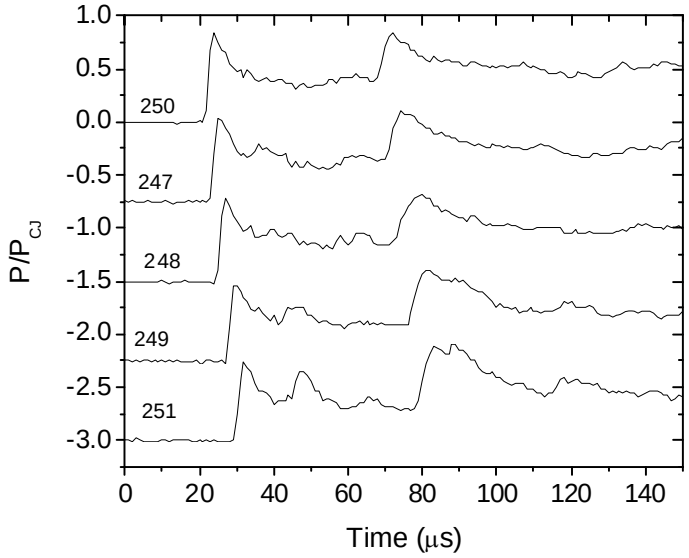

Figure 68 Spontaneous re-initiation with C_2H_2 + 4 O_2 at E5 with 26.4 mm spacer.

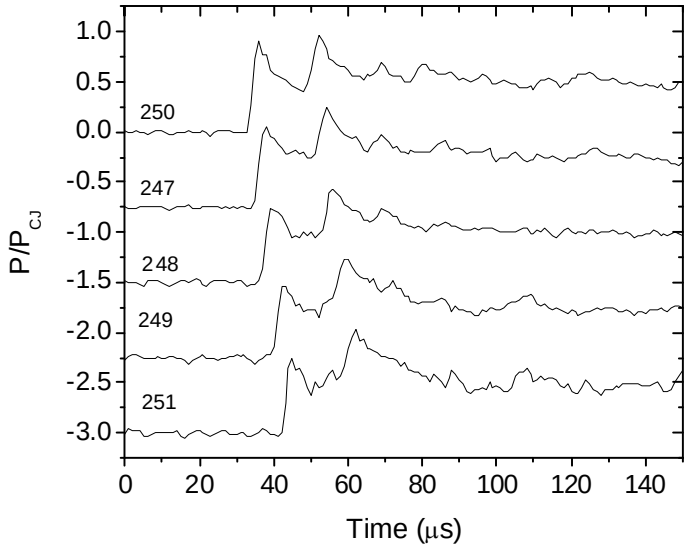

Figure 69 Spontaneous re-initiation with C_2H_2 + 4 O_2 at E6 with 26.4 mm spacer.

There is one final difference between continuous reflected re-initiation and spontaneous re-initiation that is observed when the pressure traces of E1 are compared, shown in Fig. 70. This figure shows that when spontaneous re-initiation occurred far from the endwall, as in Runs 250, 247, and 248, the magnitude of the pressure wave between the incident and reflected wave was small. However, when reflected re-initiation occurred or spontaneous re-initiation occurred in the vicinity of the endwall, as in Run 249 and Run 251, the magnitude of the middle pressure wave is large. The exact cause of this middle spike was not identified, but it was clear that the type of re-initiation had a dramatic effect on the magnitude of the middle spike.

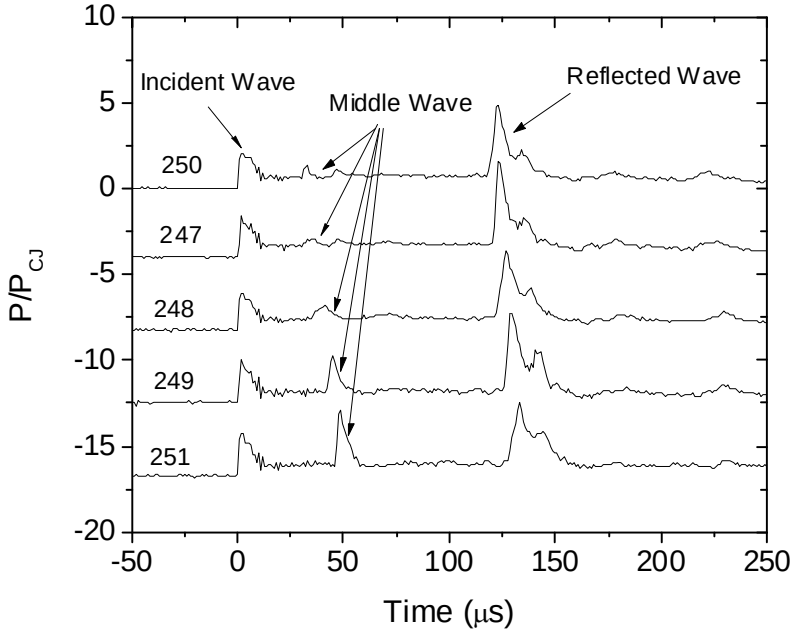

Figure 70 Presence and magnitude of middle wave depends upon type and location of re-initiation.

Radial Uniformity

Another important aspect of detonation diffraction into a confined volume which was observed in this study was the radial uniformity of the detonation wave for the continuous reflected re-initiation and spontaneous re-initiation regimes. Pressure traces demonstrating the radial uniformity are shown in Figs. 71-72 and a soot foil record, which is radially symmetric, is shown in Fig. 73.

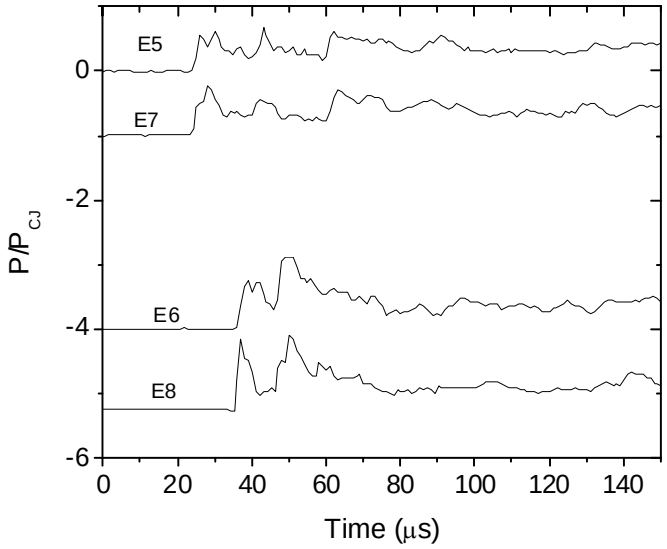

Figure 71 Comparing radial uniformity of the detonation wave for Run 395. Transducers E5 and E7 are at the same radial distance and E6 and E8 are at the same radial distance.

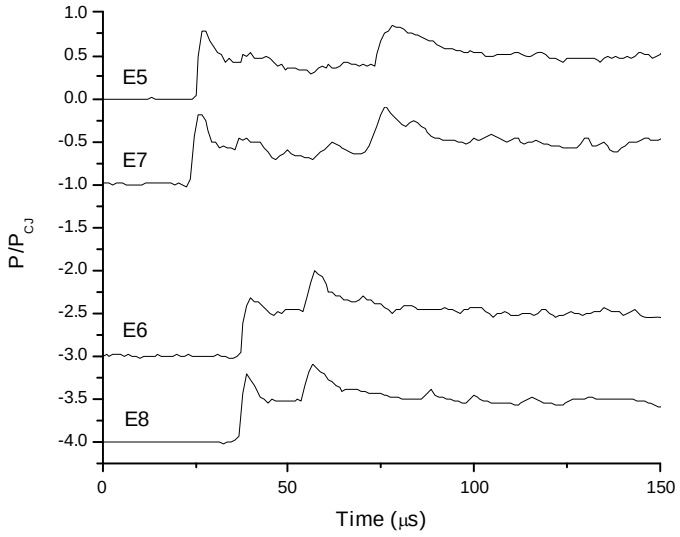

Figure 72 Comparing radial uniformity of the detonation wave for Run 165. Transducers E5 and E7 are at the same radial distance and E6 and E8 are at the same radial distance.

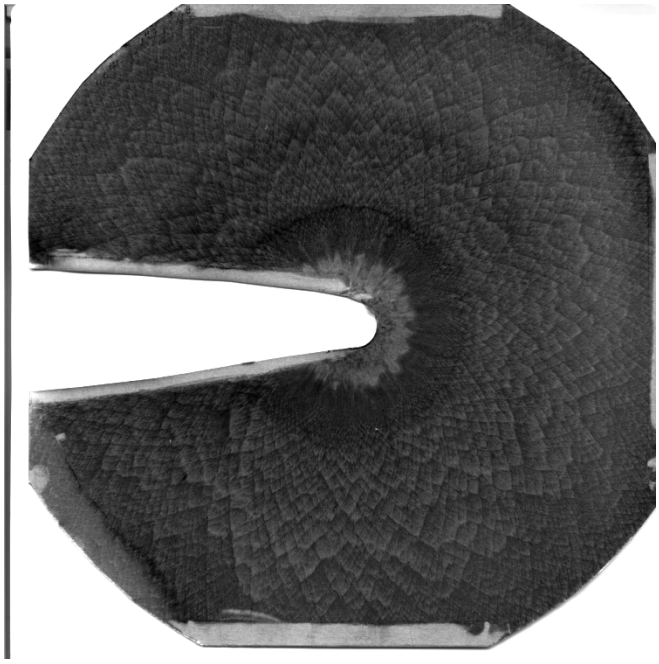

Figure 73 Soot foil record from Run 369. The soot foil record is symmetric in the radial direction.

Relatively few runs were conducted in which E7 and E8 were monitored, but the results shown in Figs. 71-72 are typical of the behavior for conditions in the continuous reflected re-initiation and spontaneous re-initiation regimes. For conditions in the discontinuous reflected re-initiation regime this radial uniformity began to break down.

Soot foil records near the critical conditions for transmission which show non-uniform radial propagation are shown in Fig. 74 and 75. These records show that in some directions the detonation failed to transmit, where no cellular structure was present, while in other directions the transmission of the detonation was successful, where typical cellular structure was present. However, it is interesting to note that

because the transmission of the detonation was successful in at least one direction that eventually the detonation will be re-established globally.

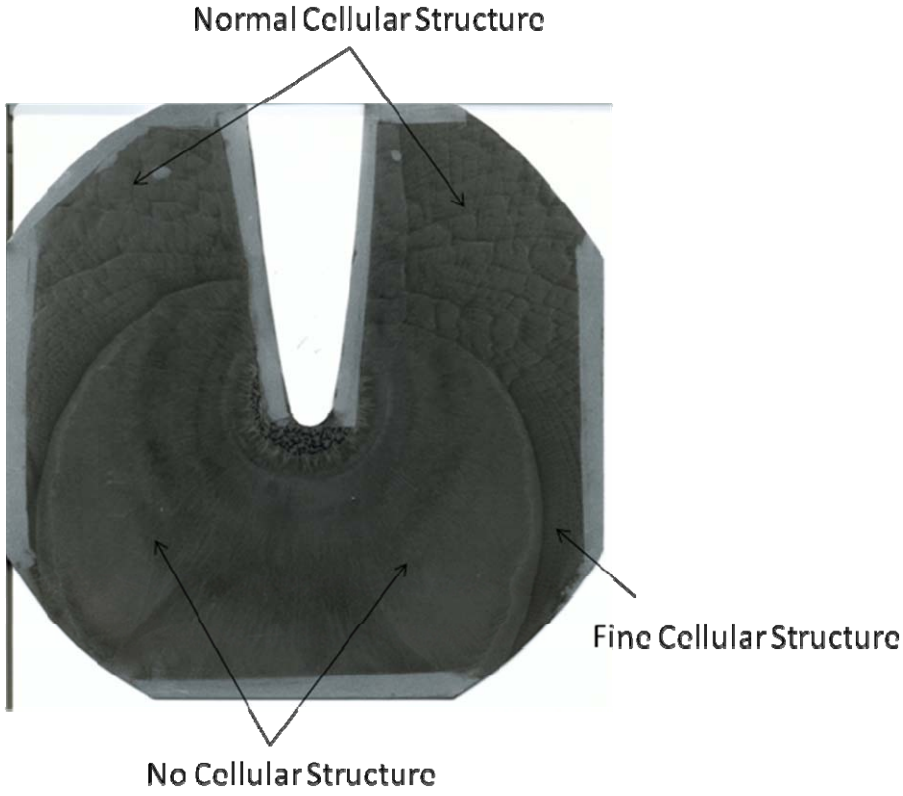

Figure 74 Soot foil record from Run 283. Transmission of the detonation was radially non-uniform.

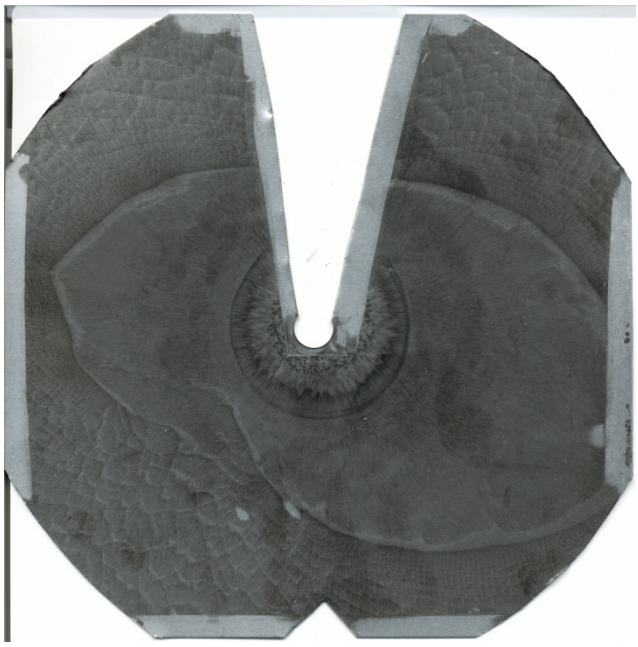

Figure 75 Soot foil record from Run 272. Transmission of the detonation was radially non-uniform.

All Conditions

A major achievement of this study was the ability to define the critical conditions for successful transmission of a planar detonation to a cylindrical detonation. All experiments performed in this study were classified as a "go" or "no go". For those runs classified as "go", no distinction is made between the methods of transmission.

The data were analyzed using two different methods, which highlight different, important features of the data. In the first method, the data were plotted as w/λ vs. w. This method highlights the fact that the results of this study showed that the value of w/λ for which successful transmission was possible decreased as the gap size was decreased. Examining the data in this way shows that the results of this study are different from the

results of Murray and Lee (1983), which indicated that the critical condition for transmission was $w/\lambda = 5.7$, regardless of gap size.

In the second method, the data were plotted as λ_s/λ vs. w, where λ_s is the critical cell size for transmission to an unconfined volume. This definition is a useful way of analyzing the data because it allows the relative ease of transmission of a planar detonation in a confined volume to be directly compared to the ease of transmission in an unconfined volume. Values of $\lambda_s/\lambda < 1$ indicate that for a given set of initial conditions, transmission to a confined volume is easier than transmission to an unconfined volume, while values of $\lambda_s/\lambda > 1$ indicate that transmission to a confined volume is more difficult than transmission to an unconfined volume. For sufficiently large gap sizes the confined volume can be approximated as an unconfined volume, and λ_s/λ should tend to 1.

Figures 76-80 show all experiments performed during this study. These figures show that there is a clear demarcation line between the conditions which were classified as a “go” and the conditions which were classified as a “no go”. The exact experimental conditions for each data point in Figs. 76-80 are given in Appendix C.

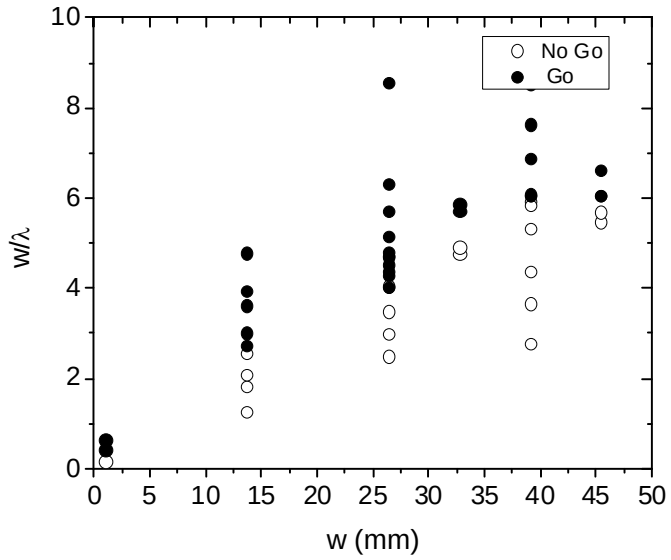

Figure 76 Results for all runs with H_2 + 0.5 O_2. Each experiment was classified as either a go or no go.

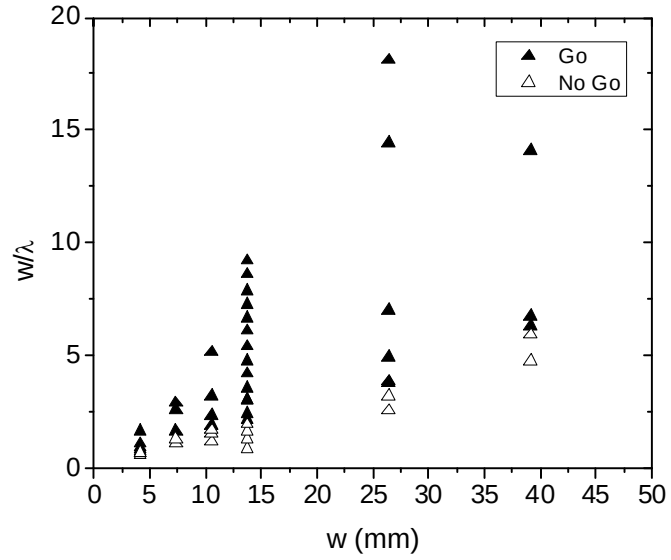

Figure 77 Results for all runs with C_2H_2 + 4 O_2. Each experiment was classified as either a go or no go.

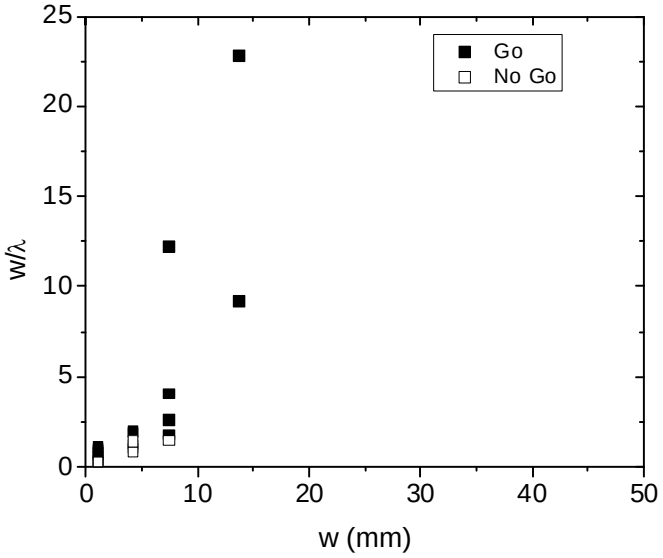

Figure 78 Results for all runs with C_2H_2 + 2.5 O_2. Each experiment was classified as either a go or no go.

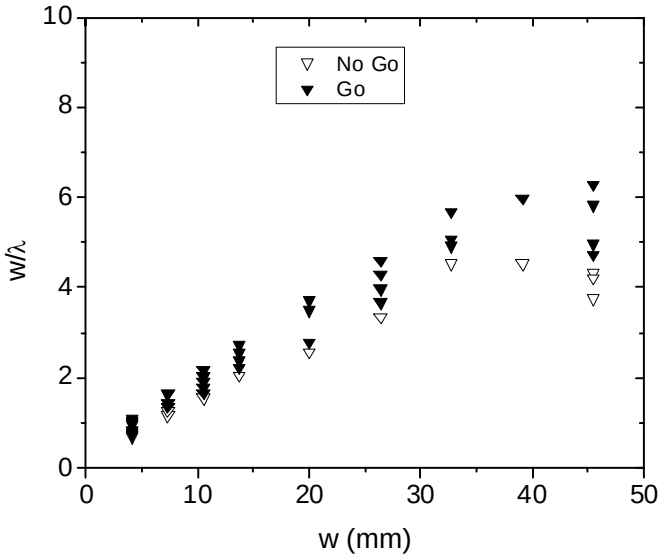

Figure 79 Results for all runs with C_2H_4 + 3 O_2. Each experiment was classified as either a go or no go.

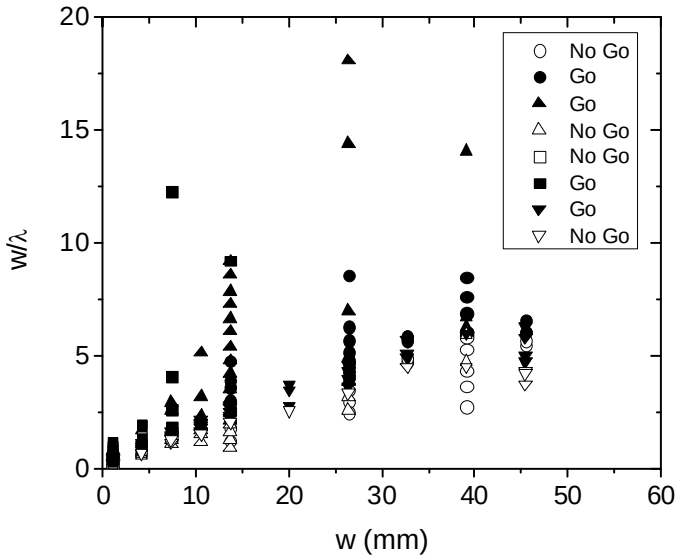

Figure 80 Results for all runs performed during this study. Each experiment was classified as either a go or no go.

Soot Foil Conditions

Figure 81 shows the location of all soot foil records shown in Appendix B. It should be noted that the majority of soot foil records are for conditions where transmission was successful, but w/λ was less than 5.7.

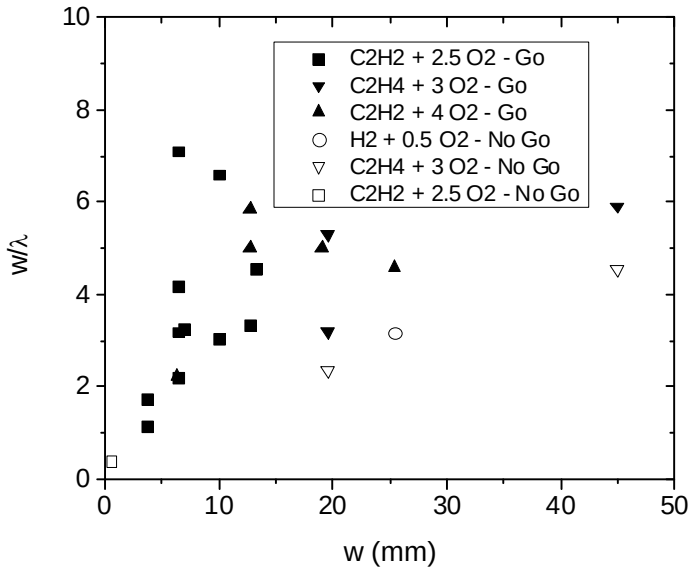

Figure 81 Conditions with soot foil records. All soot foils represented on this plot are shown in the Appendix B.

Critical Conditions

Finally, it was possible to define the critical conditions for transmission of a planar detonation into a confined volume. In this study, the data point classified as a "go" with the largest value of λ and the data point classified as a "no go" with the smallest value of λ were defined as the critical points.

The critical conditions are plotted on graphs of w/λ vs. w and λ_s/λ vs. w in Figs. 82-91. The dotted lines shown in the plots of w/λ vs. w represent a zone where transmission may or may not occur. Above this region, transmission will always occur, while below this region transmission will never occur. The corresponding pressure profile obtained for each test represented in Figs. 82-91 is given in Appendix A

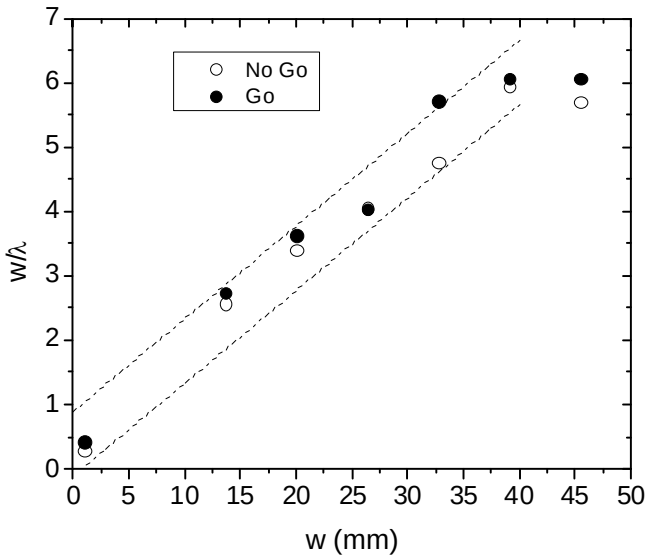

Figure 82 Critical conditions for H_2 + 0.5 O_2 plotted as w/λ vs w.

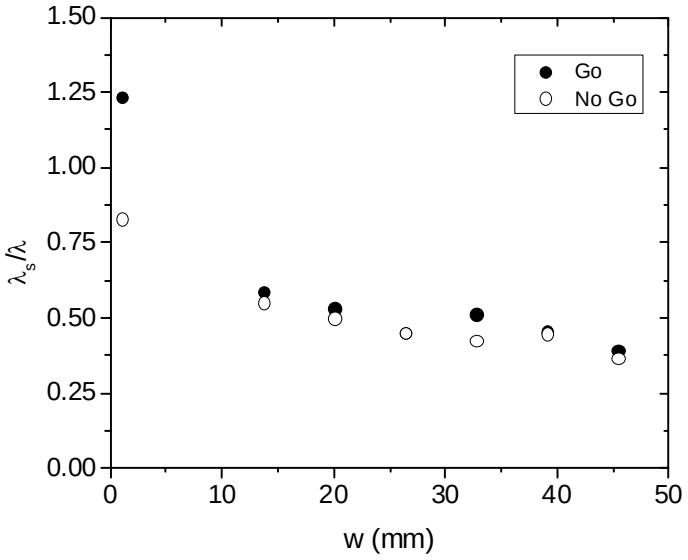

Figure 83 Critical conditions for H_2 + 0.5 O_2 plotted as λ_s/λ vs w.

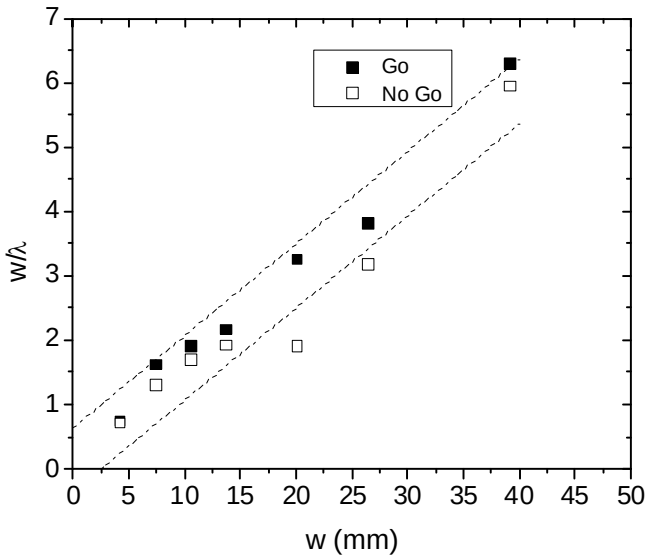

Figure 84 Critical conditions for $C_2H_2 + 4\ O_2$ plotted as w/λ vs w.

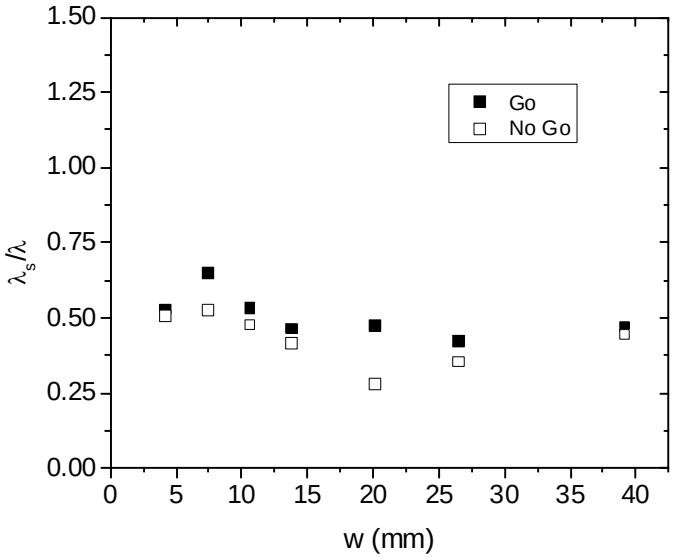

Figure 85 Critical conditions for $C_2H_2 + 4\ O_2$ plotted as λ_s/λ vs w.

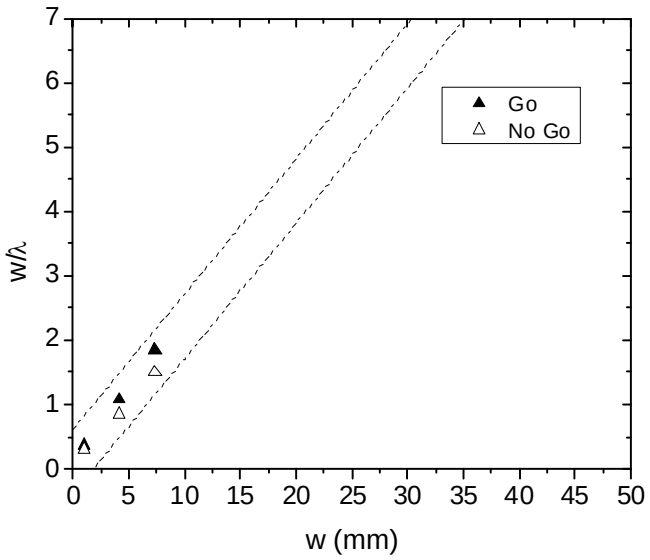

Figure 86 Critical conditions for C_2H_2 + 2.5 O_2 plotted w/λ vs w. Because only a few data points at small gap sizes were able to be collected for this mixture, critical conditions at larger gap sizes should not be extrapolated.

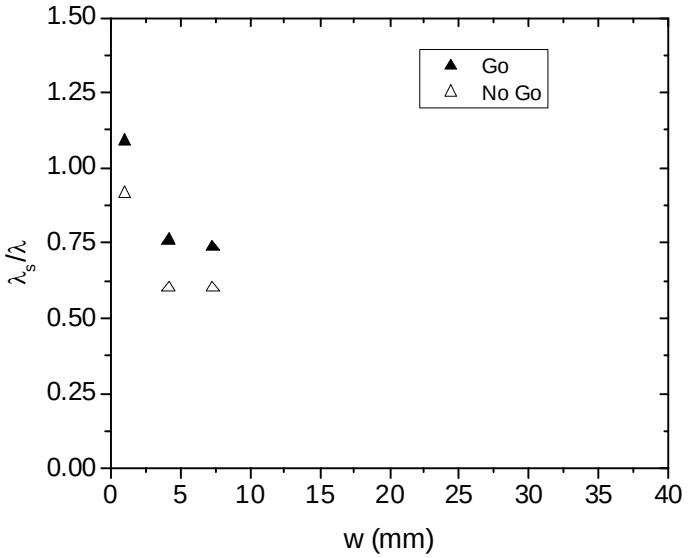

Figure 87 Critical conditions for C_2H_2 + 2.5 O_2 plotted as λ_s/λ vs w.

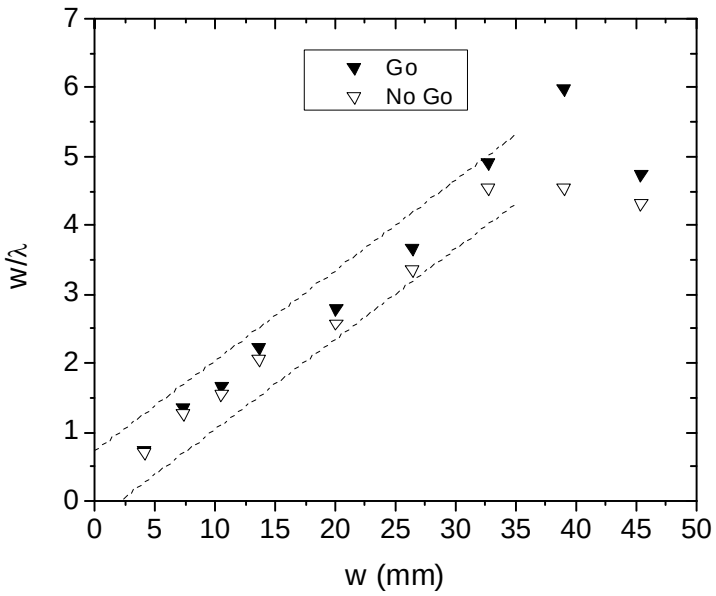

Figure 88 Critical conditions for $C_2H_4 + 3\ O_2$ plotted as w/λ vs w.

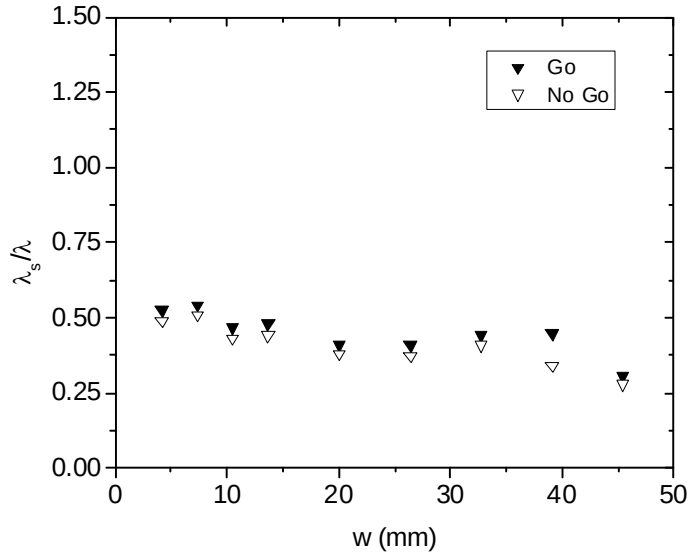

Figure 89 Critical conditions for $C_2H_4 + 3\ O_2$ plotted as λ_s/λ vs w.

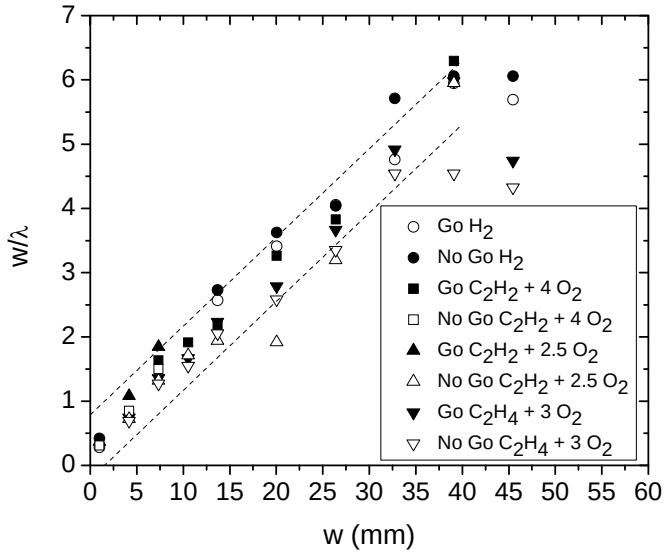

Figure 90 Universal critical conditions plotted as w/λ vs w.

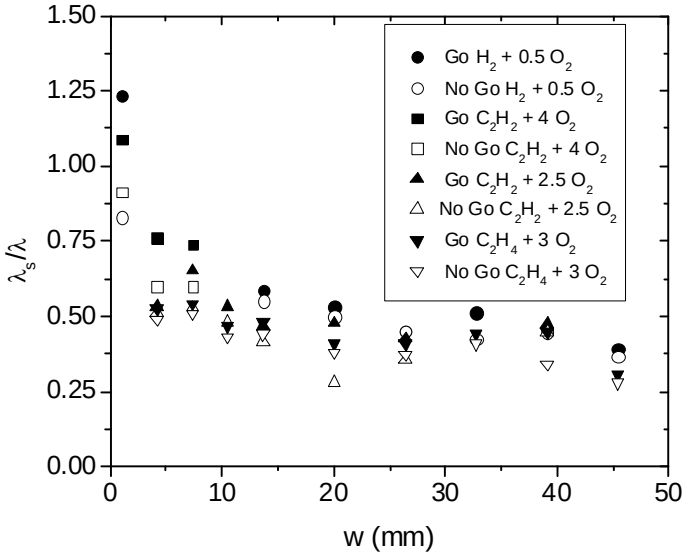

Figure 91 Universal critical conditions plotted as λ_s/λ vs w.

The plots of w/λ vs. w shows that the value of w/λ for which transmission is possible decreases as the gap size is decreased when the gap size is smaller than approximately 35 mm, but is constant for gap sizes above 35 mm. Also, if the plateau region, seen in Fig. 82 and Fig. 88, observed at gap sizes larger than 35 mm, is neglected, the trend for the plots of w/λ vs. w appears linear. However, by examining the plots of λ_s/λ vs. w it can be seen that the trend is only linear for gap sizes from 10 mm to 35 mm. Because λ_s is constant, w/λ vs. w will be linear if λ_s/λ vs. w is constant and, as seen in Figures 83, 85, 89 and 91, λ_s/λ is approximately constant for values of w between 10 and 35 mm. For gap sizes less than 10 mm, the value of λ_s/λ is no longer constant and increases as w decreases.

However, linear fits were performed for gap sizes between 10 and 35 mm, and the results are shown in Table 9. For all fits, the R^2 value was above 0.90. Again, it is important to note that the boundaries defined by the equations in Table 9 are approximate as indicated by the region marked with the dashed lines in Figs. 82, 84, 86, 88 and 90.

Table 9 Equations of linear fit performed for critical conditions

Mixture	Equation of Linear Fit	R^2 Value
$H_2 + 0.5\ O_2$	$w/\lambda = 0.133\ w + 0.735$	0.913
$C_2H_2 + 4\ O_2$	$w/\lambda = 0.151\ w - 0.0944$	0.906
$C_2H_2 + 2.5\ O_2$	Linear Fit Not valid	--
$C_2H_4 + 3\ O_2$	$w/\lambda = 0.133\ w + 0.175$	0.962
Universal	$w/\lambda = 0.140\ w + 0.237$	0.929

Figures 83, 85, 87, 89 and 91 show that λ_s/λ is less than 1 for all gap sizes other than 1 mm. As noted earlier, this result indicates that for a set of initial conditions the transmission of a detonation into a confined volume is easier than transmission of a detonation into an unconfined volume. This was expected because the reflection of the diffracted shock wave and endwall should produce conditions capable of re-initiating a detonation under conditions where a detonation diffracting into an unconfined volume might fail. However, it is interesting to note that it is actually harder to successfully transmit a detonation into a confined volume than into an unconfined volume for a 1 mm gap because λ_s/λ is greater than 1.

Comparison With Previous Results

Finally, the results of this study can be compared to the results of Murray and Lee (1983) as well as Sorin et al. (2009). The results of Murray and Lee (1983) showed

that transmission was not possible for values of w/λ less than 5.7. They hypothesized that this may be due to the hydrodynamic thickness of the detonation wave and the fact that the sonic plane behind the detonation wave may need to completely emerge from the tube for transmission into another geometry to be successful.

However, the results obtained during this study, shown in Figs. 82- 90 are clearly different. The present study shows that as the gap size is decreased, transmission becomes possible for smaller values of w/λ. In fact, at the smallest gap size tested of 1 mm, pressure signals indicated successful transmission for values of w/λ as small as 0.31.

Also, at larger gap sizes, Figs. 82 and 88 show that a plateau is reached where gap size no longer affects the value of w/λ at which transmission is successful. For stoichiometric hydrogen-oxygen, this plateau occurred at $w/\lambda \approx 6$, and for stoichiometric ethylene-oxygen this plateau occurred at $w/\lambda \approx 4.5$. It is interesting to note that these plateaus are near the transmission of $w/\lambda = 5.7$ observed by Murray and Lee (1983) for all gap sizes.

Figure 92 compares the results of the present study with the combined experimental results of Murray and Lee (1983) and Sorin et al. (2009). It should be noted that Fig. 92 shows all experimental data available on the transformation of a planar detonation wave to a cylindrical detonation wave. The qualitative trend of the studies is similar, but the results are quantitatively different. All three studies show that as w/D decreases below a certain value, λ_s/λ begins to increase. However, λ_s/λ was relatively constant in the current study for over the range of $0.25 < w/D < 1.19$, while a distinct

minimum around w/D = 1 was observed by Murray and Lee (1983) and Sorin et al. (2009). Clearly, more experimental work needs to be conducted at values of w/D less than 0.5 and values of w/D greater than 1.25 to verify the trends seen in these three studies.

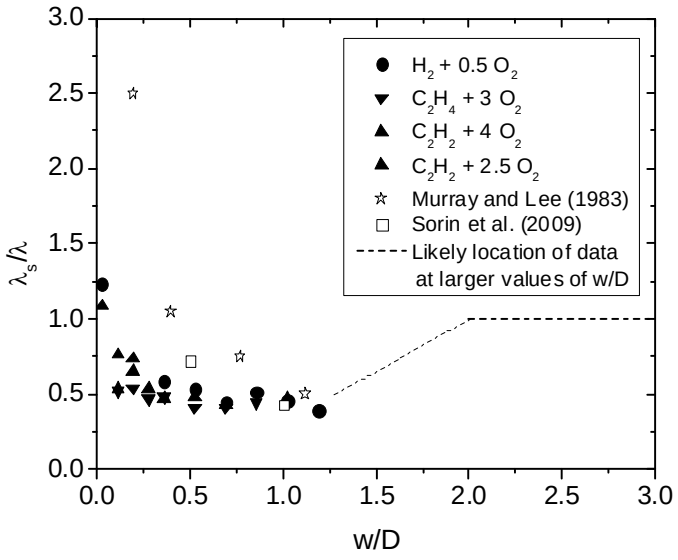

Figure 92 Comparison of results from current study with the results of Murray and Lee (1983) and Sorin et al. (2009).

CHAPTER VI

SUMMARY AND CONCLUSIONS

While the problem of detonation diffraction into an unconfined volume has been extensively researched, there has much less work on detonation diffraction into a confined volume. Therefore, experiments were conducted in which a planar detonation wave was allowed to diffract into a confined volume for four different fuel-oxidizer mixtures. The width of the confined volume was varied from 1 mm to 45.45 mm.

Empirical correlations were developed for the conditions under which successful transmission of a planar detonation into a cylindrical volume is possible. A universal correlation of $w/\lambda = 0.138\ w + 0.289$, where w is in mm, was developed for gap sizes of 10-35 mm. Above 40 mm, the correlation is not valid as the value of w/λ for which transmission is possible plateaus at a value of w/λ between 4.5 and 6, and below 10 mm the data are no longer linear with w.

These results differ from the previous study by Murray and Lee (1983), which found that successful transmission was only possible for values of w/λ greater than 5.7. Currently, no plausible explanation for the difference in results has been formulated.

The results of this study show that the critical conditions for transmission of a planar detonation into a confined, cylindrical volume are a function of the physical gap size as well as the dimensionless quantity w/λ. As the physical dimension of the gap size is decreased, transmission becomes possible for smaller values of w/λ. This study also showed that for gap sizes between 4.175 and 45.45 mm, transmission of a detonation into the confined volume was easier than transmission into a unconfined volume; but for

a gap size of 1 mm, successful transmission of a detonation into the confined volume was actually more difficult than transmission into an unconfined volume.

CHAPTER VII

RECOMMENDATIONS

To gain a better understanding of the effect a confining volume has on detonation diffraction, more experimental work needs to be done. The effect of variables such as tube diameter, expansion ratio, gap widths and mixture composition should be investigated. Specifically, while this study focused on fuel-oxygen mixtures, it would also be of interest to conduct tests with fuel-air and fuel-oxygen-helium/argon mixtures.

Also, Fig. 92 shows that further research should concentrate on values of w/D less than 0.5 and greater than 1.25. Tests at values of w/D less than 0.5 would help resolve the difference seen between the current study and the study by Murray and Lee (1983) while tests at values of w/D greater than 1.25 would fill in the mostly hypothetical curve seen in Fig. 92 and would experimentally demonstrate at what point the confined volume no longer plays a role in the transmission process.

Finally, adding flow visualization, in addition to pressure and soot foil data, to these experiments would be extremely valuable. While the pressure data and soot foil records used in this study allowed important conclusions to be drawn, the addition of flow visualization would only deepen the understanding of this topic and may help shed light on this topic which is currently not that well understood.

REFERENCES

Arienti, M. and Shepherd, J. E. 2005. A numerical study of detonation diffraction. *Journal of Fluid Mechanics,* **529,** 117-146.

Arienti, M. 2002. A numerical and analytical study of detonation diffraction, Doctoral Dissertation, California Institute of Technology, Pasadena, CA.

Austin, J. 2010. Personal Communication. Professor of the University of Illinois Urbana-Champaign, Aerospace Engineering Department.

Baumann, W., Urtiew, P. A. and Oppenheim, A. K. 1961. On the influence of tube diameter on the development of gaseous detonations. *Zeitschrift Fur Elektrochemie,* **65,** 898-902.

Bollinger, L. 1964. Formation of detonation waves in hydrogen-oxygen mixtures from 0.2 to 2 atmospheres initial pressure in a 54-meter long tube. NASA Technical Note D-2256, Ohio State University, Columbus, OH.

Bollinger, L., Fong, M. and Edse, R. 1961. Experimental measurements and theoretical analysis of detonation induction distances. *ARS Journal, **31,*** 588-595.

Bollinger, L. E. and Edse, R. 1959. Effect of initial pressure and temperature on the detonation induction distances in hydrogen-oxygen and acetylene-oxygen-nitrogen mixtures. *Proceedings of the Propellant Thermodynamics and Handling Conference*, July 1959.

Brown., C. J. and Thomas, G. O. 2000. Experimental studies of ignition and transition to detonation induced by the reflection and diffraction of shock waves. *Shock Waves,* **10,** 23-32.

Browne, S., Ziegler, J. and Shepherd, J. E. 2008a. Shock and detonation toolbox. GALCIT - Explosion Dynamics Laboratory, Pasadena, CA.

Browne, S., Ziegler, J. and Shepherd, J. E. 2008b. Numerical solution methods for shock and detonation jump conditions. Report FM2006.006, GALCIT - Explosion Dynamics Laboratory, Pasadena, CA.

Chan, C. K. and Dewitt, W. A. 1996. Deflagration-to-detonation transition in end gases. *Proceedings of the Combustion Institute,* **26,** 2679-2684.

Ciccarelli, G. and Dorofeev, S. 2008. Flame acceleration and transition to detonation in ducts. *Progress in Energy and Combustion Science,* **34,** 499-550.

Ciccarelli, G., Fowler, C. J. and Bardon, M. 2005. Effect of obstacle size and spacing on the initial stage of flame acceleration in a rough tube. *Shock Waves,* **14,** 161-166.

Craven, A. D. and Grieg, T. R. 1968. The development of detonation over-pressures in pipelines. *Institute of Chemical Engineers Symposium Series,* **25,** 41-50.

Dorofeev, S., Kochurko, A. S., Sidorov, V. P., Bezmelnitsin, A. V. and Breitung, W. M. 1996. Experimental and numerical studies of the pressure field generated by DDT events. *Shock Waves,* **5,** 375-379.

Edwards, D. H., Thomas, G. O. and Nettleton, M. A. 1981. Diffraction of a planar detonation in various fuel-oxygen mixtures at an area change. *Progress in Astronautics and Aeronautics,* **76,** 341-357.

Guirao, C. M., Knystautas, R. and Lee, J. H. 1989. A summary of hydrogen-air detonation experiments. Technical Report, Department of Mechanical Engineering, McGill University.

Guo, C., Wang, C., Xu, S. and Zhang, H. 2007. Cellular pattern evolution in gaseous detonation diffraction in a 90 degree-branched channel. *Combustion and Flame,* **148,** 89-99.

Jones, D. A., Michel, M. and Oran, E. S. 1995. Reignition of detonations by reflected shocks. *Shock Waves,* **5,** 47-57.

Knystautas, R., Lee, J. H. and Guirao, C. M. 1982. The critical tube diameter for detonation failure in hydrocarbon-air mixtures. *Combustion and Flame,* **48,** 63-83.

Kuznetsov, M., Alekseev, V., Matsukov, I. and Dorofeev, S. 2005. DDT in a smooth tube filled with a hydrogen-oxygen mixture. *Shock Waves,* **14,** 205-215.

Lam, A., Austin, J., Pintgen, F., Wintenberger, E., Shepherd, J. E., Inaba, K. and Matsuo, A. 2003. On the mechanism of soot track formation: experimental study. 19th *ICDERS*, July 27th-Aug.1st, Hakone, Japan.

Lee, J. H. 2008. *The Detonation Phenomenon,* Cambridge University Press, Cambridge.

Lee, S., Watts, J., Saretto, S., Pal, S., Conrad, C., Woodward, R. and Santoro, R. 2004. Deflagration to detonation transition processes by turbulence-generating obstacles in pulse detonation engines. *Journal of Propulsion and Power,* **20,** 1026-1036.

Li, J., Lai, W. H. and Chung, K. 2006. Tube diameter effect on deflagration-to-detonation transition of propane-oxygen mixtures. *Shock Waves,* **16,** 109-117.

Liang, Z., Karnesky, J., Shepherd, J. E. and Deiterding, R. 2008. Detonations in C_2H_4-O_2. Experimental measurements and validation of numerical simulation for incident and reflected waves. Report FM2006.009, GALCIT - Explosion Dynamics Laboratory, Pasadena, CA.

Liberman, M. A., Kuznetsov, M., Ivanov, A. and Matsukov, I. 2009. Formation of the preheated zone ahead of a propagating flame and the mechanism underlying the deflagration-to-detonation transition. *Physics Letters A,* **373,** 501-510.

Matsui, H. and Lee, J. H. 1978. On the measure of the relative detonation hazards of gaseous fuel-oxygen and air mixtures. Proceedings of the Combustion Institute, **17**, 1269-1279.

Mitrofanov, V. and Soloukhin, R. Soviet Physics - Doklady. The diffraction of multifront detonation waves. **12,** 1055-1058.

Murray, S. B. and Lee, J. H. 1983. On the transformation of planar detonation to cylindrical detonation. *Combustion and Flame,* **52,** 269-289.

Ohyagi, S., Obara, T., Hoshi, S. and Yoshihashi, T. 2002. Diffraction and re-initiation of detonation behind a backward-facing step. *Shock Waves,* **12,** 221-226.

Pantow, E. G., Fischer, M. and Kratzel, Th. 1996. Decoupling and recoupling of detonation waves associated with sudden expansion. *Shock Waves,* **6,** 131-137.

Papalexandris, M. V., Thomas, J. F., Jacobs, C. and Deledicque, V. 2007. Structural characteristics of detonation expansion from a small channel to a larger one. *Proceedings of the Combustion Institute,* **31,** 2407-2414.

Peraldi, O., Knystautas, R. and Lee, J. H. 1986. Criteria for transition to detonation in tubes. *Proceedings of the Combustion Institute,* **21,** 1629-1637.

Pintgen, F. and Shepherd, J. E. 2009. Detonation diffraction in gases. *Combustion and Flame,* **156,** 665-677.

Schultz, E. 2000. Detonation diffraction through an abrupt area expansion, Doctoral Dissertation, California Institute of Technology, Pasadena, CA.

Shepherd, J. E. 2009. Detonation in gases. *Proceedings of the Combustion Institute,* **32,** 83-98.

Shepherd, J. E. 1992. Pressure loads and structural response of the BNL high-temperature detonation tube. Technical Report, Mechanical Engineering Department, Rensselaer Polytechnic Institute, Troy, NY.

Shepherd, J.E., Teodorcyzk, A., Knystautas, R., Lee, J.H. 1991. Shock wave produced by reflected detonations. *Progress in Astronautics and Aeronautics.* **134**, 244-264.

Sorin, R., Zitoun, R. and Desbordes, D. 2009. Optimization of the deflagration to detonation transition: Reduction of length and time of transition. *Shock Waves,* **15,** 137-145.

Vasil'ev, A. A. and Trotsyuk, A. V. 2003. Experimental investigation and numerical simulation of an expanding multifront detonation wave. *Combustion Explosion and Shock Waves,* **39,** 80-90.

Vasil'ev, A. A. 1998. Critical conditions for initiation of cylindrical multifront detonation. *Combustion Explosion and Shock Waves,* **34,** 220-225.

Wang, B. L., Habermann, M., Lenartz, M., Olivier, H. and Gronig, H. 2000. Detonation formation in H_2-O_2/He/Ar mixtures at elevated initial pressures. *Shock Waves,* **10,** 295-300.

Wang, C. J. and Xu, S. L. 2007. Re-initiation phenomenon of gaseous detonation induced by shock reflection. *Shock Waves,* **16,** 247-256.

Zhang, F., Thibault, P. A. and Murray, S. B. 1998. Transition from deflagration to detonation in an end multiphase slug. *Combustion and Flame,* **114,** 13-25.

APPENDICES

APPENDIX A

PRESSURE TRACES FOR CRITICAL CONDITIONS

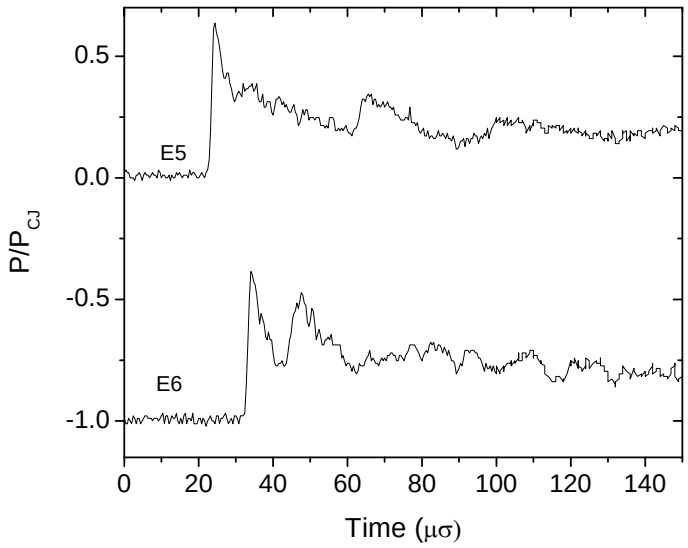

Figure A-1 Go. Run 71. 1 mm spacer. H_2+0.5 O_2.

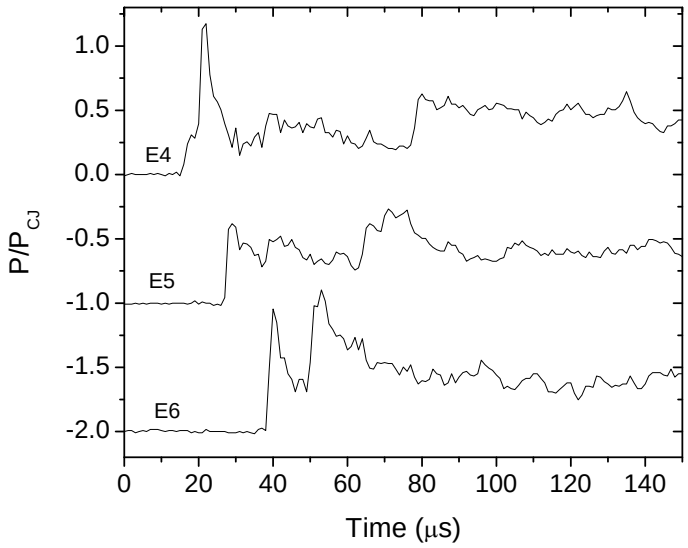

Figure A-2 Go. Run 120. 13.7 mm spacer. H_2+0.5 O_2.

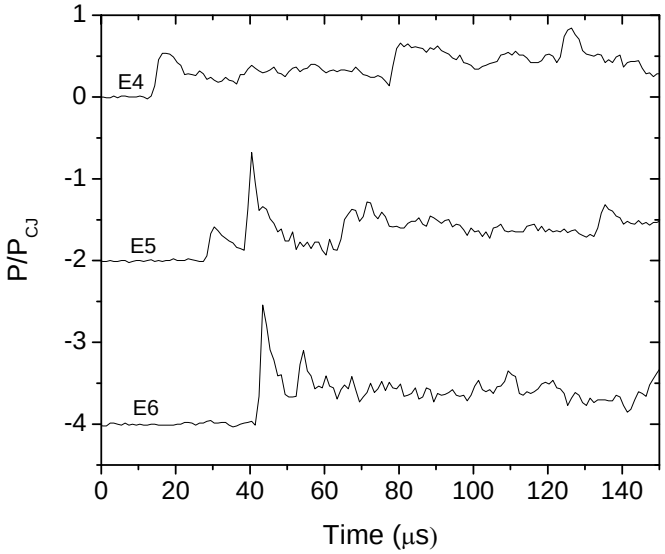

Figure A-3 Go. Run 128. 26.4 mm spacer. H_2+0.5 O_2.

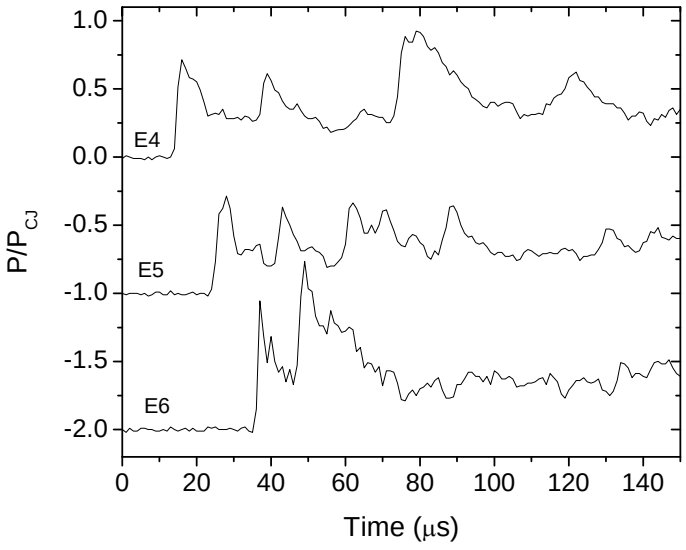

Figure A-4 Go. Run 396. 32.75 mm spacer. H_2+0.5 O_2.

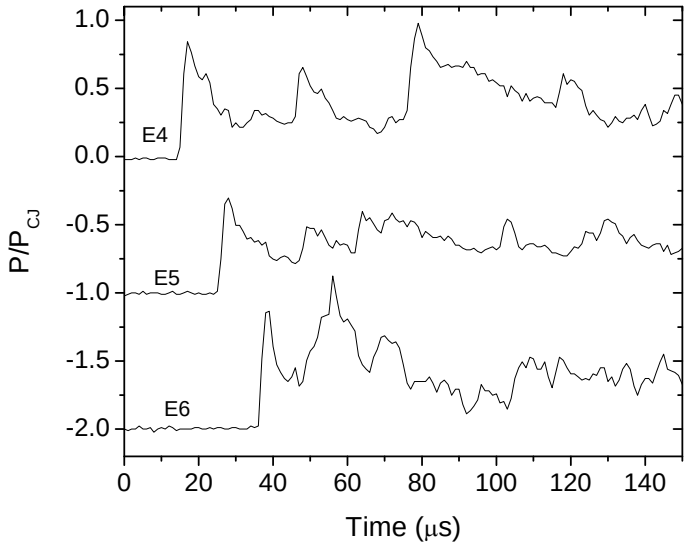

Figure A-5 Go. Run 109. 39.1 mm spacer. H_2+0.5 O_2.

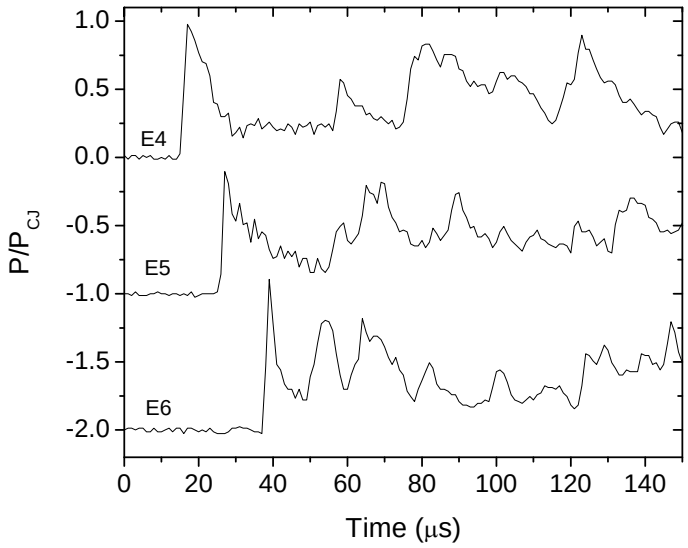

Figure A-6 Go. Run 382. 45.45 mm spacer. H_2+0.5 O_2.

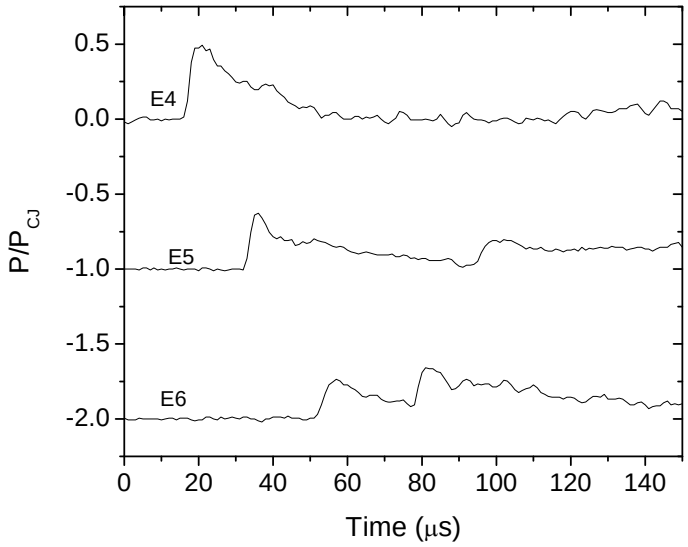

Figure A-7 No Go. Run 78. 1 mm spacer. H_2+0.5 O_2.

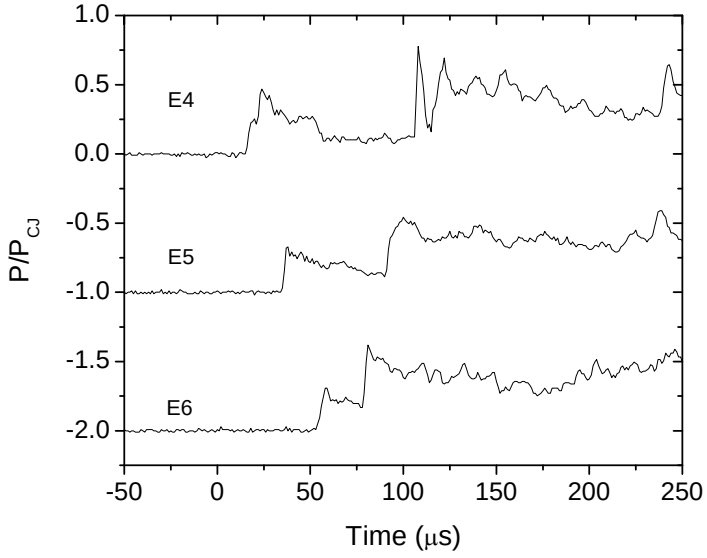

Figure A-8 No Go. Run 125. 13.7 mm spacer. H_2+0.5 O_2.

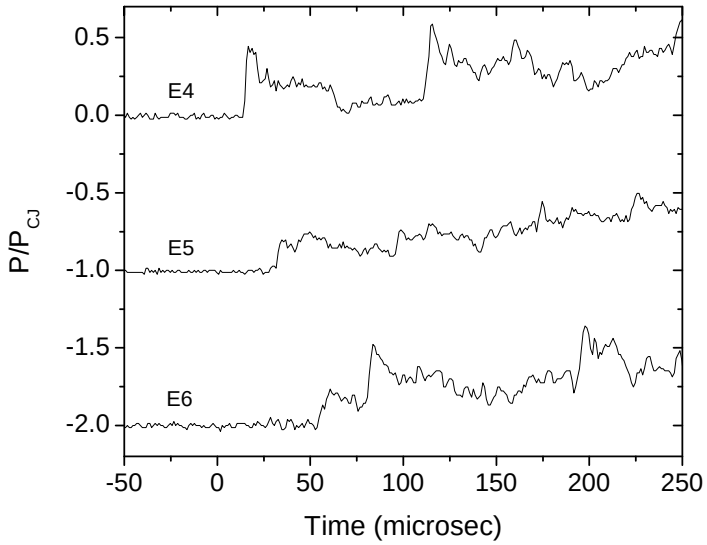

Figure A-9 No Go. Run 129. 26.4 mm spacer. H_2+0.5 O_2.

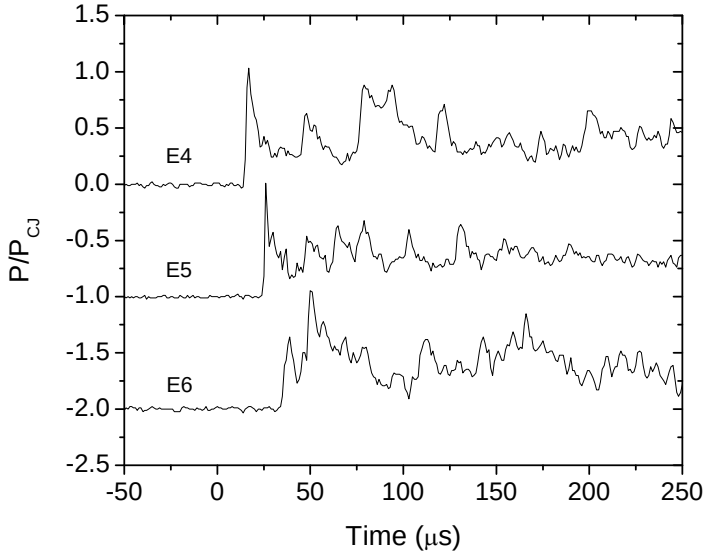

Figure A-10 No Go. Run 138. 39.1 mm spacer. H_2+0.5 O_2.

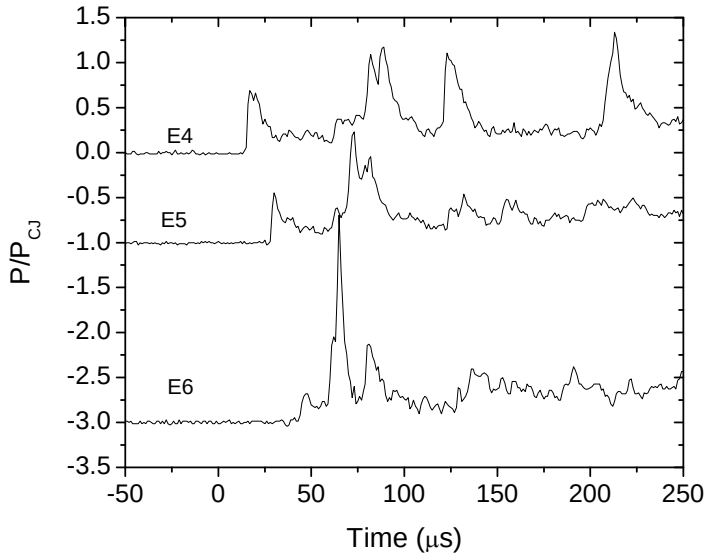

Figure A-11 No Go. Run 384. 45.45 mm spacer. H_2+0.5 O_2.

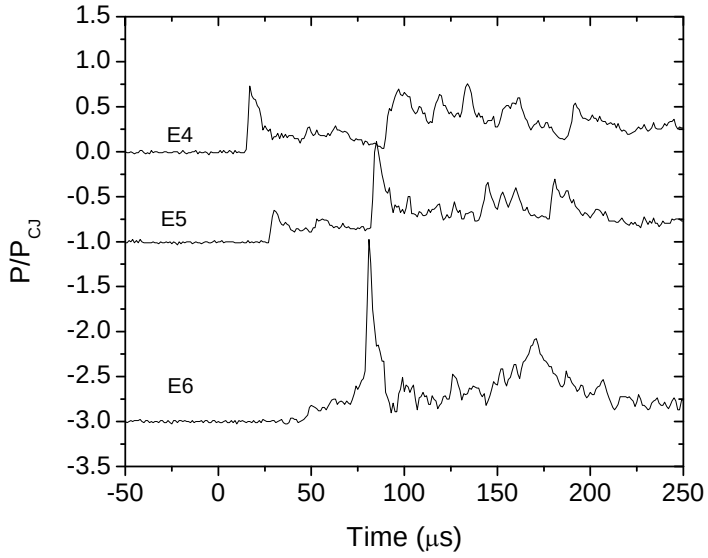

Figure A-12 No Go. Run 390. 32.75 mm spacer. H_2+0.5 O_2.

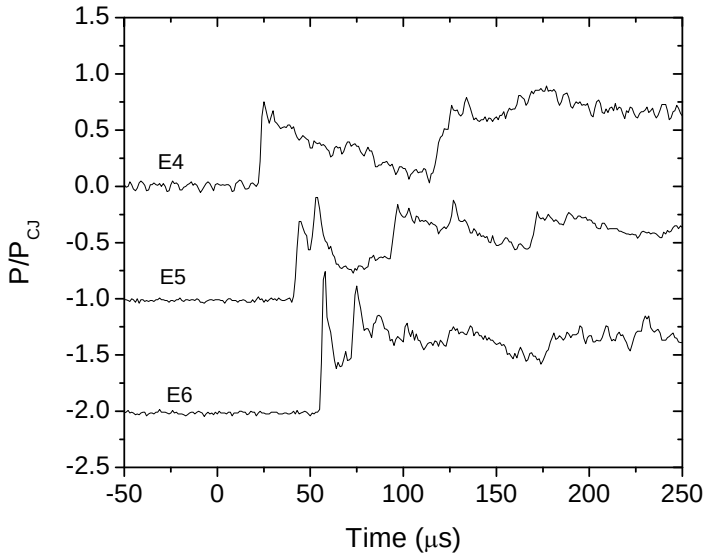

Figure A-13 Go. Run 204. 4.175 mm spacer. C_2H_2+4 O_2.

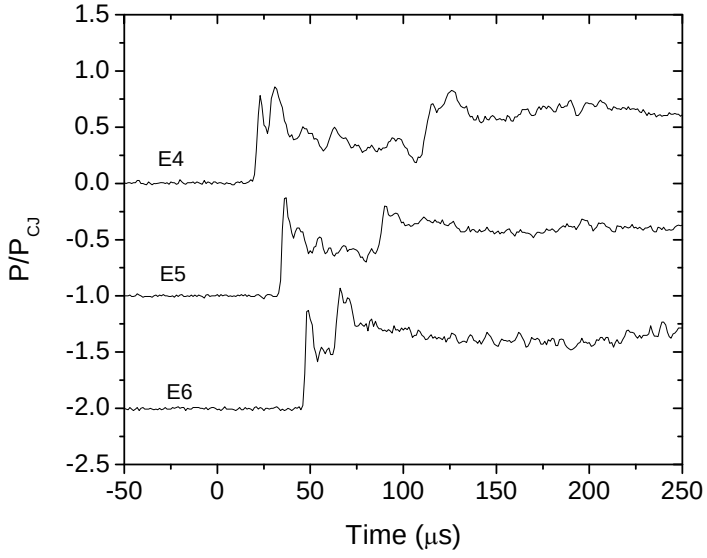

Figure A-14 Go. Run 195. 7.35 mm spacer. C_2H_2+4 O_2.

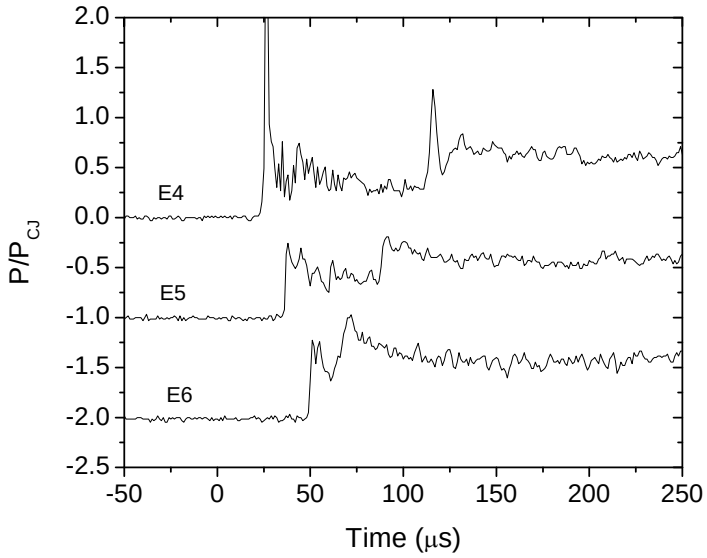

Figure A-15 Go. Run 211. 10.525 mm spacer. C_2H_2+4 O_2.

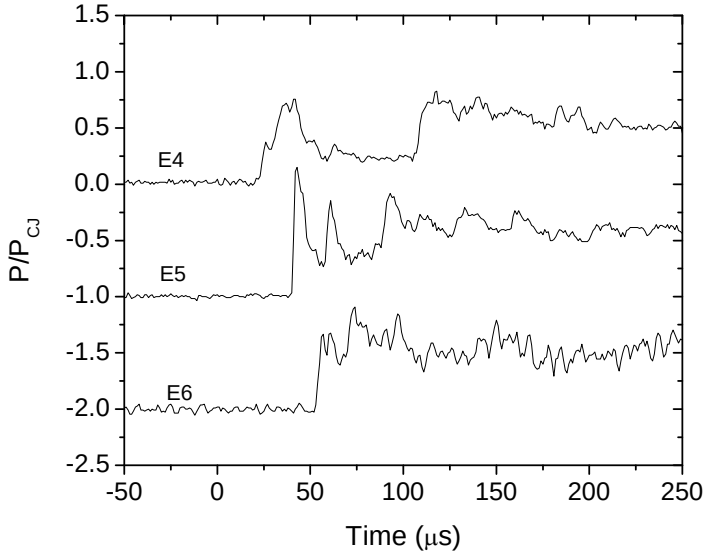

Figure A-16 Go. Run 166. 13.7 mm spacer. C_2H_2+4 O_2.

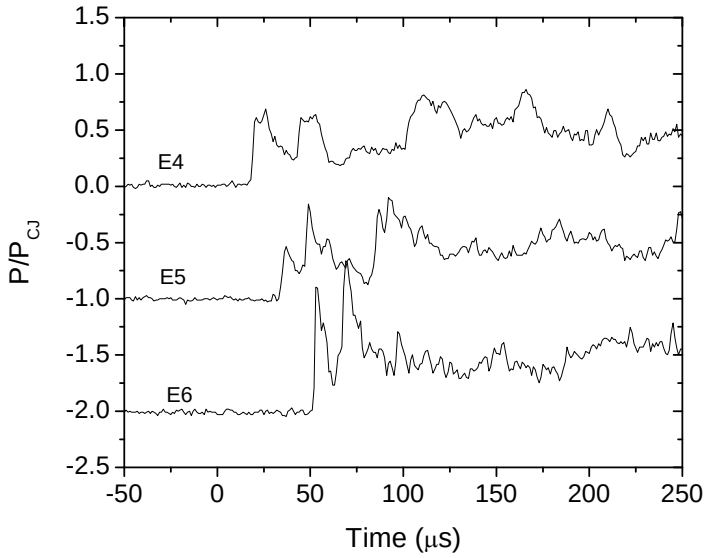

Figure A-17 Go. Run 162. 26.4 mm spacer. C_2H_2+4 O_2.

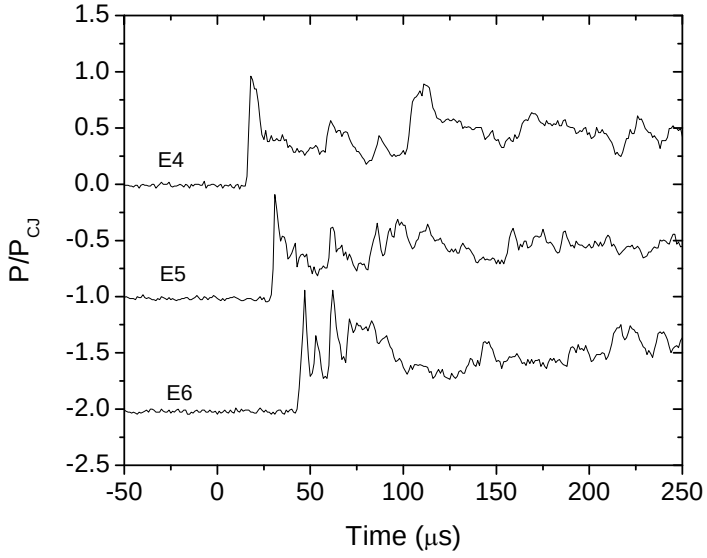

Figure A-18 Go. Run 235. 39.1 mm spacer. C_2H_2+4 O_2.

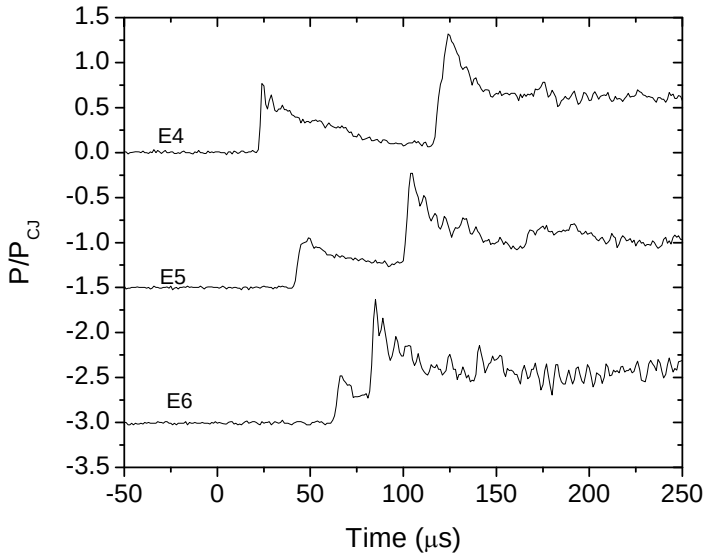

Figure A-19 Go. Run 206. 4.175 mm spacer. C_2H_2+4 O_2.

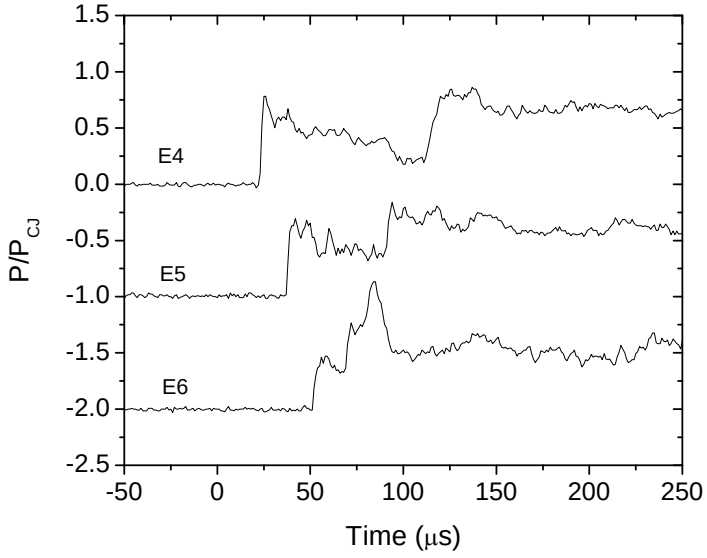

Figure A-20 Go. Run 186. 7.35 mm spacer. C_2H_2+4 O_2.

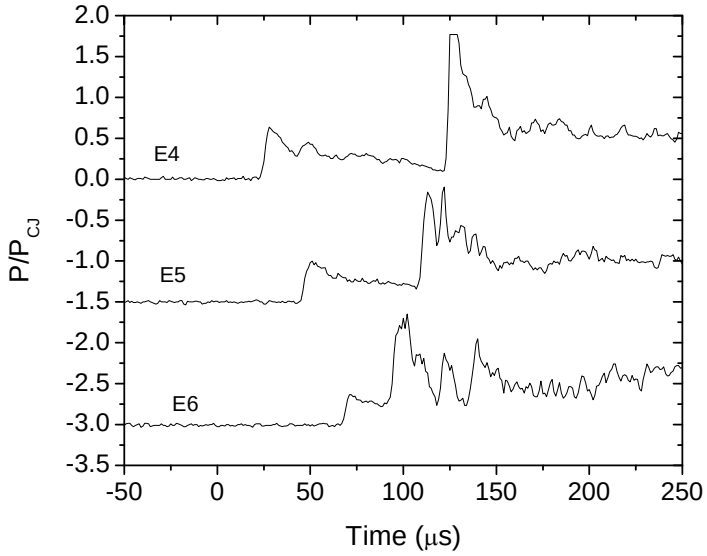

Figure A-21 Go. Run 214. 10.525 mm spacer. C_2H_2+4 O_2.

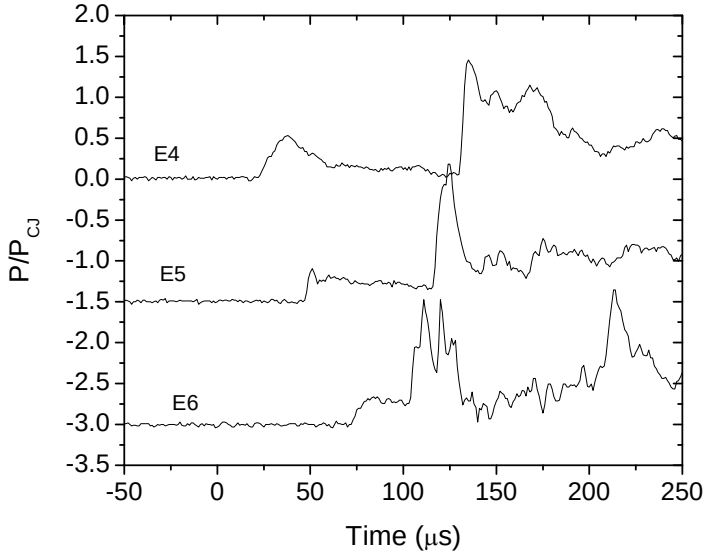

Figure A-22 Go. Run 182. 13.7 mm spacer. C_2H_2+4 O_2.

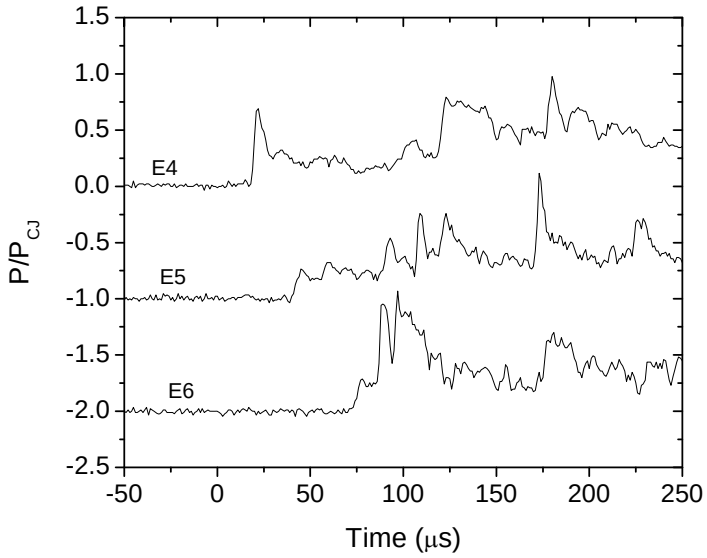

Figure A-23 Go. Run 164. 26.4 mm spacer. C_2H_2+4 O_2.

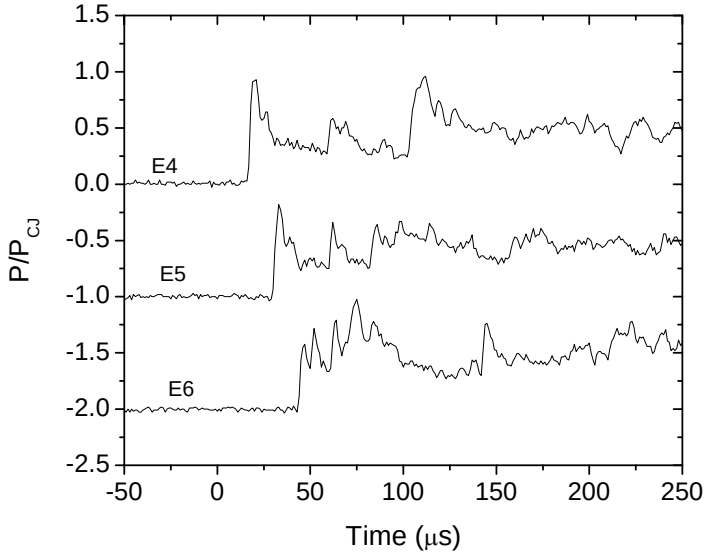

Figure A-24 Go. Run 234. 39.1 mm spacer. C_2H_2+4 O_2.

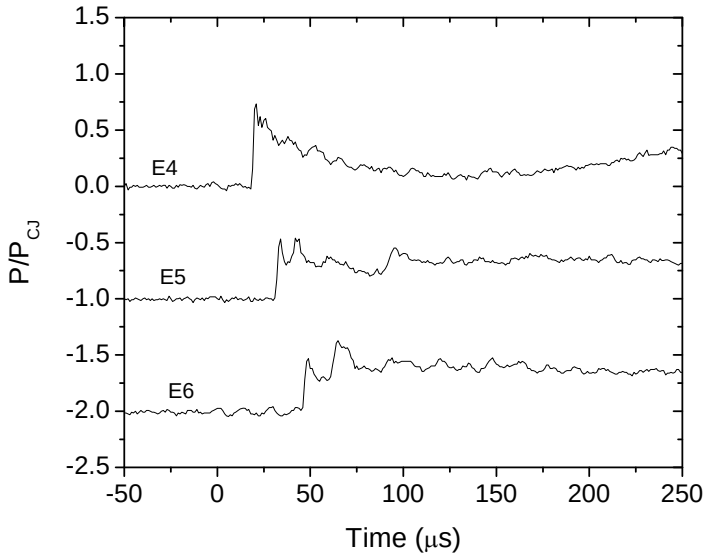

Figure A-25 Go. Run 307. 1 mm spacer. C_2H_2+2.5 O_2.

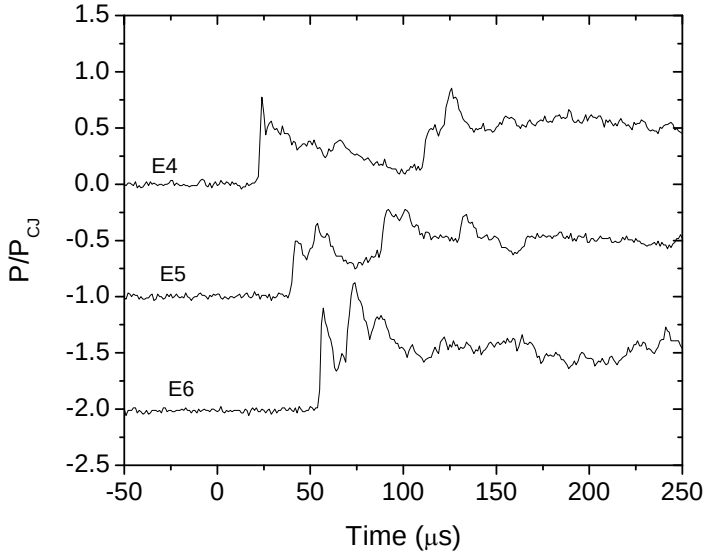

Figure A-26 Go. Run 310. 4.175 mm spacer. C_2H_2+2.5 O_2.

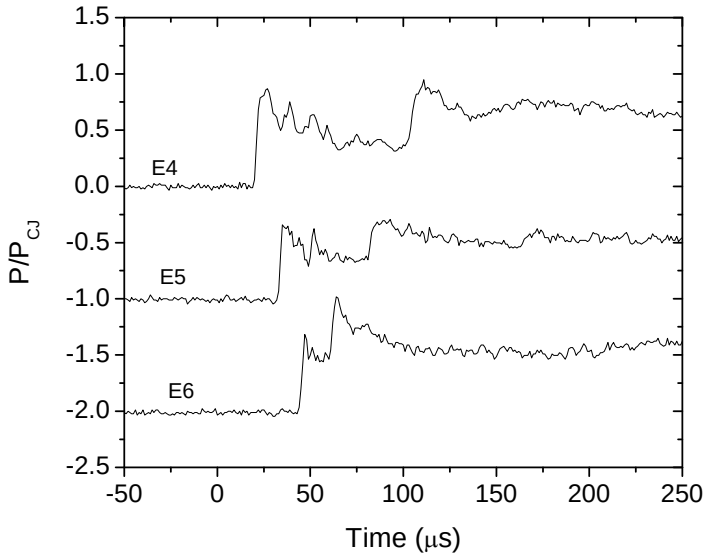

Figure A-27 Go. Run 313. 7.35 mm spacer. C_2H_2+2.5 O_2.

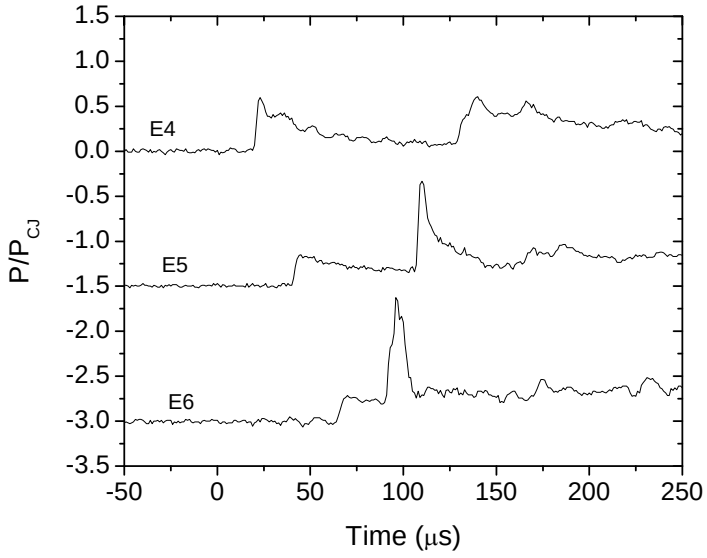

Figure A-28 No Go. Run 305. 1 mm spacer. C_2H_2+2.5 O_2.

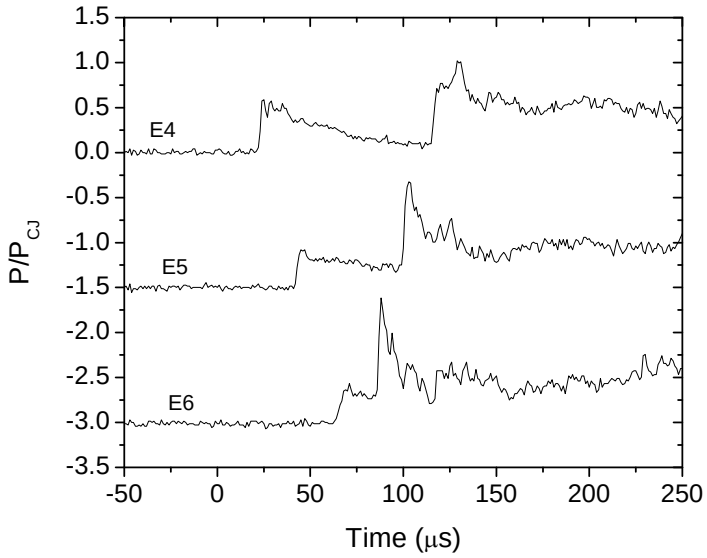

Figure A-29 No Go. Run 309. 4.175 mm spacer. C_2H_2+2.5 O_2.

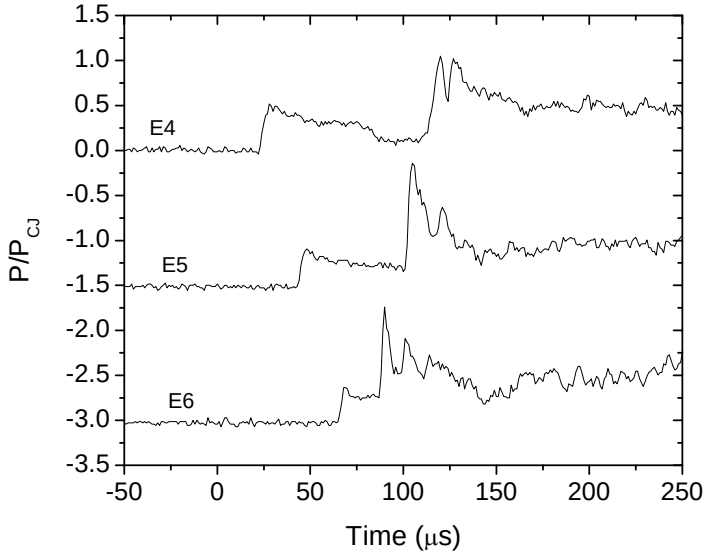

Figure A-30 No Go. Run 312. 7.35 mm spacer. C_2H_2+2.5 O_2.

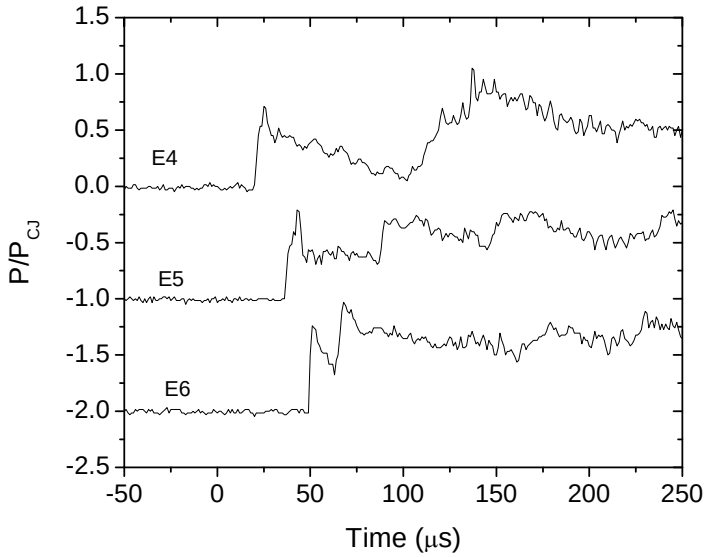

Figure A-31 Go. Run 365. 4.175 mm spacer. C_2H_4+3 O_2.

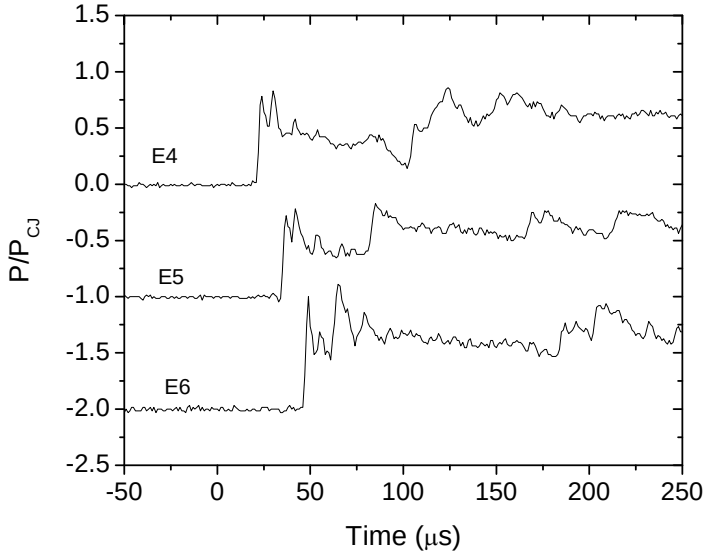

Figure A-32 Go. Run 315. 7.35 mm spacer. C_2H_4+3 O_2.

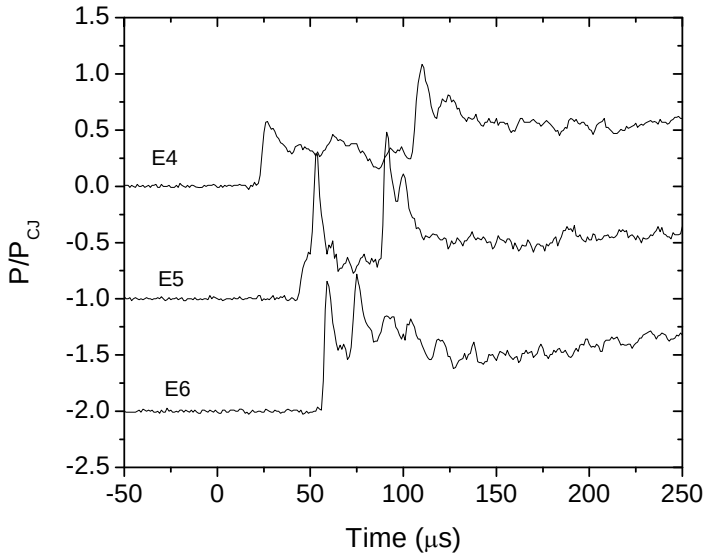

Figure A-33 Go. Run 356. 10.525 mm spacer. C_2H_4+3 O_2.

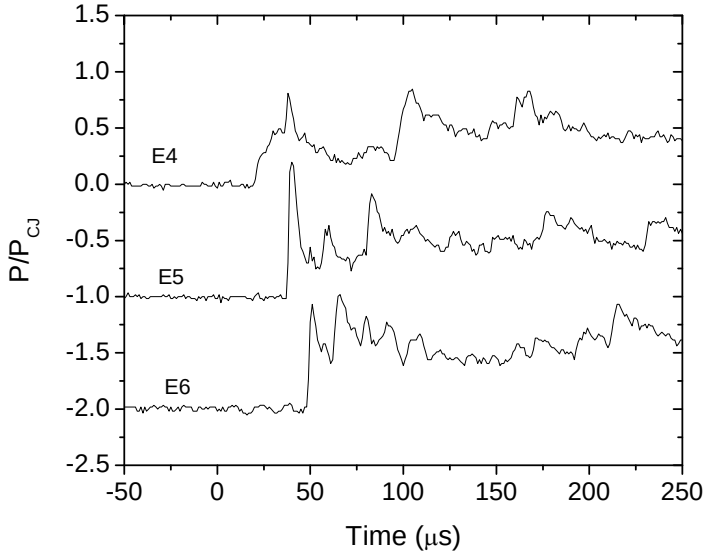

Figure A-34 Go. Run 351. 13.7 mm spacer. C_2H_4+3 O_2.

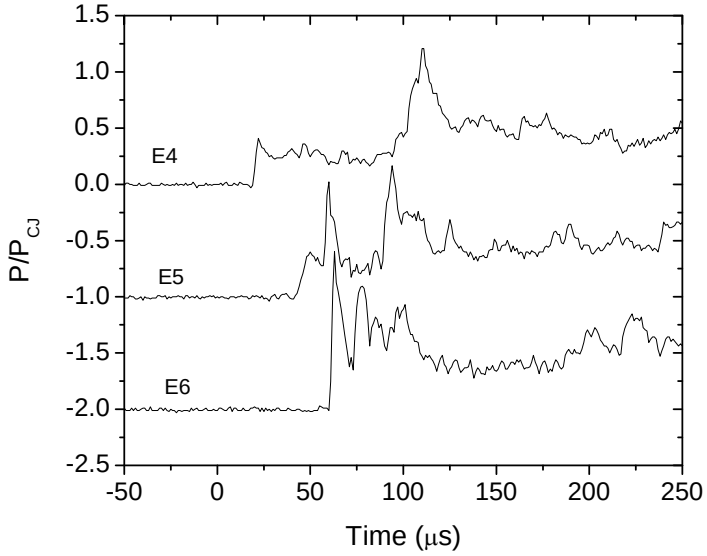

Figure A-35 Go. Run 343. 20.05 mm spacer. C_2H_4+3 O_2.

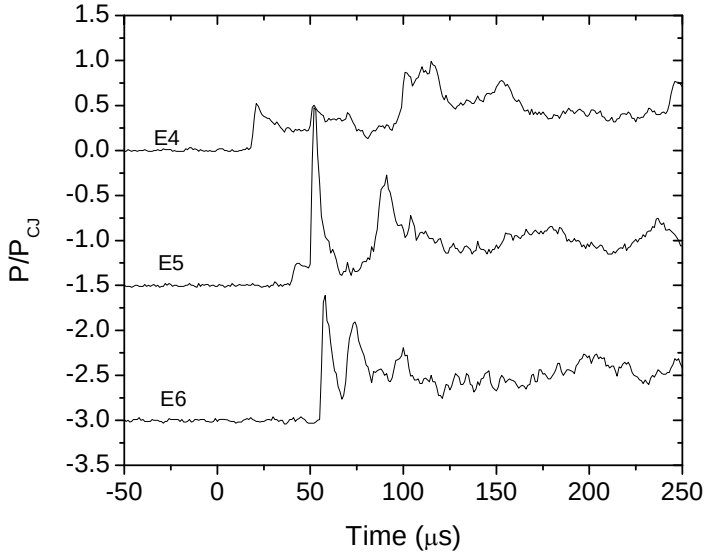

Figure A-36 Go. Run 338. 26.4 mm spacer. C_2H_4+3 O_2.

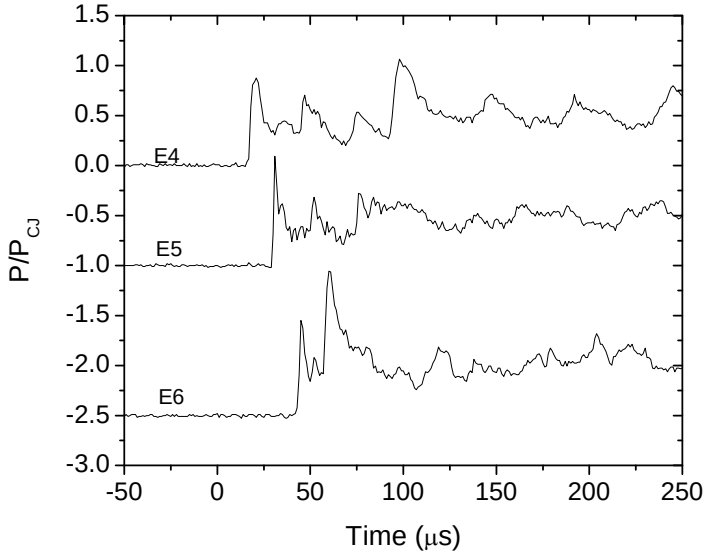

Figure A-37 Go. Run 332. 32.75 mm spacer. C_2H_4+3 O_2.

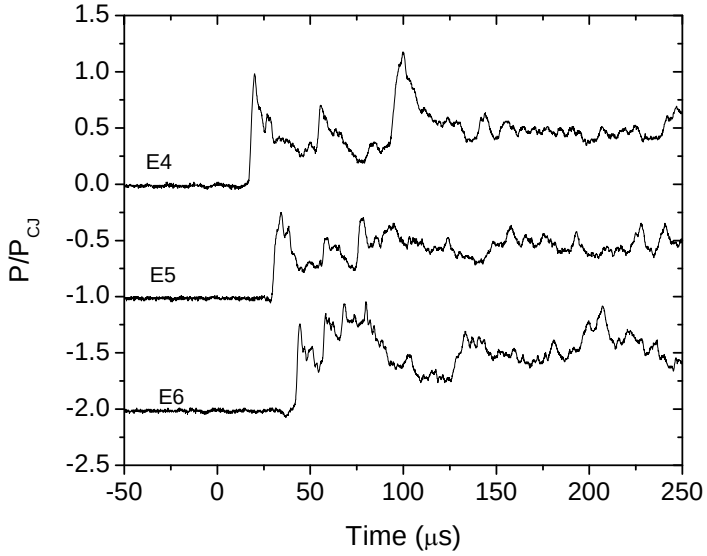

Figure A-38 Go. Run 326. 39.1 mm spacer. C_2H_4+3 O_2.

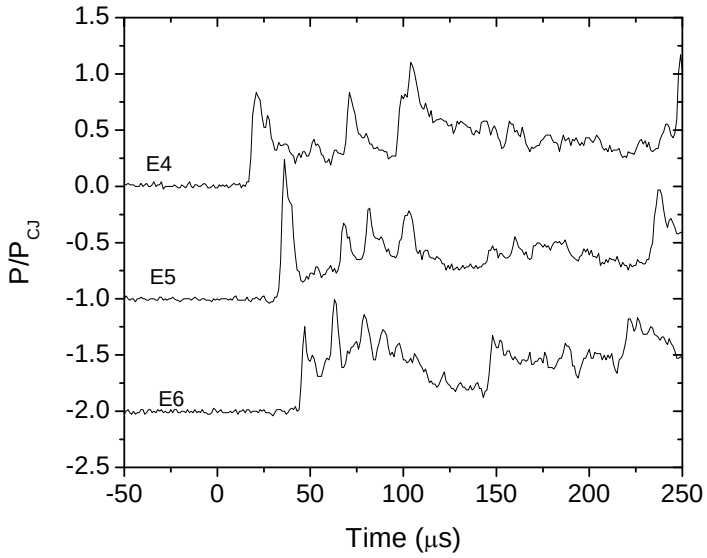

Figure A-39 Go. Run 372. 45.45 mm spacer. C_2H_4+3 O_2.

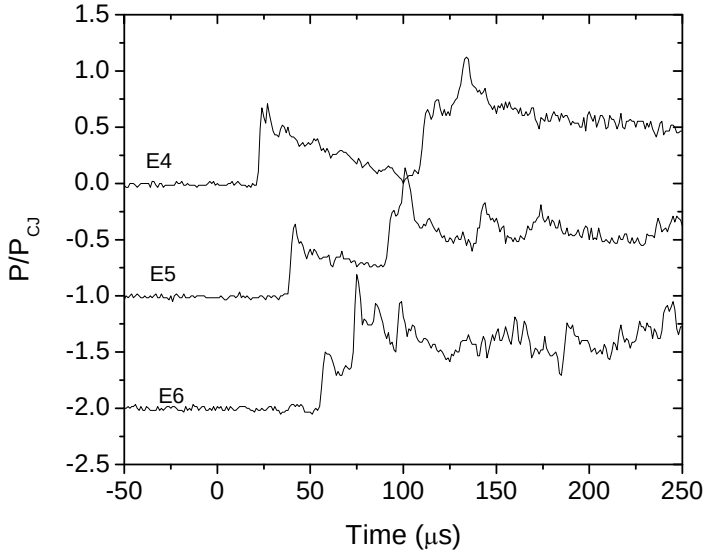

Figure A-40 No Go. Run 366. 4.175 mm spacer. C_2H_4+3 O_2.

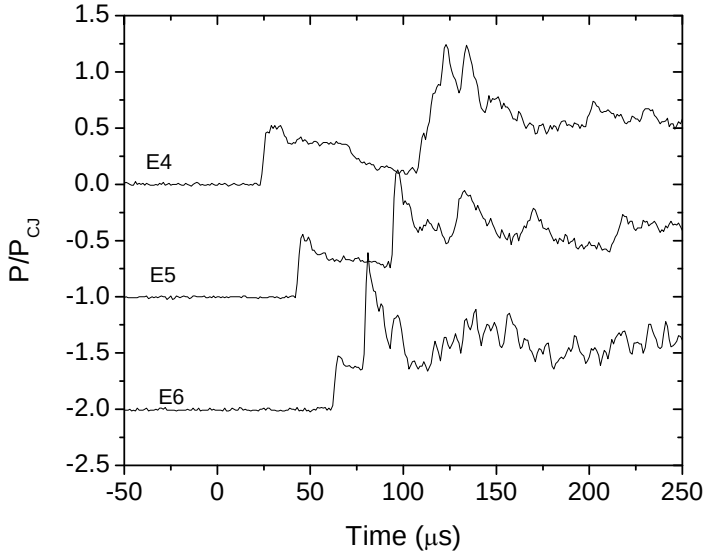

Figure A-41 No Go. Run 317. 7.35 mm spacer. C_2H_4+3 O_2.

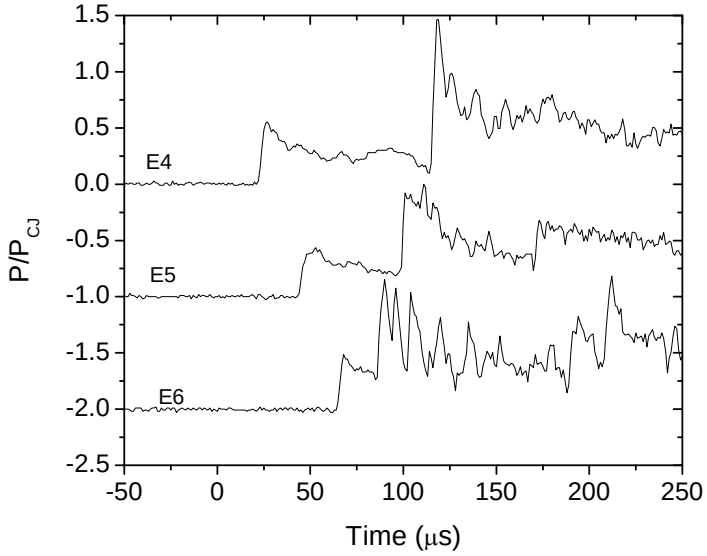

Figure A-42 No Go. Run 357. 10.525 mm spacer. C_2H_4+3 O_2.

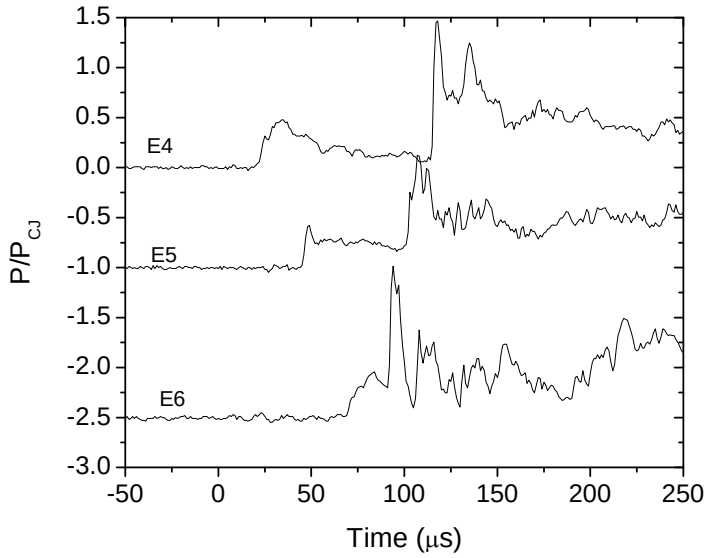

Figure A-43 No Go. Run 348. 13.7 mm spacer. C_2H_4+3 O_2.

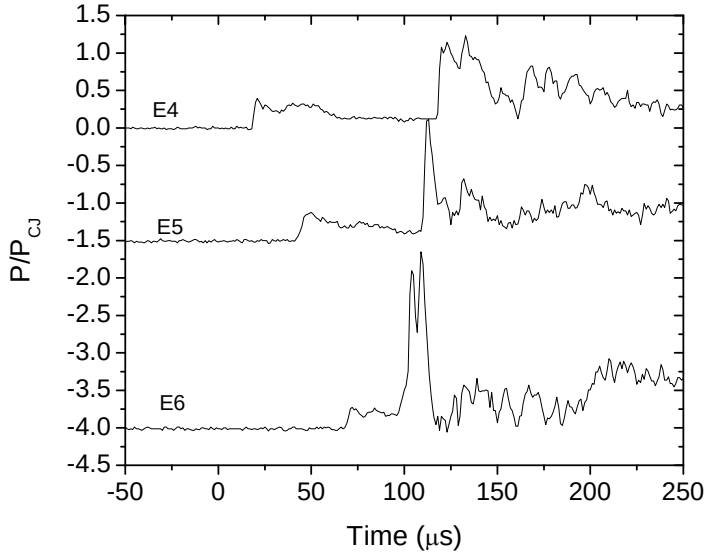

Figure A-44 No Go. Run 344. 20.05 mm spacer. C_2H_4+3 O_2.

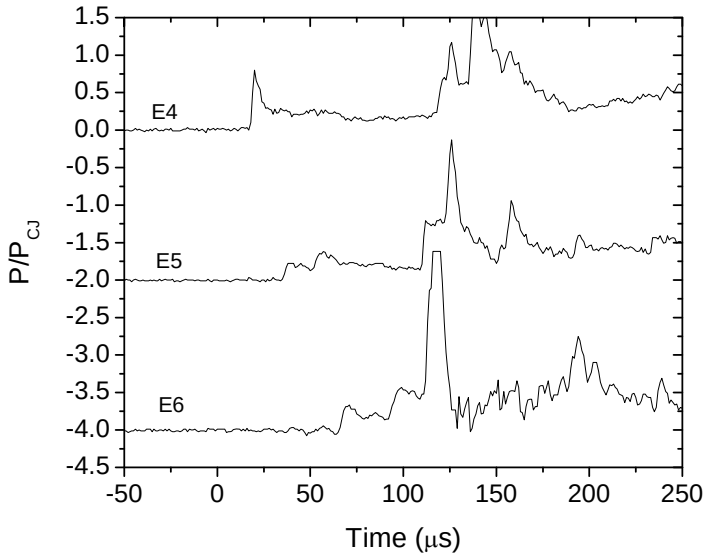

Figure A-45 No Go. Run 339. 26.4 mm spacer. C_2H_4+3 O_2.

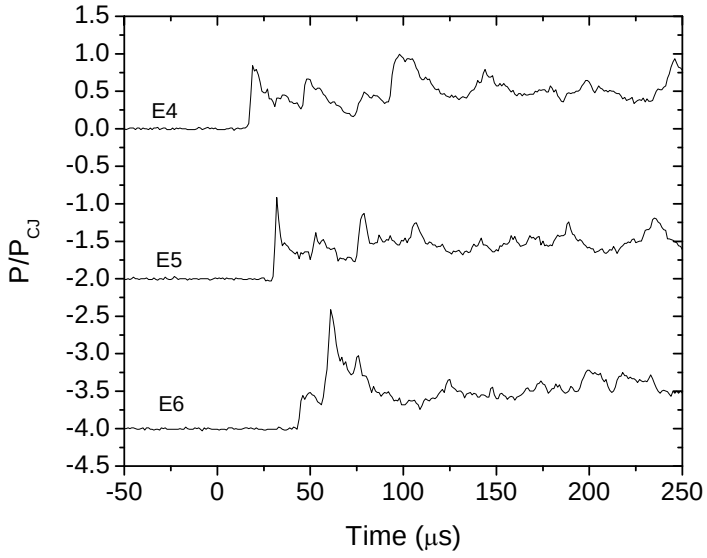

Figure A-46 No Go. Run 333. 32.75 mm spacer. C_2H_4+3 O_2.

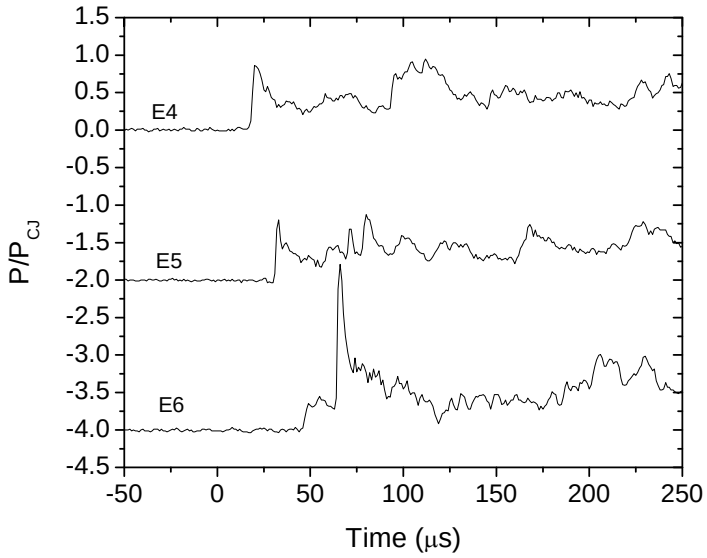

Figure A-47 No Go. Run 329. 39.1 mm spacer. C_2H_4+3 O_2.

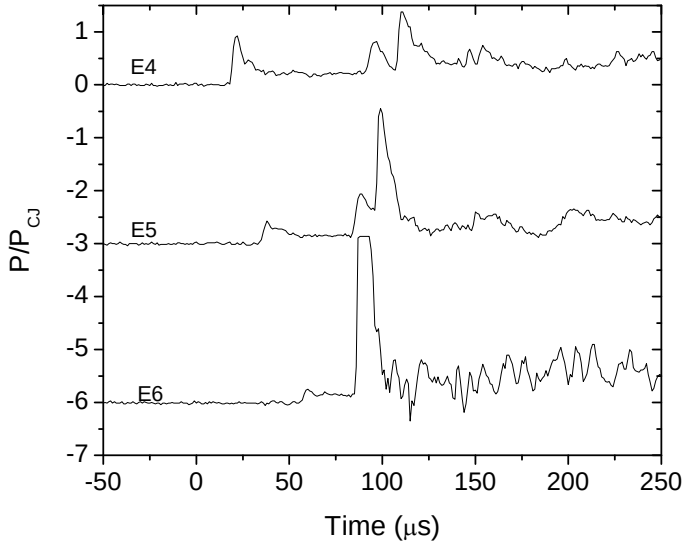

Figure A-48 No Go. Run 321. 45.45 mm spacer. C_2H_4+3 O_2.

APPENDIX B

SOOT FOIL RECORDS

Figure B-1 No Go. Run 143. 26.4 mm spacer. H_2+0.5 O_2. w/λ = 3.18.

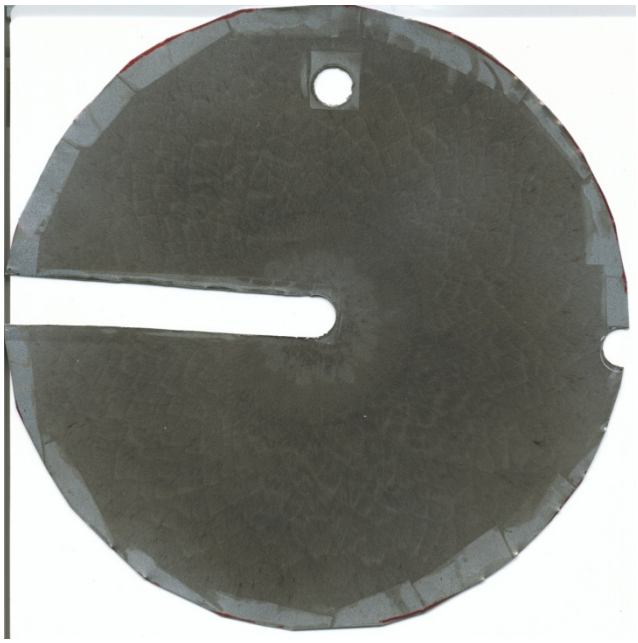

Figure B-2 Go. Run 227. 20.05 mm spacer. C_2H_2+4 O_2. w/λ = 5.02.

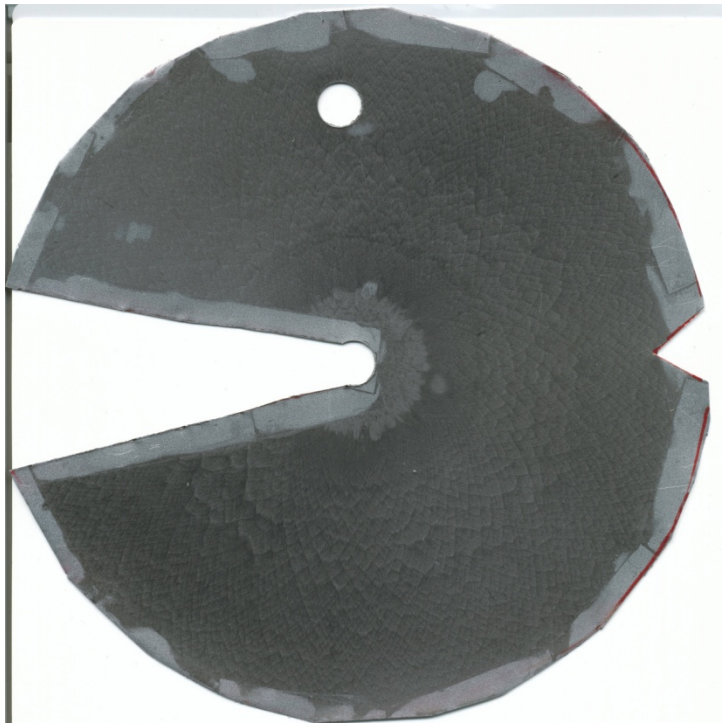

Figure B-3 Go. Run 237. 13.7 mm spacer. C_2H_2+4 O_2. w/λ = 5.86.

Figure B-4 Go. Run 240. 13.7 mm spacer. C_2H_2+4 O_2. w/λ = 5.02. Front wall.

Figure B-5 Go. Run 240. 13.7 mm spacer. C_2H_2+4 O_2. w/λ = 5.02. Back wall.

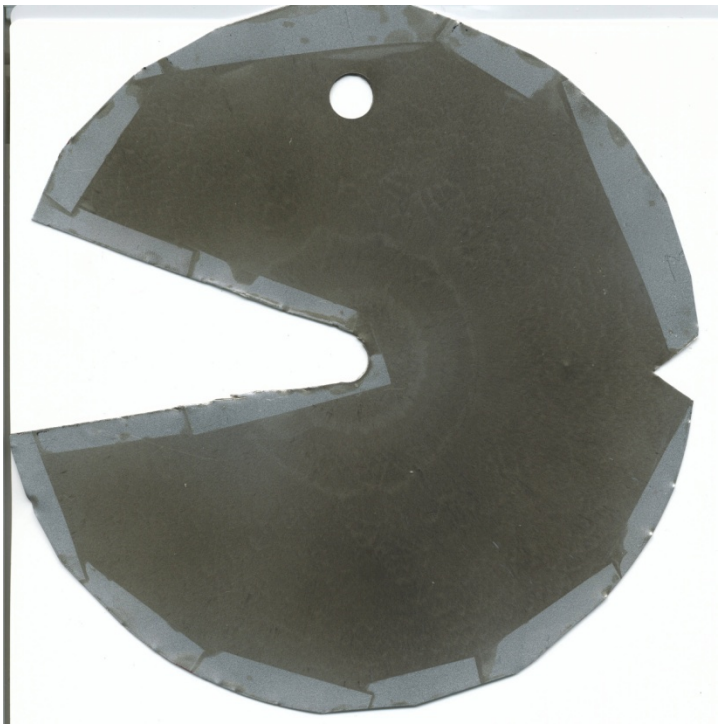

Figure B-6 Go. Run 243. 7.35 mm spacer. C_2H_2+4 O_2. w/λ = 2.23.

Figure B-7 Go. Run 244. 26.4 mm spacer. C_2H_2+4 O_2. w/λ = 4.6.

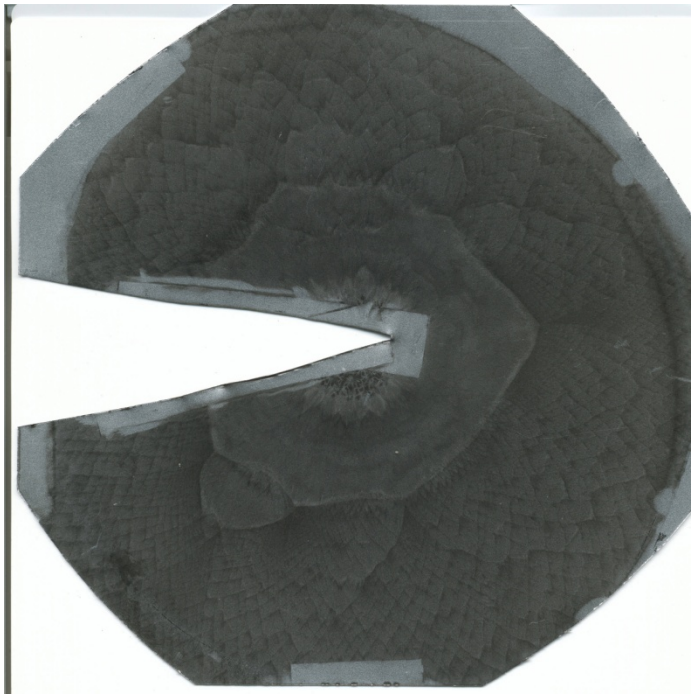

Figure B-8 Go. Run 265. 13.7 mm spacer. C_2H_2+2.5 O_2. w/λ = 3.33. Front wall.

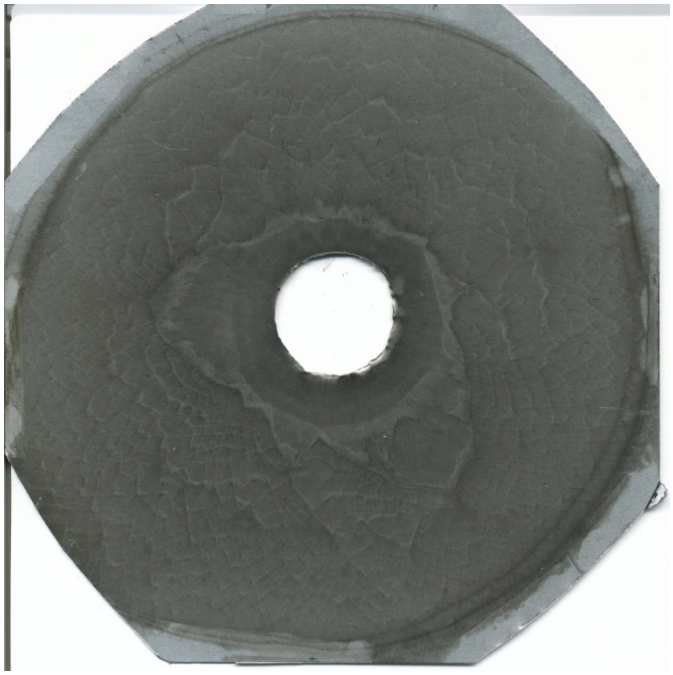

Figure B-9 Go. Run 265. 13.7 mm spacer. C_2H_2+2.5 O_2. w/λ = 3.33. Back wall.

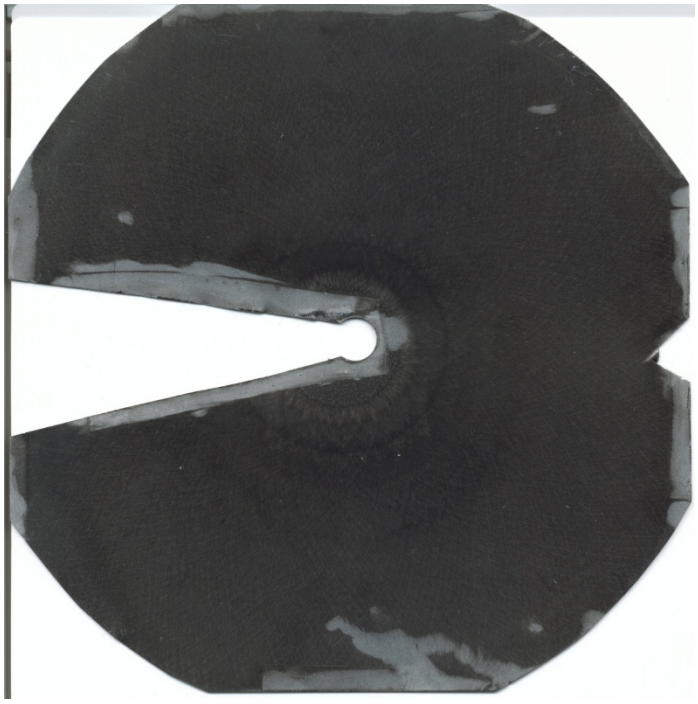

Figure B-10 Go. Run 266. 7.35 mm spacer. C_2H_2+2.5 O_2. w/λ = 7.11. Front wall.

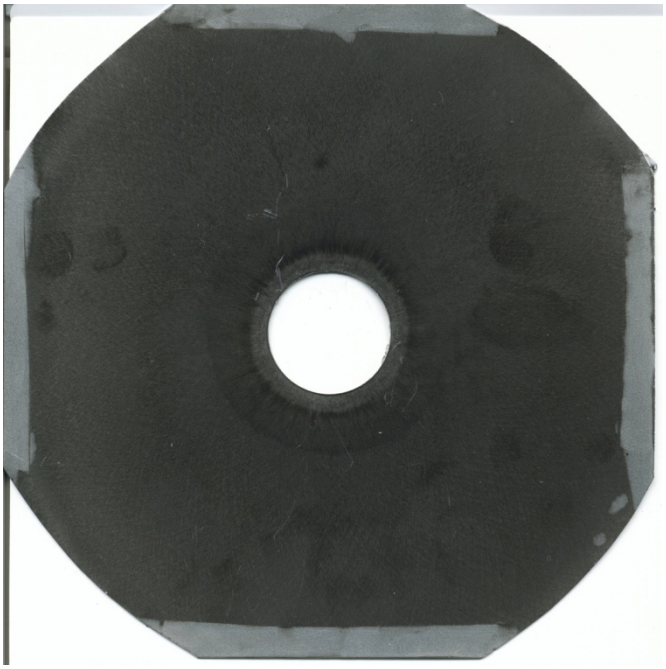

Figure B-11 Go. Run 266. 7.35 mm spacer. C_2H_2+2.5 O_2. w/λ = 7.11. Back wall.

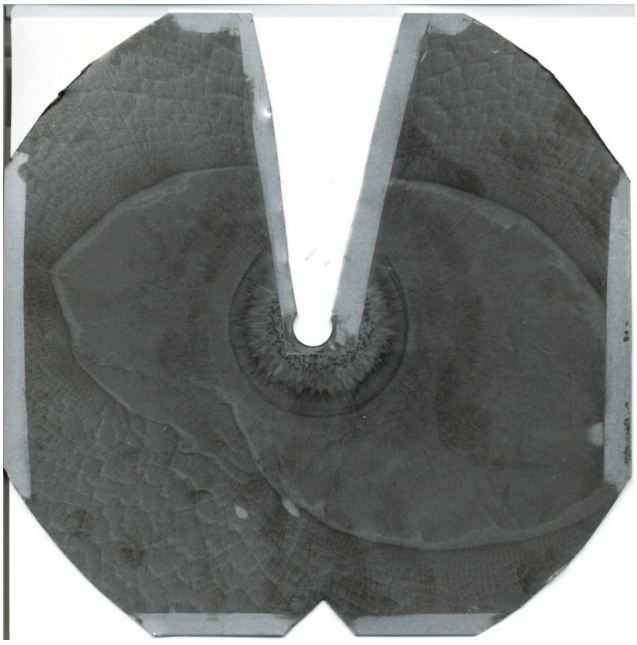

Figure B-12 Go. Run 272. 7.35 mm spacer. C_2H_2+2.5 O_2. w/λ = 2.2. Front wall.

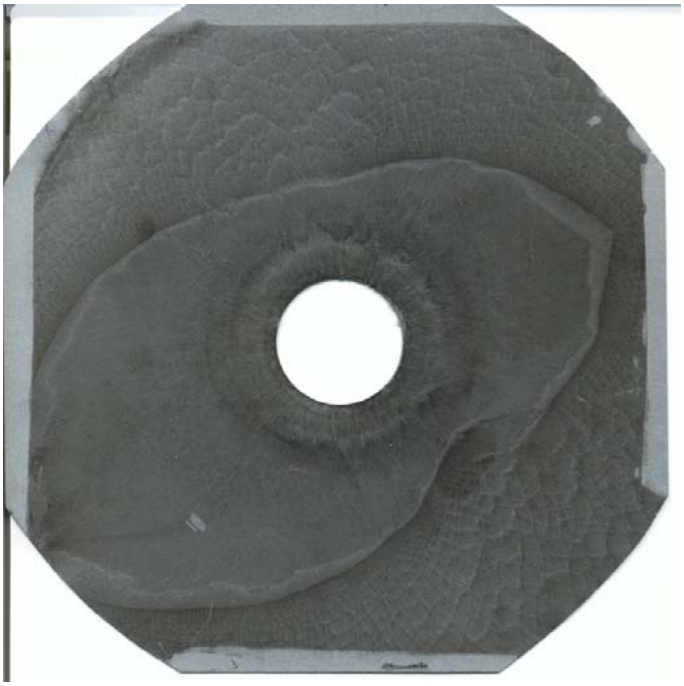

Figure B-13 Go. Run 272. 7.35 mm spacer. C_2H_2+2.5 O_2. w/λ = 2.2. Back wall.

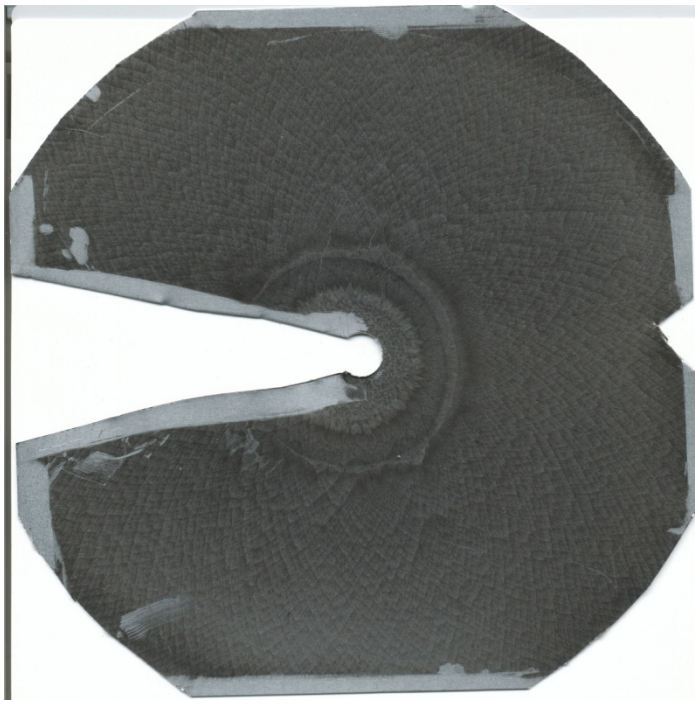

Figure B-14 Go. Run 273. 7.35 mm spacer. C_2H_2+2.5 O_2. w/λ = 4.18. Front wall.

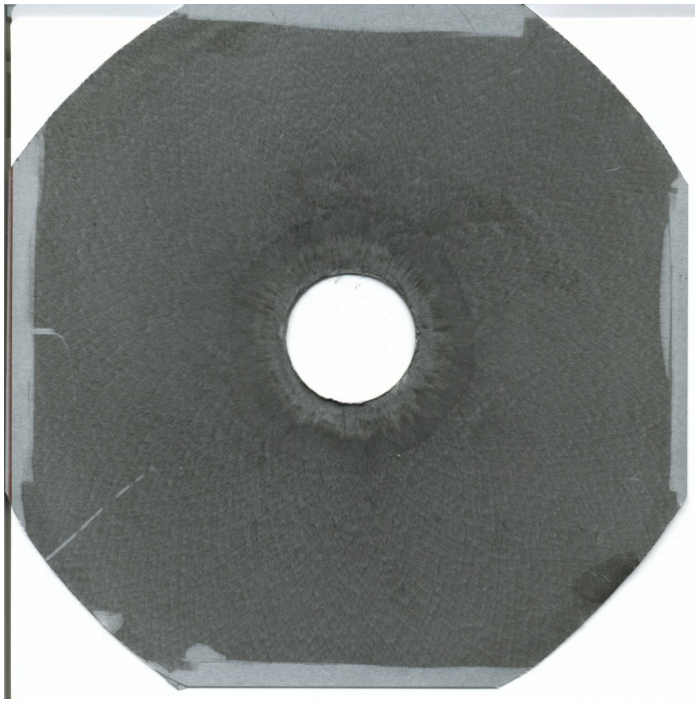

Figure B-15 Go. Run 273. 7.35 mm spacer. C_2H_2+2.5 O_2. w/λ = 4.18. Back wall.

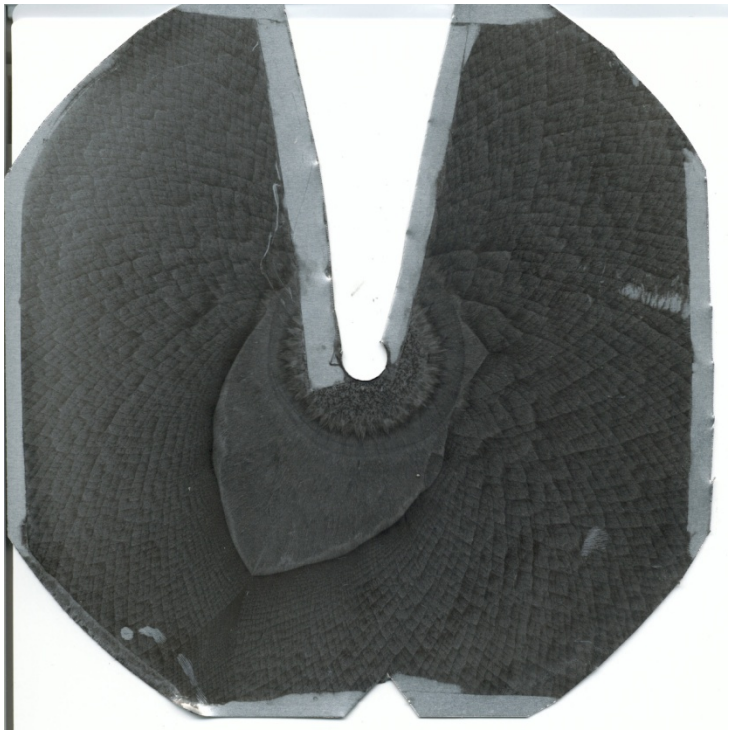

Figure B-16 Go. Run 274. 7.35 mm spacer. C_2H_2+2.5 O_2. w/λ = 3.2. Front wall.

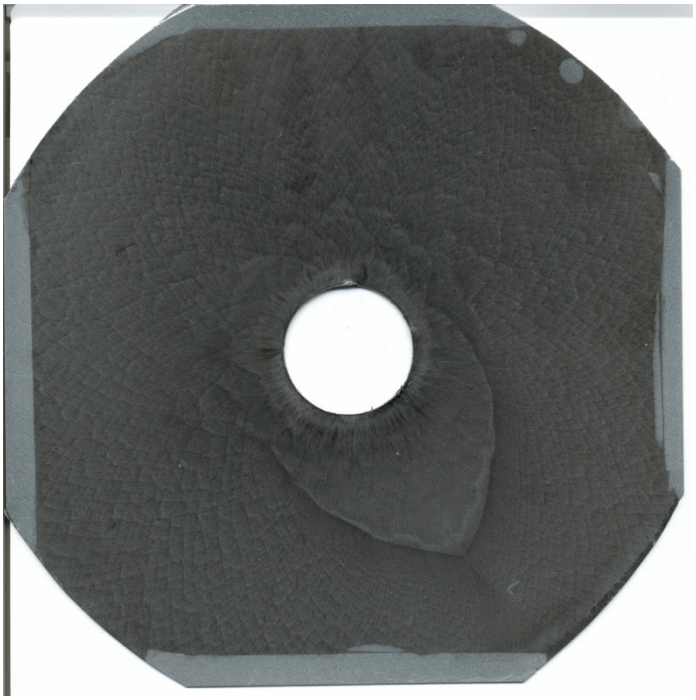

Figure B-17 Go. Run 274. 7.35 mm spacer. C_2H_2+2.5 O_2. w/λ = 3.2. Back wall.

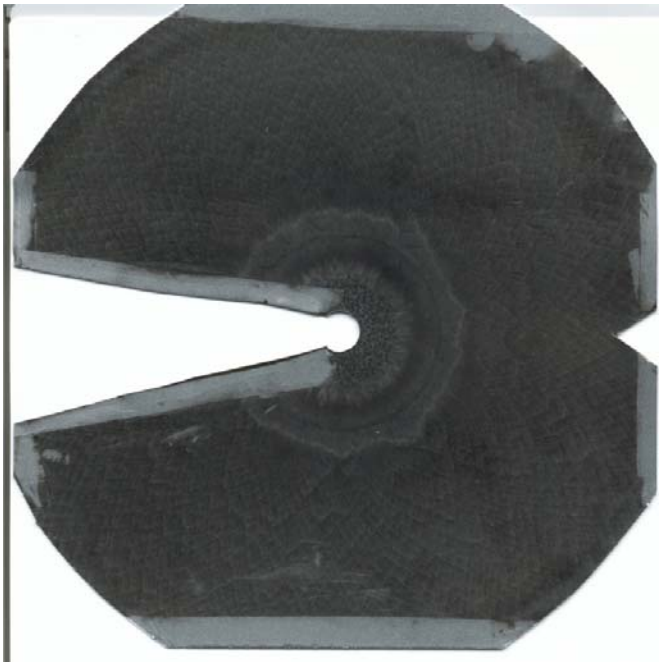

Figure B-18 Go. Run 275. 7.35 mm spacer. C_2H_2+2.5 O_2. w/λ = 3.26.

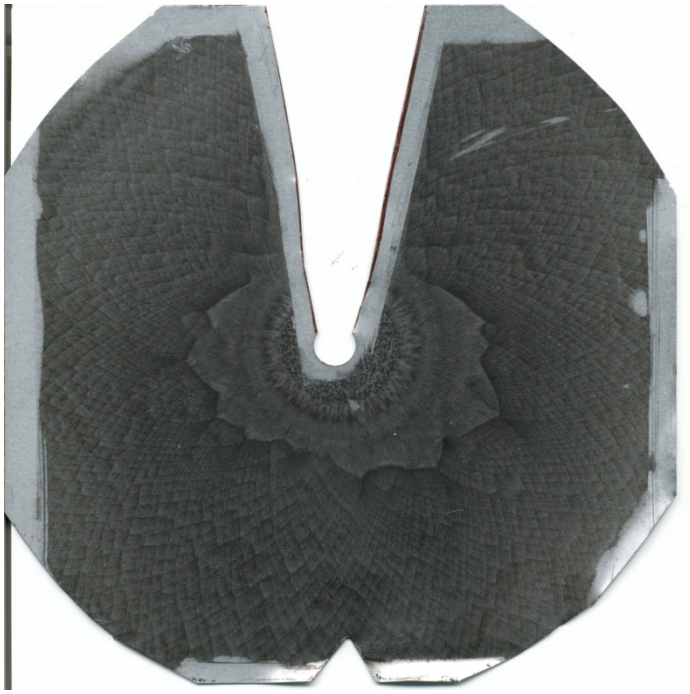

Figure B-19 Go. Run 278. 4.175 mm spacer. C_2H_2+2.5 O_2. w/λ = 1.74.

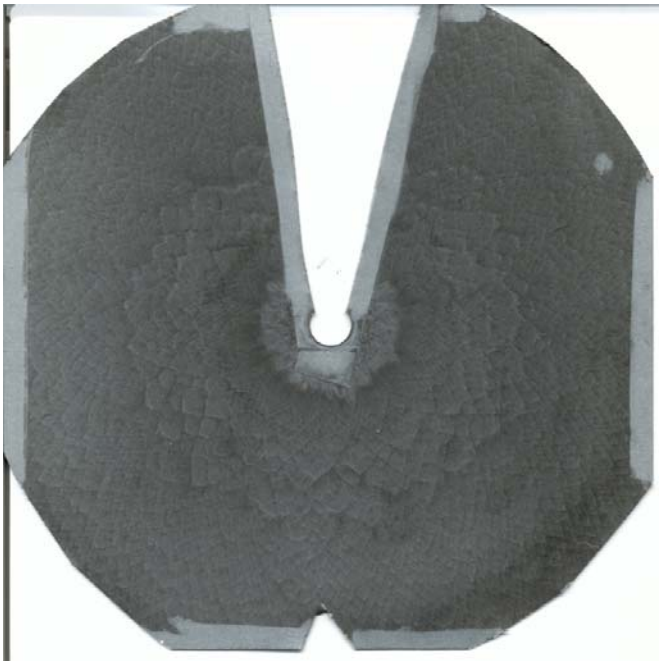

Figure B-20 Go. Run 282. 13.7 mm spacer. C_2H_2+2.5 O_2. w/λ = 4.6.

Figure B-21 Go. Run 283. 4.175 mm spacer. C_2H_2+2.5 O_2. w/λ = 1.15.

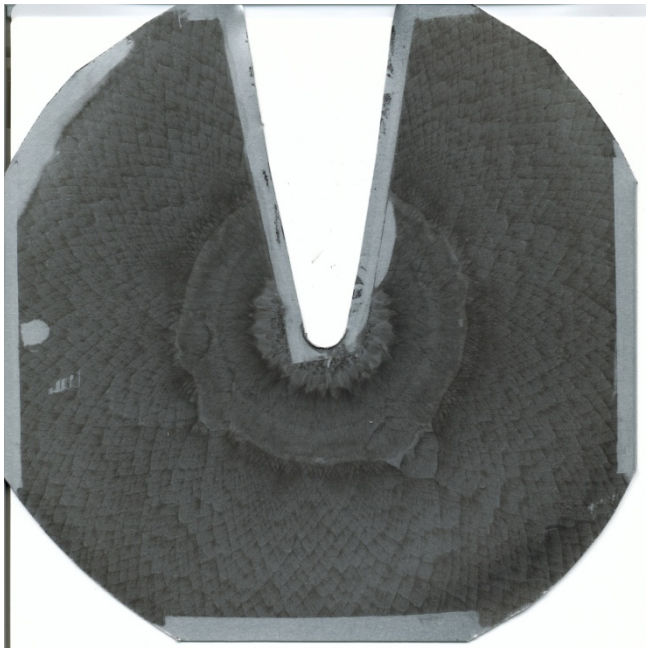

Figure B-22 Go. Run 284. 10.525 mm spacer. C_2H_2+2.5 O_2. w/λ = 3.03.

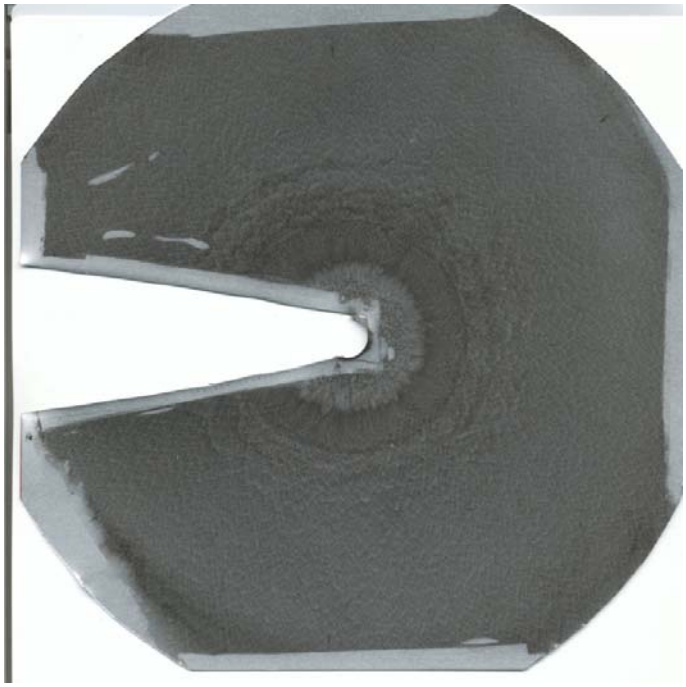

Figure B-23 Go. Run 284. 10.525 mm spacer. C_2H_2+2.5 O_2. w/λ = 6.6.

Figure B-24 No Go. Run 298. 1 mm spacer. C_2H_2+2.5 O_2. w/λ = 0.4. Due to width of soot foil actual gap was less than 0.5 mm.

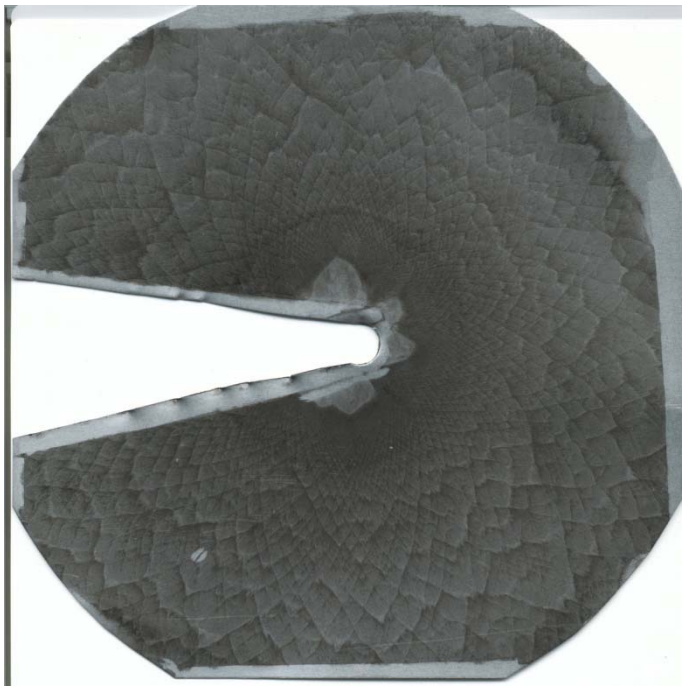

Figure B-25 Go. Run 325. 45.45 mm spacer. C_2H_4+3 O_2. w/λ = 5.9.

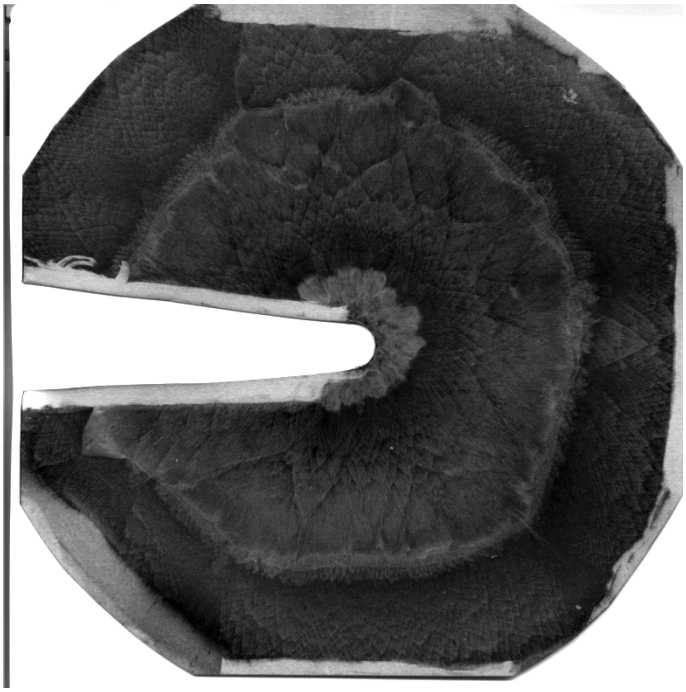

Figure B-26 Go. Run 368. 20.05 mm spacer. C_2H_4+3 O_2. w/λ = 3.2.

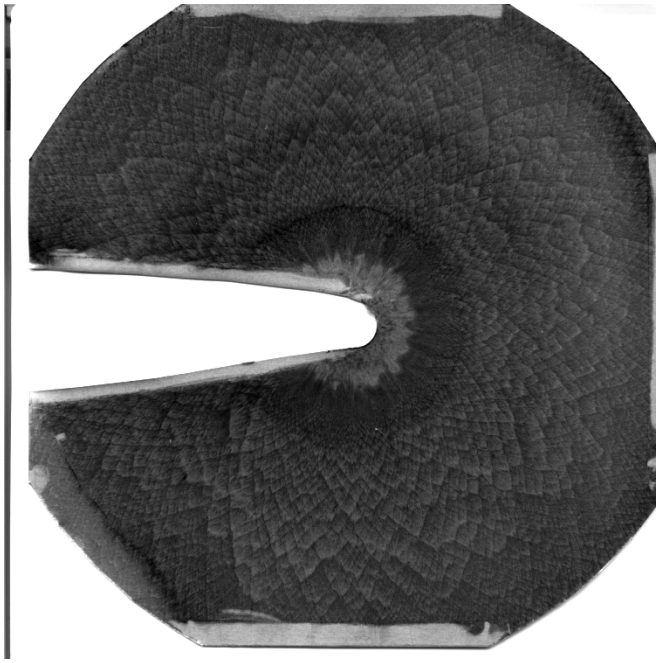

Figure B-27 Go. Run 369. 20.05 mm spacer. C_2H_4+3 O_2. w/λ = 5.3.

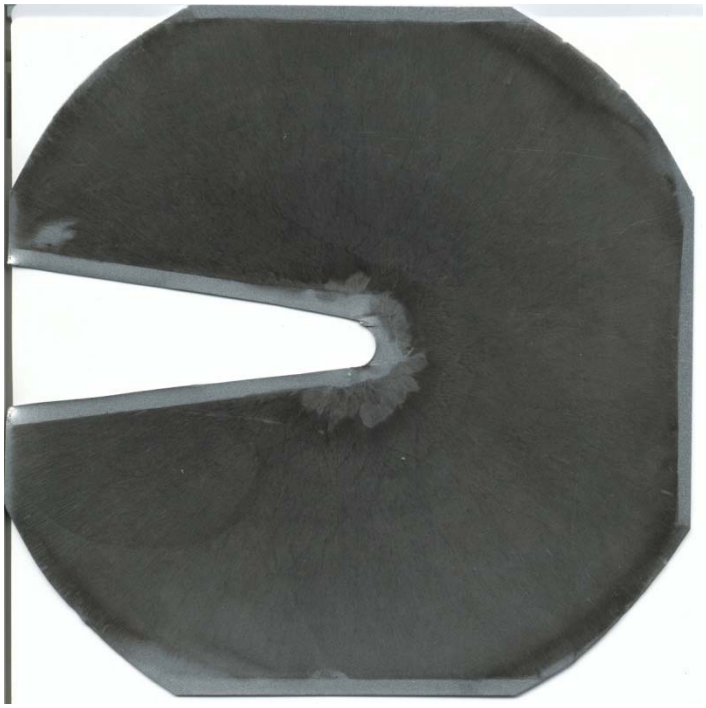

Figure B-28 No Go. Run 367. 20.05 mm spacer. C_2H_4+3 O_2. w/λ = 2.37.

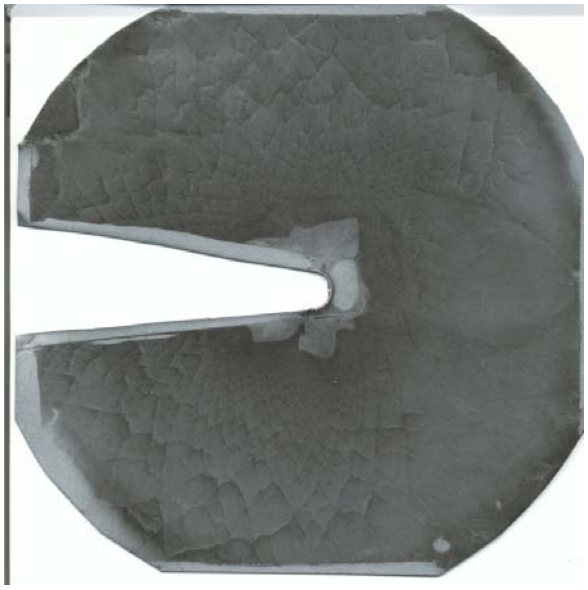

Figure B-29 No Go. Run 375. 45.45 mm spacer. C_2H_4+3 O_2. w/λ = 4.6.

APPENDIX C

ALL EXPERIMENTAL CONDITIONS FOR EXPERIMENTS WITHOUT SOOT FOILS

Table C-1 Experimental conditions for experiments without soot foils

Mixture	Gap	Fill Pressure	w/λ	Go/No Go	Run
$C_2H_2 + 2.5\ O_2$	1	100	0.991	Go	295
$C_2H_2 + 2.5\ O_2$	1	50.1	0.453	Go	296
$C_2H_2 + 2.5\ O_2$	1	70.1	0.663	Go	297
$C_2H_2 + 2.5\ O_2$	1	83.9	0.812	Go	298
$C_2H_2 + 2.5\ O_2$	1	85.2	0.827	Go	299
$C_2H_2 + 2.5\ O_2$	1	94.6	0.931	Go	300
$C_2H_2 + 2.5\ O_2$	1	104.3	1.040	Go	301
$C_2H_2 + 2.5\ O_2$	1	115.5	1.167	Go	302
$C_2H_2 + 2.5\ O_2$	1	40.2	0.353	Go	304
$C_2H_2 + 2.5\ O_2$	1	37.9	0.330	Go	306
$C_2H_2 + 2.5\ O_2$	1	42	0.371	Go	307
$C_2H_2 + 2.5\ O_2$	1	45.8	0.409	Go	308
$C_2H_2 + 2.5\ O_2$	4.175	51	1.929	Go	310
$C_2H_2 + 2.5\ O_2$	4.175	52.4	1.989	Go	311
$C_2H_2 + 2.5\ O_2$	4.175	30.6	1.081	Go	310
$C_2H_2 + 2.5\ O_2$	4.175	36.3	1.312	Go	311
$C_2H_2 + 2.5\ O_2$	7.35	60.4	4.114	Go	267
$C_2H_2 + 2.5\ O_2$	7.35	40.7	2.630	Go	268
$C_2H_2 + 2.5\ O_2$	7.35	158.5	12.284	Go	269
$C_2H_2 + 2.5\ O_2$	7.35	29.8	1.847	Go	313
$C_2H_2 + 2.5\ O_2$	13.7	71.1	9.226	Go	316
$C_2H_2 + 2.5\ O_2$	13.7	158.2	22.847	Go	317
$C_2H_2 + 2.5\ O_2$	1	30.3	0.256	No Go	303
$C_2H_2 + 2.5\ O_2$	1	36	0.311	No Go	305
$C_2H_2 + 2.5\ O_2$	4.175	39.4	1.440	No Go	310
$C_2H_2 + 2.5\ O_2$	4.175	24.8	0.852	No Go	309
$C_2H_2 + 2.5\ O_2$	7.35	24.8	1.500	No Go	312
$C_2H_2 + 4\ O_2$	4.175	50.3	0.757	Go	204
$C_2H_2 + 4\ O_2$	4.175	54.3	0.825	Go	203
$C_2H_2 + 4\ O_2$	4.175	60.2	0.927	Go	199
$C_2H_2 + 4\ O_2$	4.175	70.5	1.109	Go	198

Table C-1 continued

Mixture	Gap	Fill Pressure	w/λ	Go/No Go	Run
$C_2H_2 + 4\ O_2$	4.175	101.2	1.669	Go	197
$C_2H_2 + 4\ O_2$	7.35	60.3	1.636	Go	195
$C_2H_2 + 4\ O_2$	7.35	90.9	2.603	Go	194
$C_2H_2 + 4\ O_2$	7.35	100.6	2.919	Go	193
$C_2H_2 + 4\ O_2$	10.525	50.4	1.912	Go	211
$C_2H_2 + 4\ O_2$	10.525	60	2.329	Go	210
$C_2H_2 + 4\ O_2$	10.525	79.8	3.216	Go	208
$C_2H_2 + 4\ O_2$	10.525	121	5.150	Go	209
$C_2H_2 + 4\ O_2$	13.7	44.8	2.179	Go	166
$C_2H_2 + 4\ O_2$	13.7	49.9	2.461	Go	181
$C_2H_2 + 4\ O_2$	13.7	60.3	3.049	Go	180
$C_2H_2 + 4\ O_2$	13.7	60.4	3.055	Go	169
$C_2H_2 + 4\ O_2$	13.7	68.8	3.540	Go	179
$C_2H_2 + 4\ O_2$	13.7	80.3	4.216	Go	178
$C_2H_2 + 4\ O_2$	13.7	89.9	4.791	Go	177
$C_2H_2 + 4\ O_2$	13.7	100	5.404	Go	176
$C_2H_2 + 4\ O_2$	13.7	111.3	6.100	Go	175
$C_2H_2 + 4\ O_2$	13.7	120.3	6.660	Go	174
$C_2H_2 + 4\ O_2$	13.7	130.2	7.284	Go	173
$C_2H_2 + 4\ O_2$	13.7	139.6	7.881	Go	172
$C_2H_2 + 4\ O_2$	13.7	150.9	8.607	Go	171
$C_2H_2 + 4\ O_2$	13.7	160	9.196	Go	170
$C_2H_2 + 4\ O_2$	26.4	41.3	3.829	Go	162
$C_2H_2 + 4\ O_2$	26.4	41.4	3.840	Go	161
$C_2H_2 + 4\ O_2$	26.4	51.8	4.948	Go	160
$C_2H_2 + 4\ O_2$	26.4	70.5	7.012	Go	159
$C_2H_2 + 4\ O_2$	26.4	133.4	14.426	Go	158
$C_2H_2 + 4\ O_2$	26.4	163.1	18.110	Go	165
$C_2H_2 + 4\ O_2$	26.4	189.9	21.511	Go	247
$C_2H_2 + 4\ O_2$	26.4	149.8	16.448	Go	248
$C_2H_2 + 4\ O_2$	26.4	119.9	12.786	Go	249
$C_2H_2 + 4\ O_2$	26.4	210.8	24.208	Go	250
$C_2H_2 + 4\ O_2$	26.4	81.2	8.228	Go	251
$C_2H_2 + 4\ O_2$	39.1	45.3	6.297	Go	235
$C_2H_2 + 4\ O_2$	39.1	48.2	6.755	Go	232
$C_2H_2 + 4\ O_2$	39.1	92.4	14.103	Go	231
$C_2H_2 + 4\ O_2$	4.175	39	0.568	No Go	200

Table C-1 continued

Mixture	Gap	Fill Pressure	w/λ	Go/No Go	Run
$C_2H_2 + 4\ O_2$	4.175	44.2	0.654	No Go	205
$C_2H_2 + 4\ O_2$	4.175	47.2	0.704	No Go	207
$C_2H_2 + 4\ O_2$	4.175	48.4	0.725	No Go	206
$C_2H_2 + 4\ O_2$	7.35	42.4	1.098	No Go	196
$C_2H_2 + 4\ O_2$	7.35	49.9	1.321	No Go	186
$C_2H_2 + 4\ O_2$	10.525	33	1.184	No Go	212
$C_2H_2 + 4\ O_2$	10.525	41	1.514	No Go	213
$C_2H_2 + 4\ O_2$	10.525	45.8	1.716	No Go	214
$C_2H_2 + 4\ O_2$	13.7	20.4	0.895	No Go	184
$C_2H_2 + 4\ O_2$	13.7	28.8	1.322	No Go	183
$C_2H_2 + 4\ O_2$	13.7	35.1	1.653	No Go	167
$C_2H_2 + 4\ O_2$	13.7	40.5	1.944	No Go	182
$C_2H_2 + 4\ O_2$	26.4	29.1	2.577	No Go	163
$C_2H_2 + 4\ O_2$	26.4	35.2	3.196	No Go	164
$C_2H_2 + 4\ O_2$	39.1	35.3	4.749	No Go	233
$C_2H_2 + 4\ O_2$	39.1	43.1	5.952	No Go	234
$C_2H_4 + 3\ O_2$	4.175	117.1	1.097	Go	358
$C_2H_4 + 3\ O_2$	4.175	112.2	1.047	Go	359
$C_2H_4 + 3\ O_2$	4.175	107.2	0.997	Go	360
$C_2H_4 + 3\ O_2$	4.175	102	0.944	Go	361
$C_2H_4 + 3\ O_2$	4.175	91.9	0.843	Go	363
$C_2H_4 + 3\ O_2$	4.175	87.3	0.797	Go	364
$C_2H_4 + 3\ O_2$	4.175	82	0.744	Go	365
$C_2H_4 + 3\ O_2$	7.35	100.9	1.643	Go	314
$C_2H_4 + 3\ O_2$	7.35	84.6	1.356	Go	315
$C_2H_4 + 3\ O_2$	7.35	90	1.450	Go	318
$C_2H_4 + 3\ O_2$	10.525	94	2.178	Go	352
$C_2H_4 + 3\ O_2$	10.525	88.4	2.037	Go	353
$C_2H_4 + 3\ O_2$	10.525	83.8	1.921	Go	354
$C_2H_4 + 3\ O_2$	10.525	78.7	1.794	Go	355
$C_2H_4 + 3\ O_2$	10.525	73.6	1.668	Go	356
$C_2H_4 + 3\ O_2$	13.7	90.2	2.710	Go	347
$C_2H_4 + 3\ O_2$	13.7	80.1	2.381	Go	349
$C_2H_4 + 3\ O_2$	13.7	85	2.540	Go	350
$C_2H_4 + 3\ O_2$	13.7	75.5	2.233	Go	351
$C_2H_4 + 3\ O_2$	20.05	80.4	3.499	Go	340
$C_2H_4 + 3\ O_2$	20.05	65.2	2.785	Go	343

Table C-1 continued

Mixture	Gap	Fill Pressure	w/λ	Go/No Go	Run
$C_2H_4 + 3\ O_2$	20.05	85.1	3.722	Go	345
$C_2H_4 + 3\ O_2$	26.4	80.5	4.613	Go	335
$C_2H_4 + 3\ O_2$	26.4	75.4	4.296	Go	336
$C_2H_4 + 3\ O_2$	26.4	70.2	3.974	Go	337
$C_2H_4 + 3\ O_2$	26.4	65.2	3.667	Go	338
$C_2H_4 + 3\ O_2$	32.75	79.9	5.677	Go	331
$C_2H_4 + 3\ O_2$	32.75	70	4.915	Go	332
$C_2H_4 + 3\ O_2$	32.75	72.2	5.083	Go	334
$C_2H_4 + 3\ O_2$	39.1	71.2	5.977	Go	326
$C_2H_4 + 3\ O_2$	45.45	65	6.292	Go	323
$C_2H_4 + 3\ O_2$	45.45	60.5	5.819	Go	324
$C_2H_4 + 3\ O_2$	45.45	52.4	4.975	Go	371
$C_2H_4 + 3\ O_2$	45.45	50.1	4.738	Go	372
$C_2H_4 + 3\ O_2$	4.175	76.9	0.694	No Go	366
$C_2H_4 + 3\ O_2$	7.35	73.8	1.168	No Go	316
$C_2H_4 + 3\ O_2$	7.35	79.9	1.274	No Go	317
$C_2H_4 + 3\ O_2$	10.525	68.7	1.548	No Go	357
$C_2H_4 + 3\ O_2$	13.7	69.9	2.053	No Go	348
$C_2H_4 + 3\ O_2$	20.05	60.8	2.581	No Go	344
$C_2H_4 + 3\ O_2$	26.4	60	3.349	No Go	339
$C_2H_4 + 3\ O_2$	32.75	65.1	4.541	No Go	333
$C_2H_4 + 3\ O_2$	39.1	55.3	4.539	No Go	329
$C_2H_4 + 3\ O_2$	45.45	40.5	3.758	No Go	320
$C_2H_4 + 3\ O_2$	45.45	46.1	4.327	No Go	321
$C_2H_4 + 3\ O_2$	45.45	44.9	4.205	No Go	374
$H_2 + 0.5\ O_2$	1	756.4	0.644	Go	70
$H_2 + 0.5\ O_2$	1	509.1	0.420	Go	71
$H_2 + 0.5\ O_2$	13.7	430.1	4.800	Go	123
$H_2 + 0.5\ O_2$	13.7	331.6	3.627	Go	121
$H_2 + 0.5\ O_2$	13.7	254.8	2.731	Go	120
$H_2 + 0.5\ O_2$	13.7	358.2	3.942	Go	118
$H_2 + 0.5\ O_2$	13.7	279.2	3.013	Go	117
$H_2 + 0.5\ O_2$	26.4	274.9	5.711	Go	135
$H_2 + 0.5\ O_2$	26.4	229.3	4.697	Go	134
$H_2 + 0.5\ O_2$	26.4	400.4	8.564	Go	131
$H_2 + 0.5\ O_2$	26.4	301.6	6.310	Go	130
$H_2 + 0.5\ O_2$	26.4	199.3	4.038	Go	128

Table C-1 continued

Mixture	Gap	Fill Pressure	w/λ	Go/No Go	Run
$H_2 + 0.5\ O_2$	26.4	250.6	5.169	Go	127
$H_2 + 0.5\ O_2$	26.4	210.3	4.279	Go	398
$H_2 + 0.5\ O_2$	26.4	215	4.382	Go	400
$H_2 + 0.5\ O_2$	26.4	222.1	4.538	Go	401
$H_2 + 0.5\ O_2$	26.4	230.1	4.714	Go	402
$H_2 + 0.5\ O_2$	26.4	235	4.823	Go	403
$H_2 + 0.5\ O_2$	32.75	230.5	5.859	Go	395
$H_2 + 0.5\ O_2$	32.75	225	5.709	Go	396
$H_2 + 0.5\ O_2$	39.1	202.5	6.084	Go	139
$H_2 + 0.5\ O_2$	39.1	250.3	7.645	Go	115
$H_2 + 0.5\ O_2$	39.1	227.3	6.891	Go	114
$H_2 + 0.5\ O_2$	39.1	201.6	6.055	Go	109
$H_2 + 0.5\ O_2$	39.1	276.6	8.514	Go	108
$H_2 + 0.5\ O_2$	45.45	175.4	6.058	Go	382
$H_2 + 0.5\ O_2$	45.45	190.4	6.618	Go	387
$H_2 + 0.5\ O_2$	45.45	175.8	6.073	Go	388
$H_2 + 0.5\ O_2$	1	214.7	0.166	No Go	68
$H_2 + 0.5\ O_2$	13.7	240.9	2.570	No Go	125
$H_2 + 0.5\ O_2$	13.7	174.8	1.819	No Go	124
$H_2 + 0.5\ O_2$	13.7	124.5	1.262	No Go	122
$H_2 + 0.5\ O_2$	13.7	199.9	2.102	No Go	116
$H_2 + 0.5\ O_2$	26.4	150.9	2.992	No Go	133
$H_2 + 0.5\ O_2$	26.4	127.5	2.495	No Go	132
$H_2 + 0.5\ O_2$	26.4	174.6	3.501	No Go	129
$H_2 + 0.5\ O_2$	26.4	200	4.053	No Go	404
$H_2 + 0.5\ O_2$	32.75	190	4.758	No Go	390
$H_2 + 0.5\ O_2$	32.75	195.9	4.917	No Go	391
$H_2 + 0.5\ O_2$	39.1	198.2	5.945	No Go	138
$H_2 + 0.5\ O_2$	39.1	195.1	5.845	No Go	137
$H_2 + 0.5\ O_2$	39.1	97.7	2.774	No Go	113
$H_2 + 0.5\ O_2$	39.1	126.5	3.664	No Go	112
$H_2 + 0.5\ O_2$	39.1	149.3	4.381	No Go	111
$H_2 + 0.5\ O_2$	39.1	179	5.327	No Go	110
$H_2 + 0.5\ O_2$	45.45	160	5.487	No Go	383
$H_2 + 0.5\ O_2$	45.45	165.5	5.690	No Go	384

APPENDIX D

CONDITIONS FOR EXPERIMENTS WITH SOOT FOILS

Table D-1 Experimental conditions for experiments with soot foils

Mixture	Gap (mm)	w/λ	Run
$C_2H_2 + 2.5\ O_2$	0.49	0.40	298
$C_2H_2 + 2.5\ O_2$	3.67	1.75	278
$C_2H_2 + 2.5\ O_2$	3.67	1.16	283
$C_2H_2 + 2.5\ O_2$	6.33	7.11	266
$C_2H_2 + 2.5\ O_2$	6.33	2.20	272
$C_2H_2 + 2.5\ O_2$	6.33	4.18	273
$C_2H_2 + 2.5\ O_2$	6.33	3.19	274
$C_2H_2 + 2.5\ O_2$	6.84	3.26	275
$C_2H_2 + 2.5\ O_2$	10.02	3.04	284
$C_2H_2 + 2.5\ O_2$	10.02	6.61	285
$C_2H_2 + 2.5\ O_2$	12.68	3.33	265
$C_2H_2 + 2.5\ O_2$	13.19	4.58	282
$C_2H_2 + 4\ O_2$	6.33	2.23	243
$C_2H_2 + 4\ O_2$	12.68	5.86	237
$C_2H_2 + 4\ O_2$	12.68	5.02	240
$C_2H_2 + 4\ O_2$	19.03	5.02	227
$C_2H_2 + 4\ O_2$	25.38	4.60	244
$C_2H_4 + 3\ O_2$	19.54	2.37	367
$C_2H_4 + 3\ O_2$	19.54	3.19	368
$C_2H_4 + 3\ O_2$	19.54	5.30	369
$C_2H_4 + 3\ O_2$	44.94	5.91	325
$C_2H_4 + 3\ O_2$	44.94	4.55	375
$H_2 + 0.5\ O_2$	25.38	3.18	143

APPENDIX E

DERIVATION OF JUMP CONDITIONS

(E-1) $\rho_1 V_1 = \rho_2 V_2$

(E-2) $P_1 + \rho_1 V_1^2 = P_2 + \rho_2 V_2^2$

(E-3) $h_1 + V_1^2/2 = h_2 + V_2^2/2$

(E-5) $h_1 = c_p \ T_1$

(E-6) $h_2 = c_p \ T_2 - q$

(E-7) $P = \rho R T$

(E-8) $a = \sqrt{\gamma R T}$

(E-9) $M = \frac{v}{a}$

(E-10) $\gamma = \frac{c_p}{c_v}$

(E-11) $R = c_p - c_v$

(E-12) $c_p = \gamma R/(\gamma - 1)$

Eqn. 10 is obtained using by solving Eqns. 8 and 9 for c_p.

(E-13) $$\frac{P_2}{P_1} = \frac{1+\gamma_1 M_1^2}{1+\gamma_2 M_2^2}$$

(E-14) $$\frac{T_2}{T_1} = \frac{\gamma_1 R_1}{\gamma_2 R_2}\left(\frac{\frac{1}{\gamma_1 - 1} + \frac{1}{2}M_1^2 + \frac{q}{a_1^2}}{\frac{1}{\gamma_2 - 1} + \frac{1}{2}M_2^2}\right)$$

Eqn. 11 is obtained by solving Eqn. (2) using Eqn. (5), (6) and (7)

STEP 1: $P_1 + \rho_1 V_1^2 = P_2 + \rho_2 V_2^2$

STEP 2: $P_1 + P_1 M_1^2 \gamma_1 R_1 T_1/(R_1 T_1) = P_2 + P_2 M_2^2 \gamma_2 R_2 T_2/(R_2 T_2)$

STEP 3: $\frac{P_2}{P_1} = \frac{1+\gamma_1 M_1^2}{1+\gamma_2 M_2^2}$

Eqn. 12 is obtained by solving Eqn. 3 using Eqns. 4a, 4b, 7 and 10

STEP 1: $h_1 + V_1^2/2 = h_2 + V_2^2/2$

STEP 2: $c_{p1} T_1 + M_1^2 \gamma_1 R_1 T_1/2 = c_{p2} T_2 - q + M_2^2 \gamma_2 R_2 T_2/2$

STEP 3: $\gamma_1 R_1 T_1/(\gamma_1 - 1) + M_1^2 \gamma_1 R_1 T_1/2 = \gamma_2 R_2 T_2/(\gamma_2 - 1) - q + M_2^2 \gamma_2 R_2 T_2/2$

STEP 4: $T_1(\gamma_1 R_1/(\gamma_1 - 1) + M_1^2 \gamma_1 R_1/2 + q/T_1) = T_2(\gamma_2 R_2/(\gamma_2 - 1) + M_2^2 \gamma_2 R_2/2)$

STEP 5: $\frac{T_2}{T_1} = \frac{(\frac{\gamma_1 R_1}{\gamma_1 - 1} + \frac{M_1^2 \gamma_1 R_1}{2} + \frac{q}{T_1})}{(\frac{\gamma_2 R_2}{\gamma_2 - 1} + \frac{M_2^2 \gamma_2 R_2}{2})}$

STEP 6: $\frac{T_2}{T_1} = \frac{\gamma_1 R_1 a_1^2 (\gamma_2 - 1)(\gamma_1 - 1)\left[\frac{1}{(\gamma_1 - 1)} + \frac{M_1^2}{2} + q\right]}{\gamma_2 R_2 a_1^2 (\gamma_2 - 1)(\gamma_1 - 1)\left[\frac{1}{\gamma_2 - 1} + \frac{M_2^2}{2}\right]}$

STEP 7: $\frac{T_2}{T_1} = \frac{\gamma_1 R_1\left[\frac{1}{(\gamma_1 - 1)} + \frac{M_1^2}{2} + q\right]}{\gamma_2 R_2\left[\frac{1}{\gamma_2 - 1} + \frac{M_2^2}{2}\right]}$

APPENDIX F

FACILITY DRAWINGS

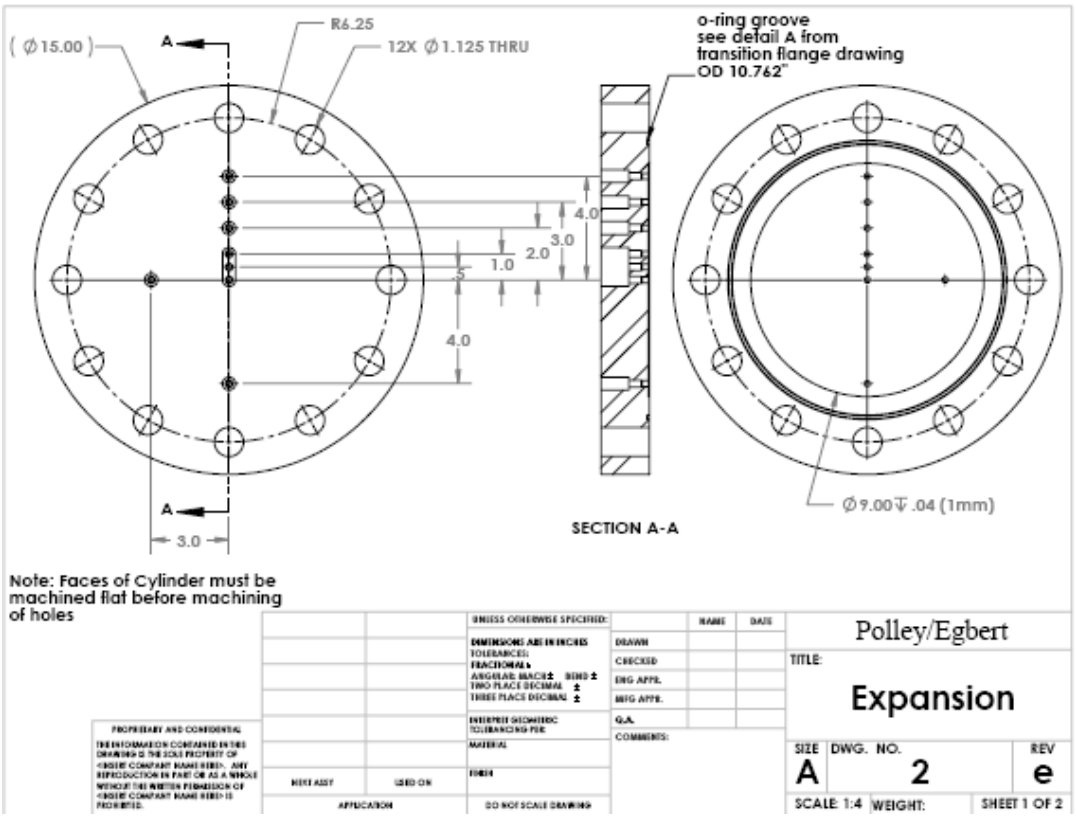

Figure F-1 Drawing of expansion volume endwall.

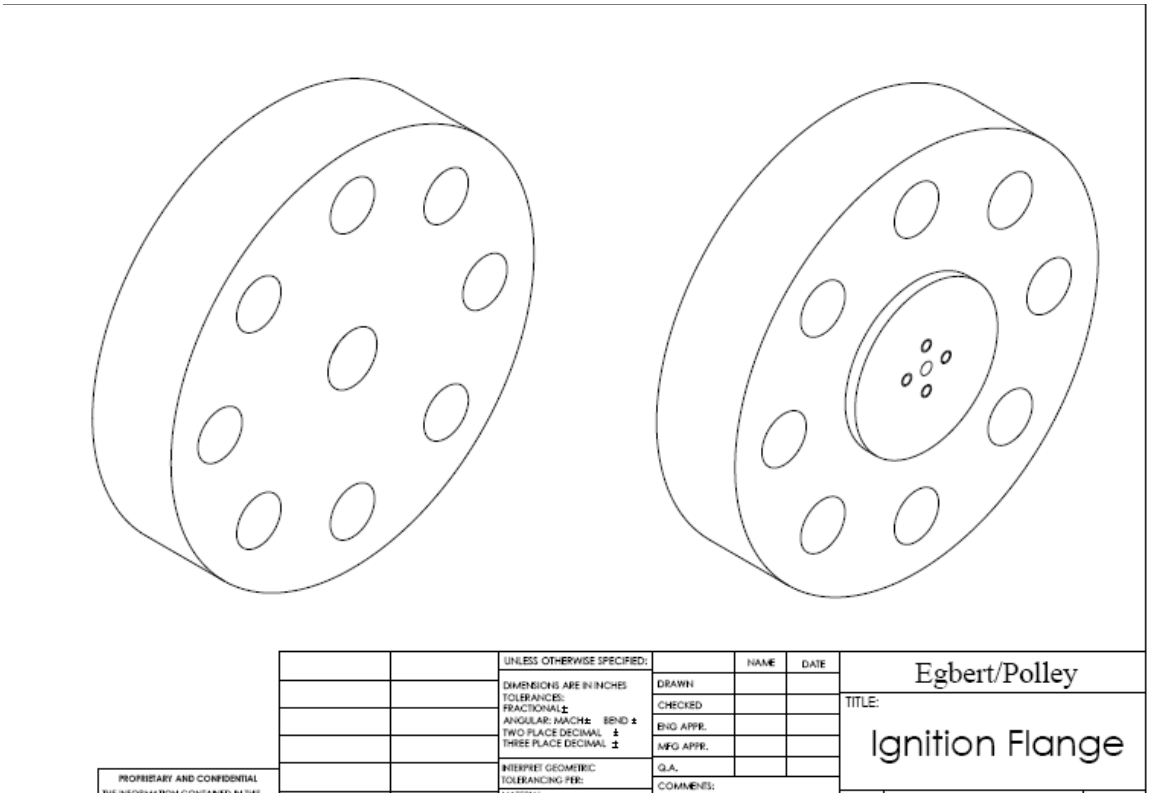

Figure F-2 Drawing of ignition flange. The center hole is for glow plug while four outer holes are for rods holding the turbulence-generating obstacles.

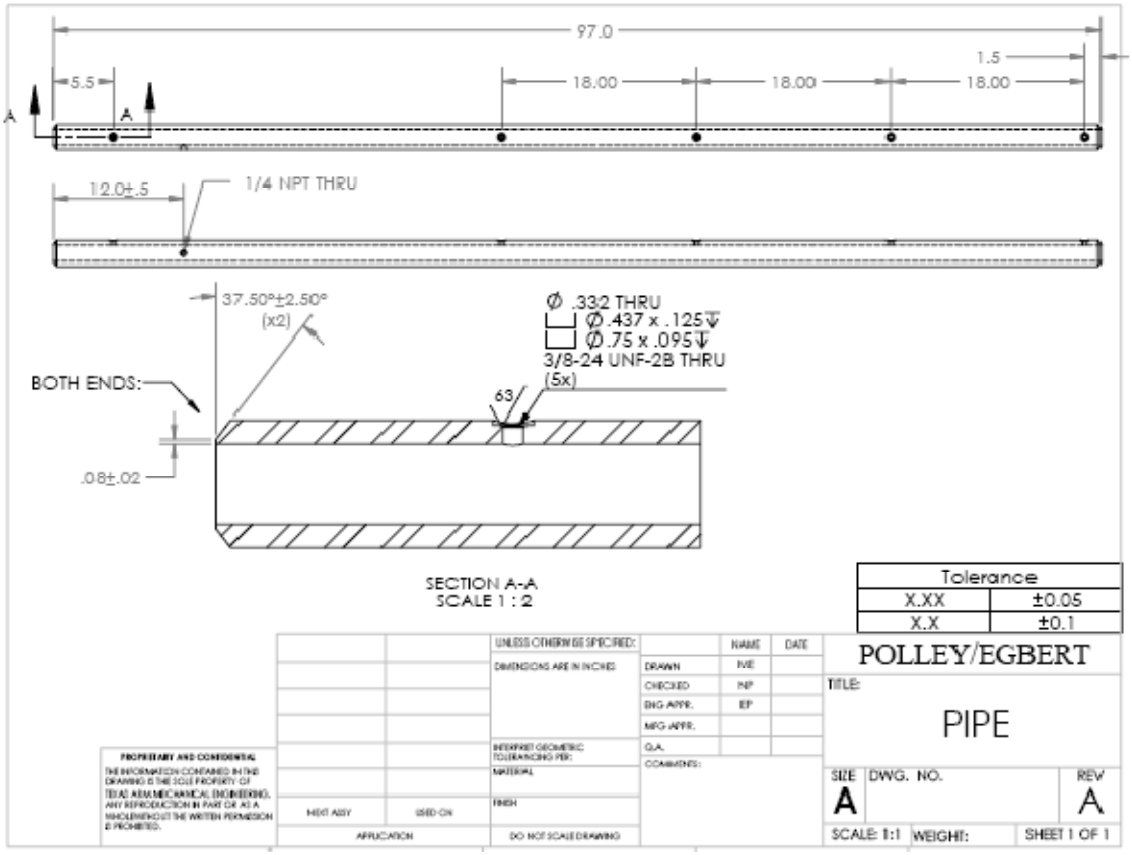

Figure F-3 Drawing of detonation tube.

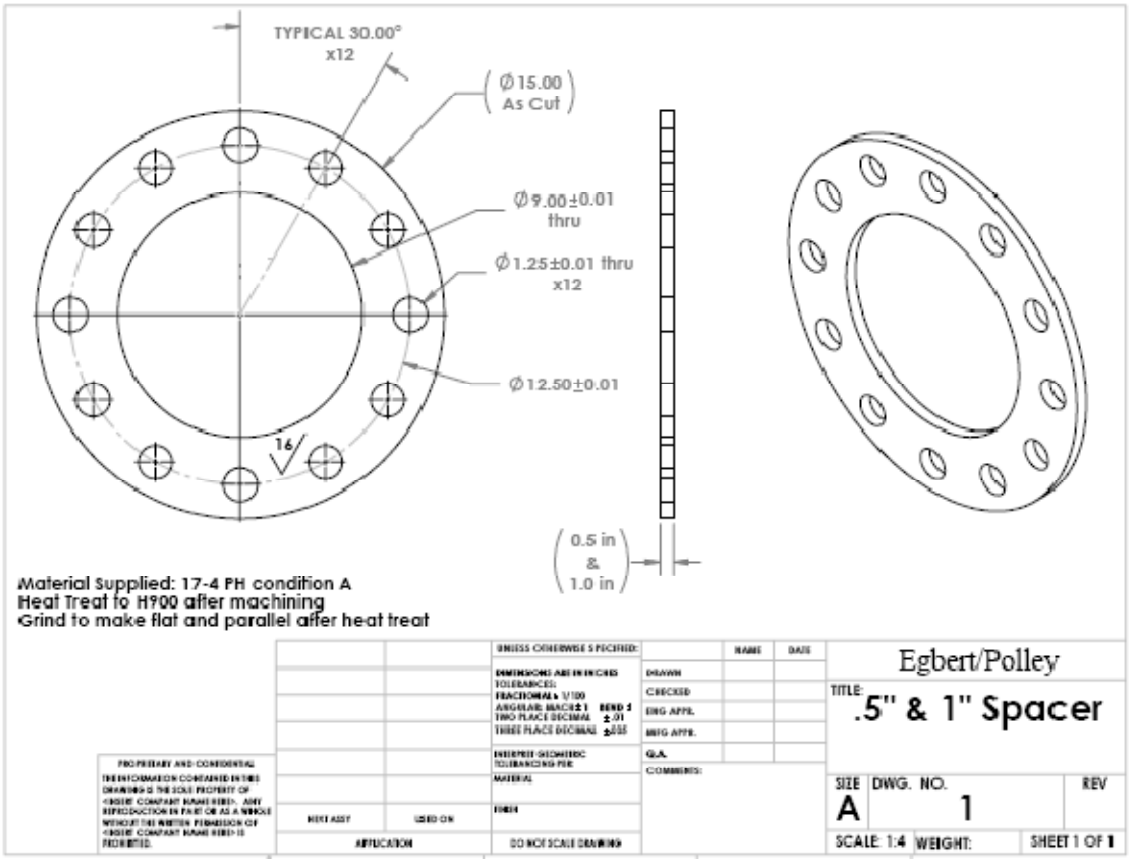

Figure F-4 Generic drawing for expansion volume spacers. The only difference between spacers is their thickness and whether or not an o-ring groove is included.

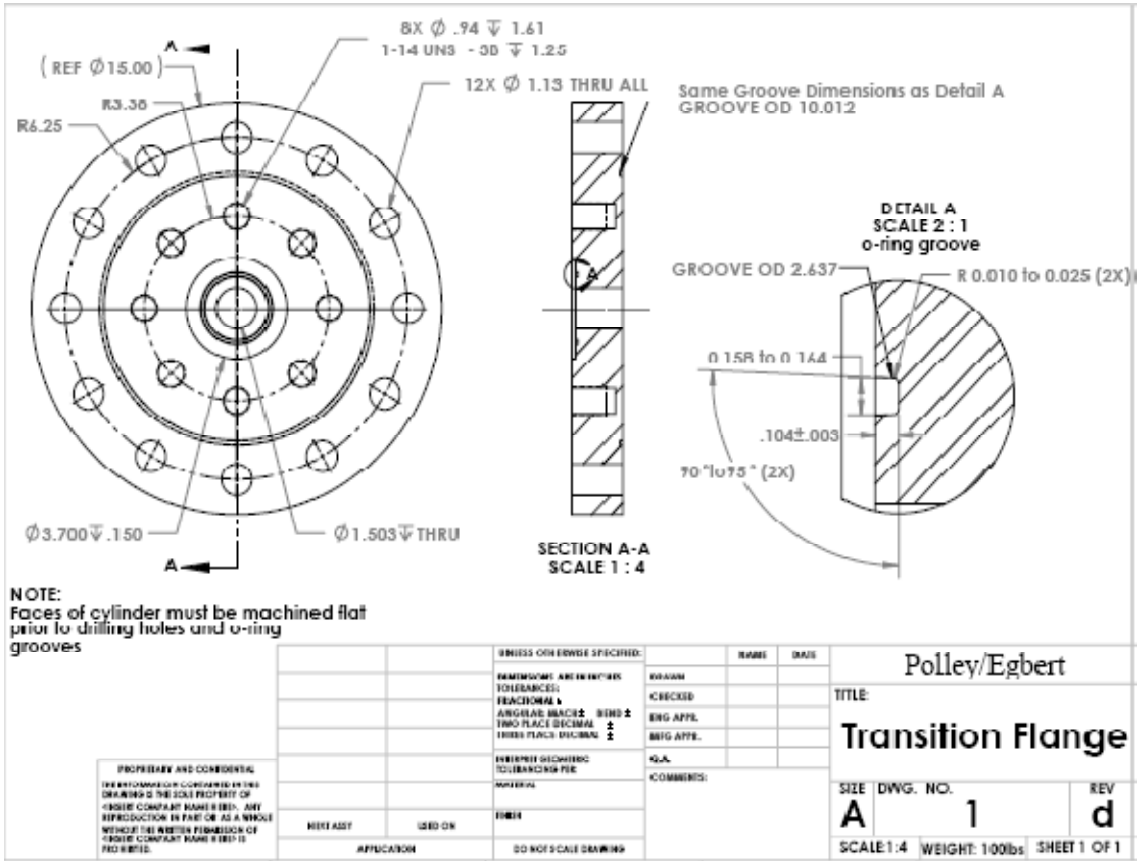

Figure F-5 Drawing of transition flange. This flange connects the smaller detonation tube to the larger expansion volume.

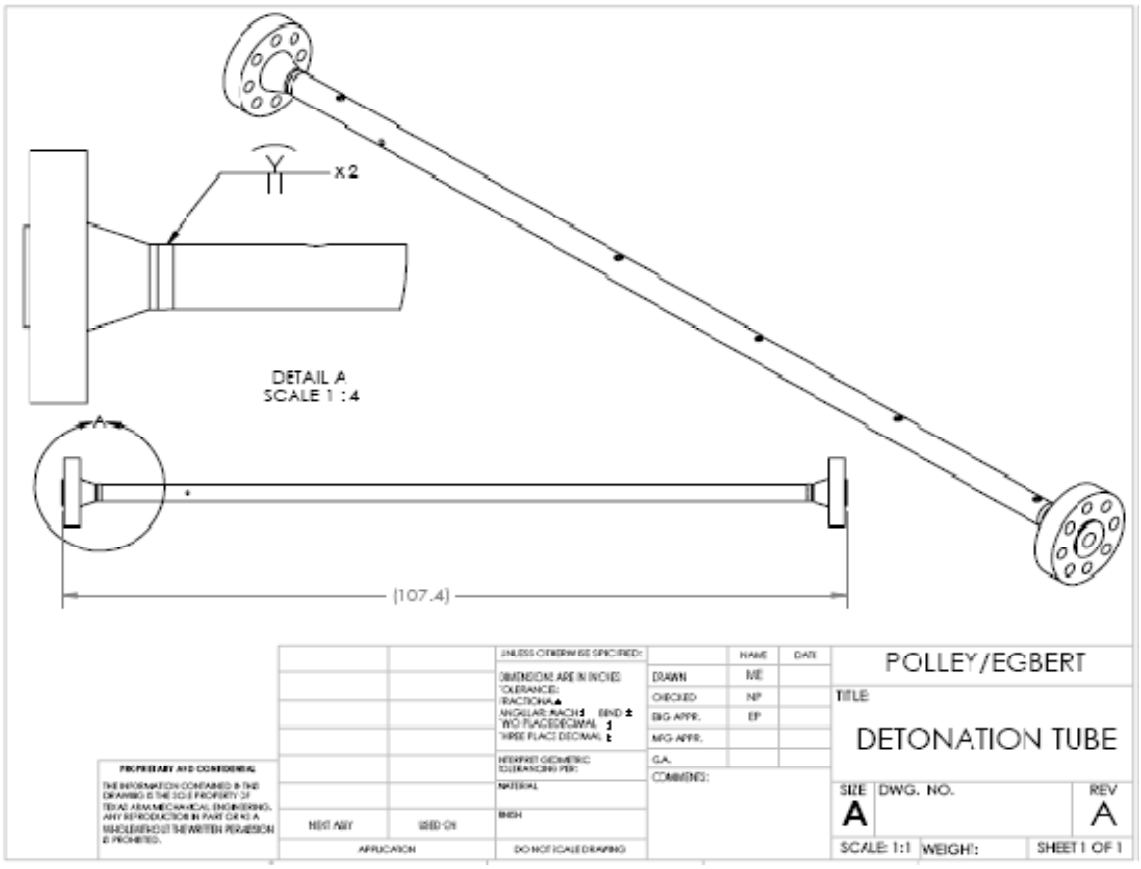

Figure F-6 Drawing of the detonation tube with the 2500# flanges welded to the ends of the tube.

VITA

Name:	Nolan Lee Polley
Address:	3123 TAMU College Station, TX 77843
Email Address:	polley@tamu.edu
Education:	B.S., Mechanical Engineering, University of Wisconsin-Madison, 2008 M.S., Mechanical Engineering, Texas A&M University, 2010